



**HAL**  
open science

## FI-flows of 3d N=4 Theories

Antoine Bourget, Simone Giacomelli, Julius F. Grimmering

► **To cite this version:**

Antoine Bourget, Simone Giacomelli, Julius F. Grimmering. FI-flows of 3d N=4 Theories. Journal of High Energy Physics, 2023, 2023 (04), pp.015. 10.1007/JHEP04(2023)015 . hal-03998607

**HAL Id: hal-03998607**

**<https://hal.science/hal-03998607v1>**

Submitted on 23 Aug 2024

**HAL** is a multi-disciplinary open access archive for the deposit and dissemination of scientific research documents, whether they are published or not. The documents may come from teaching and research institutions in France or abroad, or from public or private research centers.

L'archive ouverte pluridisciplinaire **HAL**, est destinée au dépôt et à la diffusion de documents scientifiques de niveau recherche, publiés ou non, émanant des établissements d'enseignement et de recherche français ou étrangers, des laboratoires publics ou privés.



Distributed under a Creative Commons Attribution 4.0 International License

## FI-flows of 3d $\mathcal{N}=4$ theories

---

Antoine Bourget,<sup>a,b</sup> Simone Giacomelli<sup>c,d</sup> and Julius F. Grimminger<sup>e</sup>

<sup>a</sup> *Université Paris-Saclay, CNRS, CEA, Institut de physique théorique,  
91191, Gif-sur-Yvette, France*

<sup>b</sup> *Laboratoire de Physique de l'École normale supérieure, ENS, Université PSL, CNRS,  
Sorbonne Université, Université de Paris,  
F-75005 Paris, France*

<sup>c</sup> *Dipartimento di Fisica, Università di Milano-Bicocca,  
Piazza della Scienza 3, I-20126 Milano, Italy*

<sup>d</sup> *INFN, sezione di Milano-Bicocca,  
Piazza della Scienza 3, I-20126 Milano, Italy*

<sup>e</sup> *Theoretical Physics Group, The Blackett Laboratory, Imperial College London,  
Prince Consort Road, London, SW7 2AZ, U.K.*

*E-mail:* [antoine.bourget@polytechnique.org](mailto:antoine.bourget@polytechnique.org),  
[simone.giacomelli@unimib.it](mailto:simone.giacomelli@unimib.it), [julius.grimminger17@imperial.ac.uk](mailto:julius.grimminger17@imperial.ac.uk)

**ABSTRACT:** We study the 3d  $\mathcal{N} = 4$  RG-flows triggered by Fayet-Iliopoulos deformations in unitary quiver theories. These deformations can be implemented by a new quiver algorithm which contains at its heart a problem at the intersection of linear algebra and graph theory. When interpreted as magnetic quivers for SQFTs in various dimensions, our results provide a systematic way to explore RG-flows triggered by mass deformations and generalizations thereof. This is illustrated by case studies of SQCD theories and low rank 4d  $\mathcal{N} = 2$  SCFTs. A delightful by-product of our work is the discovery of an interesting new 3d mirror pair.

**KEYWORDS:** Brane Dynamics in Gauge Theories, Differential and Algebraic Geometry, Extended Supersymmetry, Supersymmetric Gauge Theory

ARXIV EPRINT: [2302.03698](https://arxiv.org/abs/2302.03698)

---

## Contents

<b>1</b>	<b>Introduction</b>	<b>1</b>
1.1	Summary	3
1.2	A new 3d mirror pair	7
<b>2</b>	<b>Warm-up with branes: affine <math>A</math>-&amp;<math>D</math>-type Dynkin quivers</b>	<b>8</b>
2.1	Type A	8
2.1.1	Affine $A$ -Type Dynkin Quiver with higher rank nodes	17
2.1.2	Affine $A$ -Type Dynkin Quiver with higher rank nodes and one flavor	19
2.2	Type D	21
<b>3</b>	<b>FI-flows via FI-subtractions</b>	<b>23</b>
3.1	Rephrasing into linear algebra	23
3.2	Example solutions and complexity	27
3.3	How to find extremal solutions?	29
<b>4</b>	<b>SQCD</b>	<b>31</b>
4.1	Unitary gauge group	32
4.2	Special unitary gauge group	36
<b>5</b>	<b>SCFTs and non-Lagrangian theories</b>	<b>40</b>
5.1	4d SCFTs	40
5.2	Instanton moduli spaces	48
<b>6</b>	<b>Outlook</b>	<b>50</b>
<b>A</b>	<b>The meson propagation theorem</b>	<b>51</b>
<b>B</b>	<b>Weyl orbits</b>	<b>54</b>
<b>C</b>	<b>Hilbert series check of the mirror pair</b>	<b>58</b>
<b>D</b>	<b>Minimal deformations of <math>ADE</math> singularities</b>	<b>59</b>
D.1	Type $A_n$	60
D.2	Type $D_n$	60
D.2.1	$D_n \rightarrow A_{n-1}$	60
D.2.2	$D_n \rightarrow A_{k-1}D_{n-k}$	60
D.3	Type $E_6$	61
D.3.1	$E_6 \rightarrow D_5$	61
D.3.2	$E_6 \rightarrow A_1A_4$	61
D.3.3	$E_6 \rightarrow A_2A_1A_2$	62
D.3.4	$E_6 \rightarrow A_5$	63
D.4	Type $E_7$	64

D.4.1	$E_7 \rightarrow E_6$	64
D.4.2	$E_7 \rightarrow A_1 D_5$	64
D.4.3	$E_7 \rightarrow A_2 A_4$	65
D.4.4	$E_7 \rightarrow A_3 A_1 A_2$	66
D.4.5	$E_7 \rightarrow A_5 A_1$	67
D.4.6	$E_7 \rightarrow D_6$	67
D.4.7	$E_7 \rightarrow A_6$	68
D.5	Type $E_8$	68
D.5.1	$E_8 \rightarrow E_7$	68
D.5.2	$E_8 \rightarrow A_1 E_6$	69
D.5.3	$E_8 \rightarrow A_2 D_5$	69
D.5.4	$E_8 \rightarrow A_3 A_4$	69
D.5.5	$E_8 \rightarrow A_4 A_1 A_2$	70
D.5.6	$E_8 \rightarrow A_6 A_1$	71
D.5.7	$E_8 \rightarrow D_7$	71
D.5.8	$E_8 \rightarrow A_7$	71

## 1 Introduction

In this paper we address the systematic study of Fayet-Iliopoulos (FI) deformations [1] of 3d  $\mathcal{N} = 4$  unitary quiver gauge theories. In the literature, the moduli spaces of vacua of 3d  $\mathcal{N} = 4$  theories, as well as other quantities, are typically studied in two extreme settings: either all FI terms are set to a generic non-zero value, the Coulomb branch is lifted and the Higgs branch is resolved;<sup>1</sup> or all FI terms (and masses) are taken to be zero, Higgs, Coulomb and all mixed branches are present and singular, see figure 1. In the following we will consider all options of FI terms such that there is at least one supersymmetric vacuum.

FI parameters of a 3d  $\mathcal{N} = 4$  theory are a real triplet valued in the Cartan subalgebra of the Coulomb branch symmetry algebra

$$\zeta \in \mathbb{R}^3 \otimes \mathfrak{t}_{\mathcal{C}} . \tag{1.1}$$

Different choices of FI can trigger different RG flows, hence there is a notion of *stratification* in the space of FI deformations [3]. Rather than obtaining such a stratification through some geometric observable on the space of FI deformations, we will use quantum field theory considerations and focus on the notion of *minimal* deformations. We consider a deformation as minimal if the rank of the Coulomb branch global symmetry of the quiver drops by one.<sup>2</sup>

<sup>1</sup>Alternatively sometimes all mass terms are set to generic values. Masses and FI terms are exchanged by 3d mirror symmetry [2].

<sup>2</sup>Typically a FI deformation can trigger an RG flow to multiple SCFTs expressed by various quivers  $Q_i$  with Coulomb branches  $\mathcal{C}_i$ . In this case it is the rank of the combined global symmetry of all  $\mathcal{C}_i$ s which should drop by one.

We conjecture that these deformations precisely parametrize the lowest dimensional loci in the full deformation space, see figure 1. Consecutive minimal deformations will eventually lead to completely deforming the theory. In algebraic geometry we are studying the hyper-Kähler quotient

$$\mathbb{H}^n //_{\zeta} G \tag{1.2}$$

where  $G$  is the gauge group and  $\zeta \in \mathbb{R}^3 \otimes \mathfrak{t}_{\mathbb{Z}(G^\vee)}$  is the level of the moment map. In other words we are studying resolutions / deformations of the Higgs branch [4, 5]. However, it is important to note that the physical deformation parameters present in the quantum field theory need not coincide with the allowed deformation parameters of the Higgs branch as a geometric space. A simple example is a discrete gauge theory with one hypermultiplet charged under the gauge group  $\mathbb{Z}_k$ : the Higgs branch is  $A_{k-1} = \mathbb{C}^2/\mathbb{Z}_k$ , which geometrically has  $k - 1$  deformation parameters, but there are no such parameters in the discrete gauge theory.<sup>3</sup> We will only use the deformations visible in the Lagrangian theory, i.e. the center of the gauge group. For this reason we will not consider orthosymplectic quivers or non-simply laced quivers, and we are not able to probe rank enhancement of topological symmetry in unitary quivers, as happens for moduli spaces of instantons [11] and other examples [12]. Furthermore we limit our study to good theories in the sense of [13], since FI deformations of bad theories not only deform the Higgs branch but also partially lift it [14, 15], see also [16, appendix B] for a brane explanation.

This technique of FI deformations is very useful in the context of magnetic quivers, to study mass deformations of theories with 8 supercharges in spacetime dimension higher than 3. FI deformations on magnetic quivers were used successfully to

- derive magnetic quivers for 4d  $\mathcal{N} = 2$  S-fold theories from magnetic quivers for 6d  $\mathcal{N} = (1, 0)$  SCFTs [17],
- study mass deformations of 5d  $\mathcal{N} = 1$  SCFTs, and generate their RG-flow trees [18],
- derive magnetic quivers for 4d  $\mathcal{N} = 2$  theories on the worldvolume of D3 branes probing 7-branes on orbifolds [19].

In the following we will implicitly pick a 3d  $\mathcal{N} = 2$  subalgebra, and work only with complex F-terms / moment maps and complex FI parameters, as opposed to a real triplet. Because of the underlying hyper-Kähler structure there is no loss of generality. As discussed in [17–19], and as will be reviewed and generalized below, one can study the F-term equations of motion in presence of a complex FI term, and use meson propagation to obtain the theory at the endpoint of the flow triggered by the FI deformation. This can be turned into a graphical quiver subtraction algorithm.<sup>4</sup> The main result of the present paper is

---

<sup>3</sup>It has been understood for a long time that it is not sufficient to characterize theories by geometry alone, but that one needs to specify allowed deformations. Fundamental instances are the frozen singularities in string theory [6], see also [7], and this idea is particularly important in the classification of theories from their moduli space geometry [8–10].

<sup>4</sup>The FI quiver subtraction algorithm computes the type of singularities in the Higgs branch of the theory resolved by an FI term. This is not to be confused with what is commonly referred to as quiver

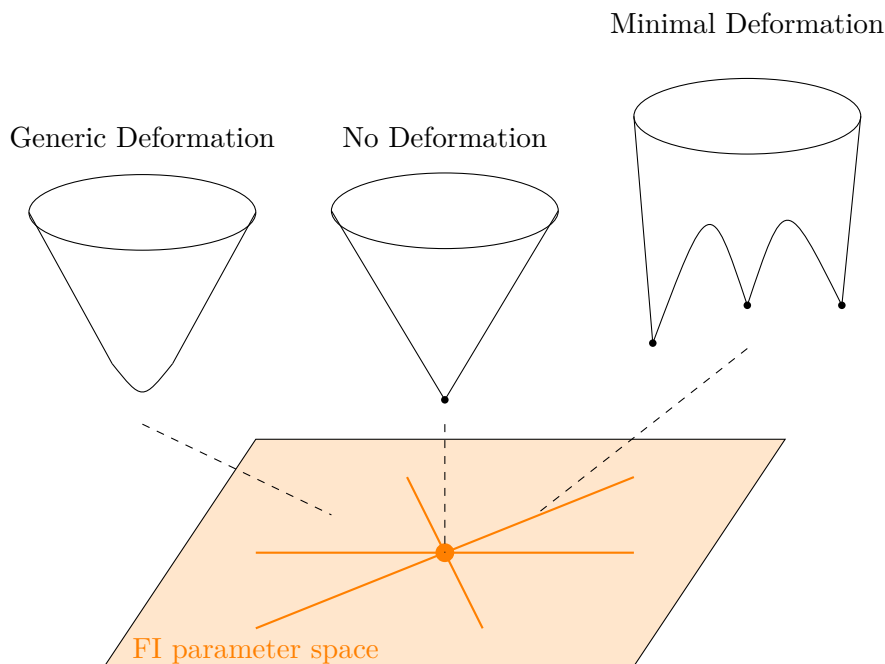


**Figure 1.** Stratification of FI space (orange plane). At the origin, the HB (black) is singular while at a generic point it is resolved. The CB is lifted at a generic point; on the locus of a *minimal* deformation, the CB symmetry drops in rank by one, by definition of minimality.

a precise rule that identifies the quivers that have to be subtracted, given a minimal FI deformation. We give an executive summary in the next subsection 1.1.

### 1.1 Summary

Let  $Q$  be a good unitary quiver. We work in the framework of complexified gauge transformations, in which the Higgs branch  $\mathcal{H}_Q$  is the algebraic variety obtained by imposing F-term constraints and invariance under the complexified gauge group. The FI parameters are deformation parameters for the F-term equations, hence for the Higgs branch  $\mathcal{H}_Q$ . Under this deformation, the conical singularity generically breaks down into several singularities, see figure 2. The goal of this paper is to identify the singularities thereby created as Higgs branches of other quivers  $Q_i \equiv Q_i(Q; \zeta)$ .

Our first result is a reformulation of this question as a well defined problem, that we call the *FI-Meson problem*, which lies at the intersection between linear algebra and graph theory. This problem takes as an input the quiver  $Q$  and the deformation  $\zeta$  and the output is the finite set  $\mathcal{S}$  of *solutions*, which are subquivers  $S$  satisfying two conditions:

- $\alpha)$  Any node in  $Q$  where  $\zeta$  takes a non-zero value is present in  $S$  with the same rank
- $\beta)$  The ranks of the other nodes are constrained by [Theorem 1](#).

---

subtraction [20, 21] which computes symplectic leaves and transverse slices in the Coulomb branch of the theory with mass and FI terms set to zero. The two algorithms are different in a number of ways, as detailed below.

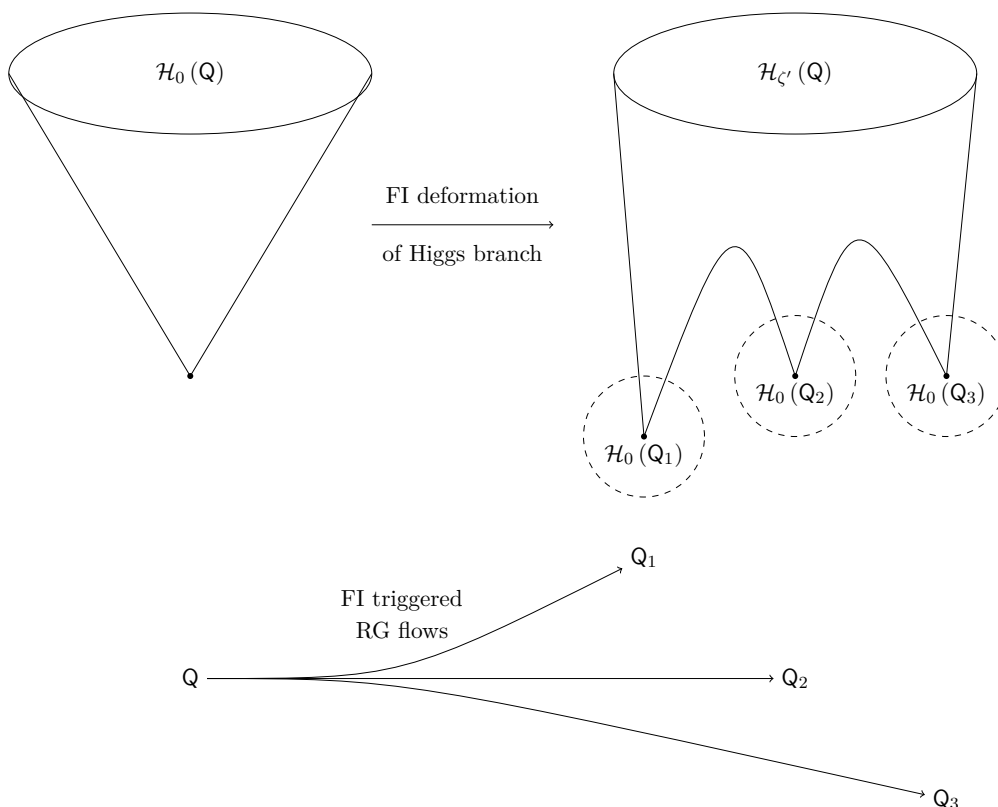


**Figure 2.** Top: schematic depiction of the conical Higgs branch  $\mathcal{H}_0(Q)$  of a good unitary quiver  $Q$  with FI term  $\zeta = 0$  (left), and the deformed Higgs branch  $\mathcal{H}_{\zeta'}(Q)$  after turning on an FI term  $\zeta = \zeta' \neq 0$  (right). The singularity of the undeformed Higgs branch splits into several separated singularities, which in turn can be described locally as Higgs branches of good unitary quivers  $Q_i$  which are determined from  $Q$  and  $\zeta$ .

Bottom: rG flows triggered by  $\zeta = \zeta'$ . The SCFT  $Q$  may flow to a number of SCFTs  $Q_i$  depending on a precise choice of Higgs branch VEV, i.e. choosing one of the singularities in the deformed Higgs branch.

While a split into three singularities is shown, in general any number of separated singularities may be produced by a non-zero FI term. Determining all  $Q_i(Q; \zeta)$  for a choice of  $Q$  and  $\zeta$  is the question we address in this paper.

The set of solutions is partially ordered, see figure 3, and it admits a finite number of local minima that we call the *extremal solutions*  $S_i(\zeta)$

$$(Q, \zeta) \xrightarrow{\text{FI-Meson}} \mathcal{S} \supset \min(\mathcal{S}) = \{S_i(\zeta)\}. \tag{1.3}$$

Our second result provides a one-to-one correspondence between the extremal solutions  $S_i(\zeta)$  to the FI-Meson problem and the quivers  $Q_i(Q; \zeta)$ . When the solutions  $S_i(\zeta)$  are known, the quivers  $Q_i(Q; \zeta)$  are obtained straightforwardly using a quiver subtraction algorithm,

$$Q - S_i(\zeta) = Q_i(Q; \zeta). \tag{1.4}$$

This subtraction algorithm has two steps: first one subtracts the ranks of the nodes of  $S_i(\zeta)$

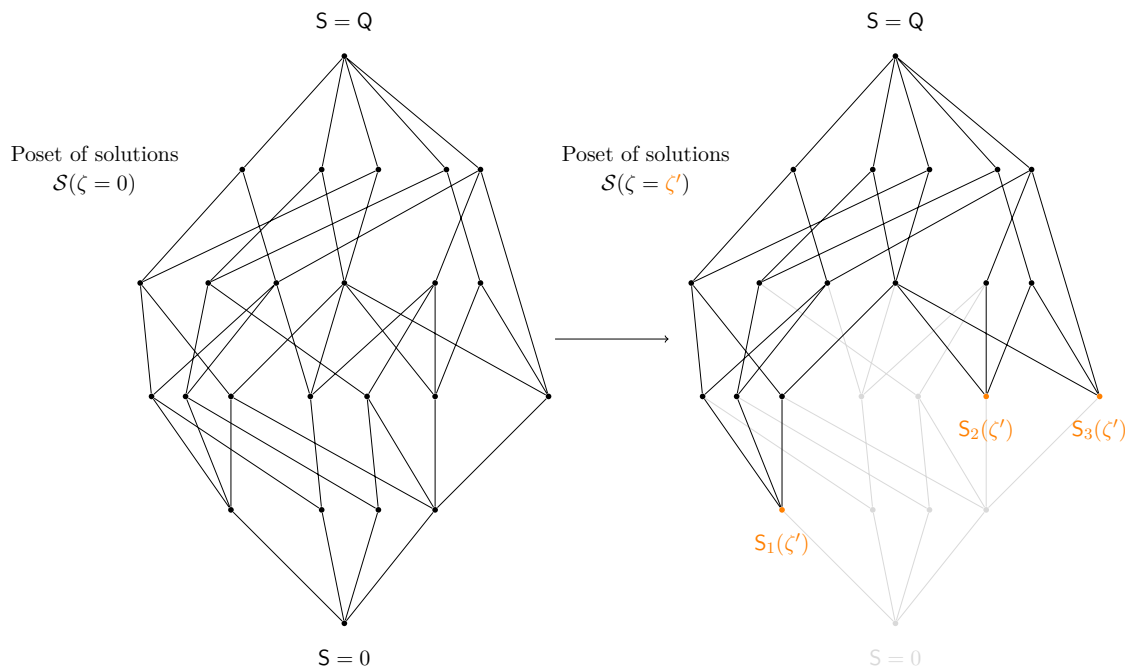


**Figure 3.** The geometric deformations and RG flows of figure 2 are mirrored in the poset of solutions  $\mathcal{S}(\zeta)$  to the FI-Meson problem. When  $\zeta = 0$ , the poset  $\mathcal{S}(\zeta)$  has a unique minimal element  $S = 0$ , meaning that there is no deformation. For generic values  $\zeta = \zeta' \neq 0$ , the poset  $\mathcal{S}(\zeta')$  can have several minima  $S_i(\zeta')$ . These minima are in one-to-one correspondence with the singularities after deformation, using the subtraction (1.4).

from those of  $Q$ , and then one *rebalances* using one or several additional nodes (which can have arbitrarily high rank).

The main practical difficulty is that the FI-Meson problem remains generically hard to solve. However it can be addressed explicitly for small enough quivers; in addition, when a brane system is available, the analysis can be greatly simplified, as illustrated at length in subsequent sections. In this case the FI deformations are interpreted as brane moves, and the singularities in figure 2 are visible as brane intersections. In general, the solution set  $\mathcal{S}$  has several minima. Geometrically, this means that the singularity breaks into several singularities, as illustrated in figure 2 and figure 3. Physically, this implies that turning on FI parameters triggers a flow towards *more than one theory*.

As an application of our methods, we compare the results it produces with what is known from other approaches. One interesting example is SQCD, which although elementary displays a surprisingly rich variety of phenomena. As another example, the graphs of mass deformations of certain families of SCFTs in various dimensions have been worked out from field theory and / or higher dimensional compactification, and they match with our results applied on their magnetic quivers.

**Comparison of two quiver subtraction algorithms.** It should be emphasized that the FI subtraction algorithm shares some superficial similarities with the ‘symplectic leaf



quiver subtraction' developed in [21, 22] to uncover the stratification of the Coulomb branch of the quiver (which is a symplectic singularity) into symplectic leaves. This is the geometric incarnation of a generalized Higgs mechanism along Coulomb branch directions. However, *these two algorithms are very different* and should not be confused. As will be amply shown in the present work,

- The identification of the quiver to be subtracted,  $S$ , is straightforward in the symplectic leaf algorithm (one simply goes through the list of known minimal symplectic singularities). In the FI algorithm, it is an algorithmically hard problem.
- Typically, in the symplectic leaf algorithm one subtracts quivers of affine type, i.e. good quivers. In the FI algorithm, one typically subtracts bad or ugly quivers.
- The rebalancing process in the FI algorithm is rich, it can involve several non-abelian nodes, while it just involves one abelian node in the symplectic leaf algorithm.
- In the symplectic leaf algorithm, the subtracted quiver  $S$  corresponds to the theory obtained in the IR after Higgsing along the Coulomb branch, while in the FI algorithm,  $Q - S$  is the IR theory that remains at one of the most singular points in the resolved Higgs branch.

### FI deforming 3d theories vs mass deforming SCFTs in higher dimensions.

While studying FI deformations of 3d  $\mathcal{N} = 4$  theories is interesting in its own right, we are mainly motivated by the possibility to study mass deformation triggered RG flows between SCFTs with 8 supercharges in various dimensions. As depicted in figure 2 a single FI deformation of a 3d  $\mathcal{N} = 4$  SCFT  $Q$  can trigger different RG flows to distinct 3d  $\mathcal{N} = 4$  SCFTs  $Q_i$ , depending on a choice of vacuum. However for e.g. a 5d  $\mathcal{N} = 1$  SCFTs  $\mathcal{T}$  with magnetic quiver  $Q$  any mass deformation triggers a flow to either a single new strongly coupled SCFT  $\mathcal{T}'$ , or to a weakly coupled theory. Let us consider a mass deformation to a new SCFT. This mass deformation can be mapped to an FI deformation  $\zeta'$  of  $Q$ . If this FI deformation leads to multiple RG flows  $Q_i$ , then the Higgs branch of  $\mathcal{T}'$  is the union of the Coulomb branches of  $Q_i$ , see figure 4.

**Plan of the paper.** In section 1.2 we present a new 3d mirror which is found by studying FI deformations of the magnetic quiver of SU SQCD. In section 2 we study the simplest examples,  $A$ - and  $D$ -type Dynkin quivers, through their brane system and through FI quiver subtraction. These basic examples clarify what happens, when there are several inequivalent solutions to the equations of motion, i.e. several inequivalent FI quiver subtractions. In section 3 we develop a more general understanding of both solving equations of motion and deriving rules for FI quiver subtraction. In section 4 we apply what we learned to FI deform magnetic quivers of SQCD theories with unitary and special unitary gauge groups to obtain the mass deformations of SQCD, yielding interesting results about the moduli space of SQCD and the effective low-energy theories at its singular points. We will in particular see that the low-energy theory in general involves matter fields in the determinant



number of hypermultiplets in the fundamental and determinant representations:

(1.6a)

is the 3d mirror dual of

(1.6b)

where the solid and dotted lines denote the fundamental and determinant representations of  $U(N)$  respectively. The duality between (1.6) and (1.6b) has been recently discussed in [23], generalizing the findings of [18, 25].

## 2 Warm-up with branes: affine $A$ -& $D$ -type Dynkin quivers

In this section we consider FI deformations of  $A$ - and  $D$ -type Dynkin quivers. These FI deformations are mapped to mass deformations in the respective 3d mirror theories, which are good  $U(1)$  and  $SU(2)$  gauge theories with fundamental hypermultiplets [2].

(2.1)

(2.2)

### 2.1 Type A

**Mass deformations of SQED.** The affine  $A$ -type Dynkin quivers are dual to SQED with charge 1 hypers. We begin this section by studying mass deformations of the latter theory, as it may be more common to the reader. We employ the Hanany-Witten brane system [26]. Our conventions are summarized in figure 5.

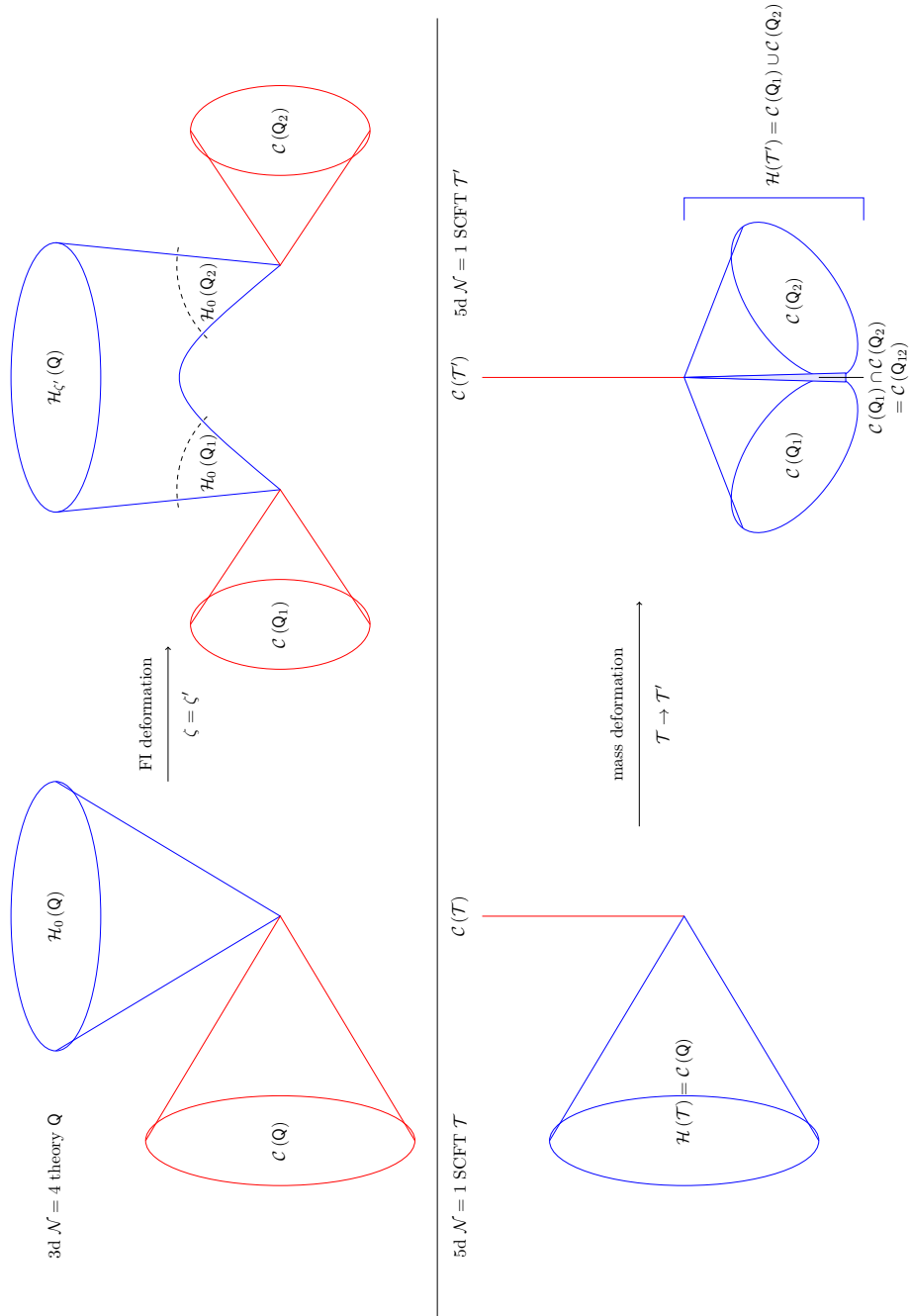


**Figure 4.** Top left: Higgs and Coulomb branch of 3d  $\mathcal{N}=4$  theory  $\mathbf{Q}$  intersecting at the origin of the full moduli space (mixed branches are not drawn). Top right: FI deformed Higgs branch with two most singular points, where Coulomb branches  $\mathcal{C}(\mathbf{Q}_1)$  and  $\mathcal{C}(\mathbf{Q}_2)$  respectively emanate. Bottom left: Higgs and Coulomb branch of 5d  $\mathcal{N}=1$  SCFT  $\mathcal{T}$  with magnetic quiver  $\mathbf{Q}$ . Bottom right: Higgs and Coulomb branch of 5d  $\mathcal{N}=1$  SCFT  $\mathcal{T}'$  resulting from a flow triggered by the FI deformation of  $\mathcal{T}$  which is described by the FI deformation  $\zeta'$  of magnetic quiver  $\mathbf{Q}$ . The Higgs branch of  $\mathcal{T}'$  is the union  $\mathcal{C}(\mathbf{Q}_1) \cup \mathcal{C}(\mathbf{Q}_2)$  with non-trivial (but possibly point-like) intersection  $\mathcal{C}(\mathbf{Q}_1) \cap \mathcal{C}(\mathbf{Q}_2)$ .

(1)

	$x^0$	$x^1$	$x^2$	$x^3$	$x^4$	$x^5$	$x^6$	$x^7$	$x^8$	$x^9$
NS5	x	x	x	x	x	x				
D3	x	x	x				x			
D5	x	x	x					x	x	x

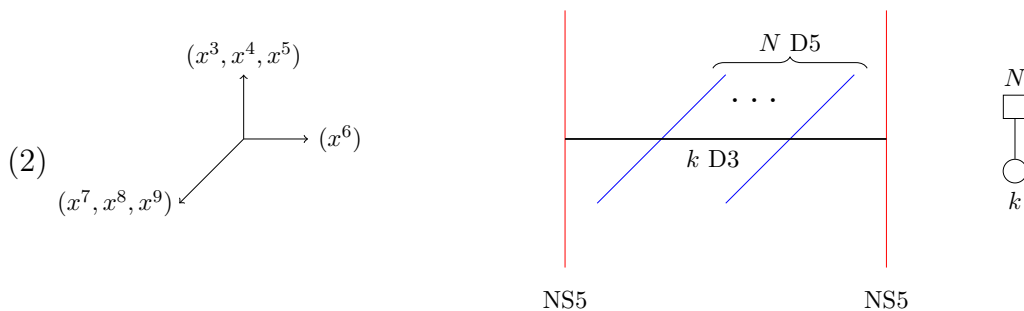


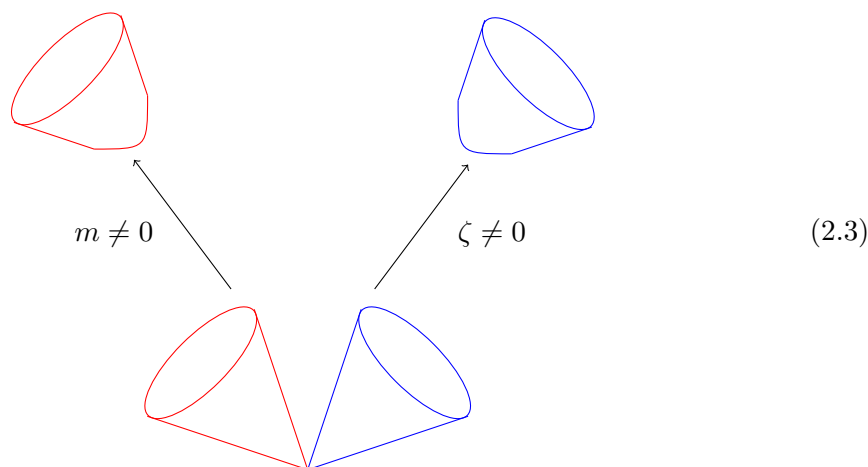
**Figure 5.** (1) The Type IIB set-up: the 'x' mark the spacetime directions spanned by the various branes. The  $x^6$  direction can be seen as an  $S^1$  direction when we engineer unframed affine quivers later in this section. (2) Depiction of the brane system for  $U(k)$  with  $N$  flavors, with all deformation parameters turned off, at the origin of its moduli space.

**Example 1.** Let us begin by studying the example of SQED with two flavors, which is self-mirror, (2.1) with  $N_f = 2$ . This theory has one<sup>6</sup> mass parameter  $m$  and one FI parameter  $\zeta$ . The moduli space for  $m = \zeta = 0$  consists of a Coulomb branch  $A_1$  and a Higgs branch  $a_1$ .<sup>7</sup> If  $m \neq 0$  the Higgs branch is lifted and the Coulomb branch is resolved. If  $\zeta \neq 0$  the Coulomb branch is lifted and the Higgs branch is resolved. If both parameters are turned on then there is no supersymmetric vacuum and we do not consider such a case.

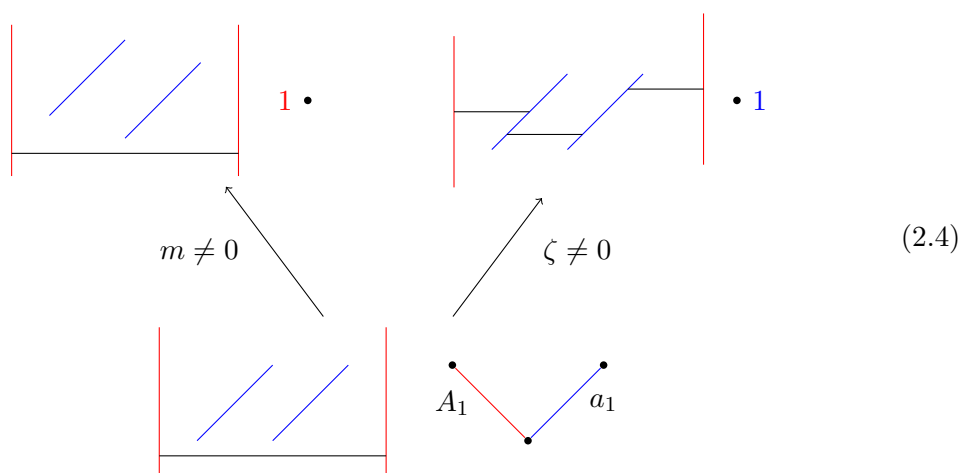
<sup>6</sup>All parameters come as triplets of  $SU(2)_C$  or  $SU(2)_H$ , where the former group acts on the Coulomb branch and the latter group on the Higgs branch. We consider one such triplet as a single parameter.

<sup>7</sup>We use the standard notations that  $a_N$  denotes the closure of the minimal nilpotent orbit of  $\mathfrak{sl}(N+1, \mathbb{C})$ , while  $A_N$  is the Kleinian singularity  $\mathbb{C}^2/\mathbb{Z}_{N+1}$ . Note that  $A_1 = a_1$  and we only make the distinction to fit with later examples.

We can depict the moduli space of the theory depending on  $m$  and  $\zeta$  schematically:



where the **Coulomb branch** is depicted in red and the **Higgs branch** is depicted in blue. We can visualize this much less schematically using brane systems and Hasse diagrams:



where we denote the dimension of the smooth factor of the Coulomb branch or Higgs branch at the bottom of the Hasse diagram without giving its precise geometry. The notation is taken from [27].

**Example 2.** Let us turn to SQED with 5 flavors, i.e the left hand side of (2.1) with  $N_f = 5$ . There are four masses  $m_1, m_2, m_3, m_4$  and one FI deformation  $\zeta$ .<sup>8</sup> A web of various deformations is depicted in figure 6. There, we see the effect of turning on  $m_1 \neq 0$ , followed by  $m_2 \neq 0$ , followed by  $m_3 \neq 0$ , etc. However, there are other mass deformations,

<sup>8</sup>The four masses parametrize the Cartan subalgebra of  $\mathfrak{su}(5)$ , they correspond to the differences of the mass parameters for the individual hypers. A global shift in all the masses is equivalent to a shift of the scalar in the vector multiplet.

for instance

(2.5)

where we set  $m_2 \neq 0$  while still keeping the other masses zero. The Hasse diagram after deformation deserves some explanations. There are now two singular points in the Coulomb branch (corresponding to the D3 brane hitting each one of the two stacks of D5 branes). As we flow to  $m_2 \rightarrow \infty$  we have to make a choice, and decide which stack of branes to keep. In the field theory this means the flow can lead to two different theories, depicted on the level of Hasse diagrams as follows:

(2.6)

or in terms of quivers:

(2.7)

The two theories on the right hand side of (2.7) represent the two distinct endpoints of the RG-flow triggered by the mass deformation.

**General case.** The examples above are immediately generalized as follows. For SQED with  $N_f$  flavors, there are  $2^{N_f-1}$  phases corresponding to whether  $m_i$  is zero or not, for  $i = 1, \dots, N_f - 1$ . The minimal deformations are those where only one mass  $m_i$  is non-zero. This mass triggers a flow where two theories can ultimately be reached:

(2.8)

If  $i = 1$  or  $i = N_f - 1$ , one of the theories is free, and one can safely focus on the interacting one, but even this is an arbitrary choice. Turning on another mass  $m_j$  can be analyzed in exactly the same way on the resulting pair of theories. For this reason, we will mostly focus in the following on *minimal* mass deformations. In the next subsection, we give a geometric interpretation of this minimality.

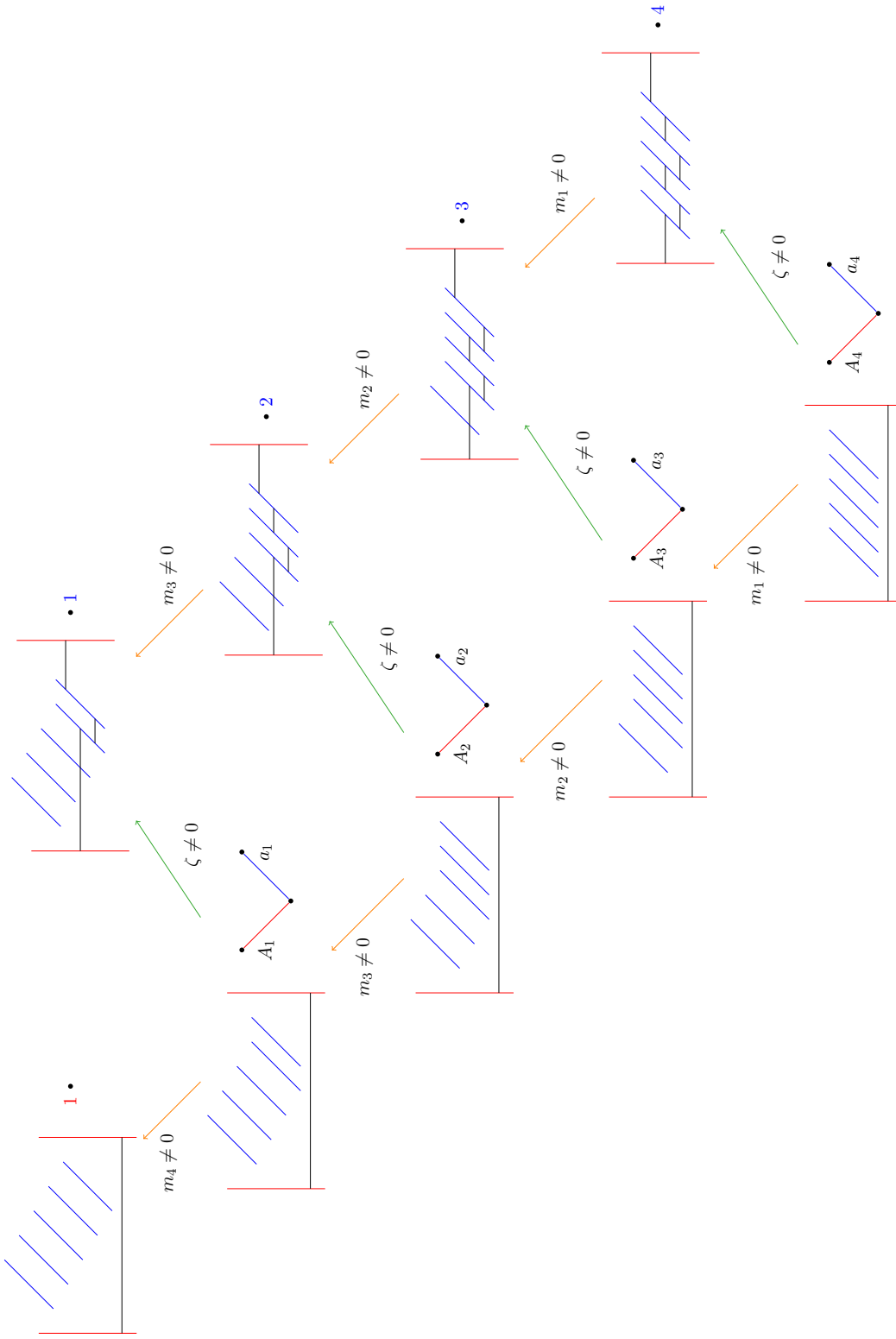


**Figure 6.** Brane diagrams for various phases of SQED with  $N_f = 5$ . There are four mass parameters (turned sequentially on the orange arrows) and one FI term (green arrow). In each case we draw the Hasse diagram of the full moduli space, with the quaternionic dimension explicitly written when it is smooth. Importantly, not all phases appear on this diagram, see for instance (2.5).

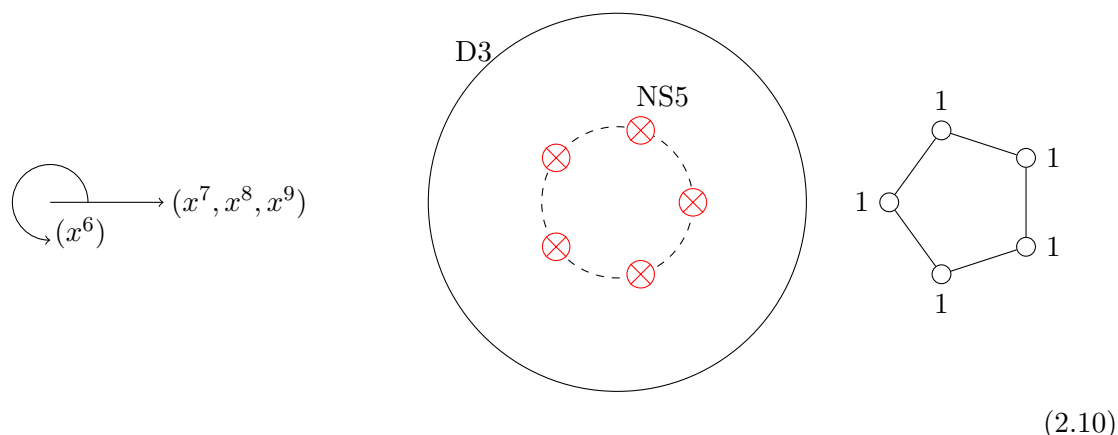


**FI deformation of magnetic quiver.** The mass deformations for SQED correspond to FI deformations for the mirror quiver, on the right of (2.1). When turning on an FI parameter in a unframed unitary quiver — with gauge nodes  $U(n_i)$  and corresponding FI terms  $\zeta_i$  — one needs to respect the condition [17, (3.16)]

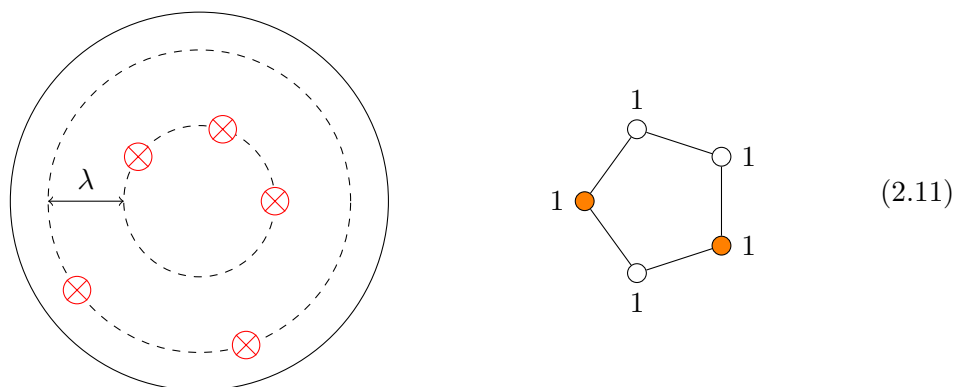
$$\sum_i n_i \zeta_i = 0. \tag{2.9}$$

Using the same labeling of the nodes as before, the minimal mass deformation  $m_i \neq 0$  corresponds to  $\zeta_i = -\zeta_0 \neq 0$ .

We can realize the unframed mirror quiver in a Hanany-Witten brane setup with the  $x^6$  direction as a circular dimension. For concreteness we pick  $N_f = 5$ . We depict the brane system for our theory in the Higgs phase, suppressing the  $(x^3, x^4, x^5)$  directions:

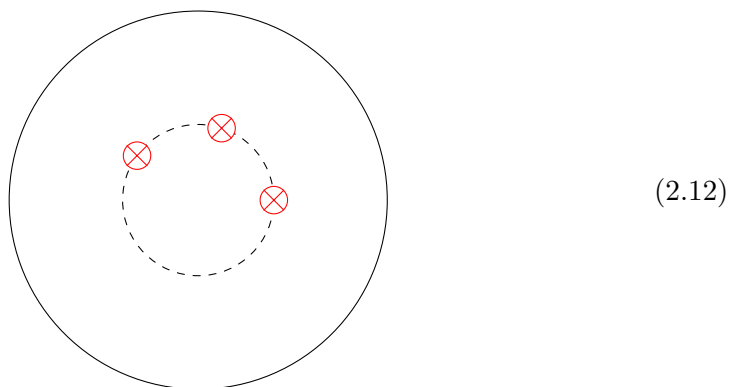


The dashed line denotes the  $(x^7, x^8, x^9)$  position the 5 NS5 branes are at. Consider the deformation (2.5), (2.7). We depict in orange the two nodes where the FI terms  $\lambda$  and  $-\lambda$  are turned on respectively:

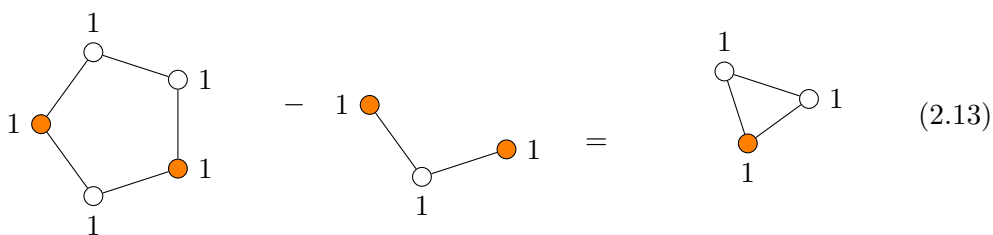


We now have 3 NS5 branes at one  $(x^7, x^8, x^9)$  position, and 2 NS5 branes at another  $(x^7, x^8, x^9)$  position, the two  $(x^7, x^8, x^9)$  positions are depicted by two dashed lines. The split of the one dashed line in (2.10) into two dashed lines in (2.11) reflects that the singular conical Higgs branch of the quiver in (2.10) is partially resolved creating two singularities. Either of the two singularities locally looks like the Higgs branch of a new quiver. Taking the limit  $\lambda \rightarrow \infty$  we are sending NS5 branes off to infinity. There are two possible scenarios:

1. We are left with

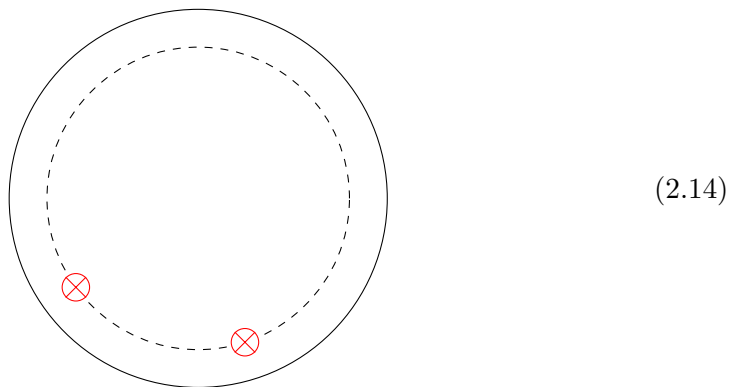


which corresponds to the FI quiver subtraction

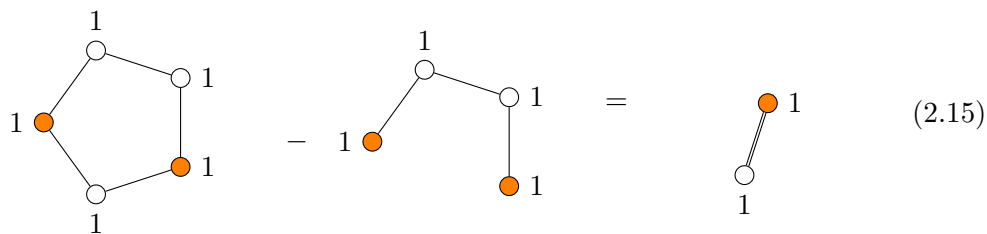


The subtraction algorithm will be explained in full generality in section 3; suffice it to say here that the orange node on the right hand side of (2.13), which is read from the brane system, will be interpreted later on as a rebalancing node.

2. We are left with



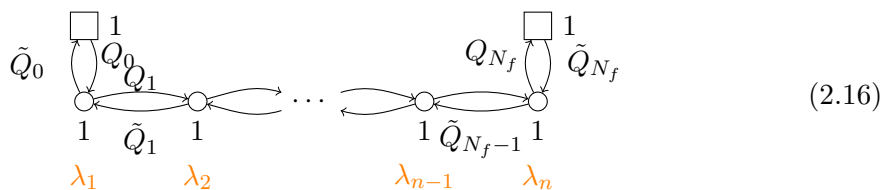
which corresponds to the FI quiver subtraction



The two quivers we obtain are the magnetic quivers of the two resulting quivers in (2.7).

**Higgs branch deformation via bug calculus.** The conclusions of the previous section can be reproduced by looking at FI deformations of the 3d mirror theory, given on the right hand side of (2.1). The nodes are labeled by  $i \in \mathbb{Z}_{N_f} = \{0, 1, \dots, N_f - 1\}$ . Let us denote by  $Q_i$  and  $\tilde{Q}_i$  the chiral multiplets that form hypermultiplets  $(Q_i, \tilde{Q}_i)$  between nodes  $i$  and  $i + 1$ .

It is useful to pick a framed version of the mirror quiver to analyze the FI deformations via ‘bug calculus’ [5]. We can pick without loss of generality the ungauging node to be  $i = 0$ . We then turn on FI terms  $\lambda_i \in \mathbb{R}$  on the node  $i = 1, \dots, N_f - 1$ . We denote this situation with the diagram



The vacuum equations read

$$Q_i \tilde{Q}_i - \tilde{Q}_{i+1} Q_{i+1} = \lambda_{i+1} . \tag{2.17}$$

One can form the usual three invariants  $X = Q_{N_f} Q_{N_f-1} \dots Q_1 Q_0$ ,  $Y = \tilde{Q}_0 \tilde{Q}_1 \dots \tilde{Q}_{N_f-1} \tilde{Q}_{N_f}$  and  $Z = Q_0 \tilde{Q}_0$ . The equation for the deformed  $A_{N_f-1}$  singularity is

$$XY = Z(Z - \lambda_1)(Z - (\lambda_1 + \lambda_2)) \dots (Z - (\lambda_1 + \dots + \lambda_{N_f-1})) . \tag{2.18}$$

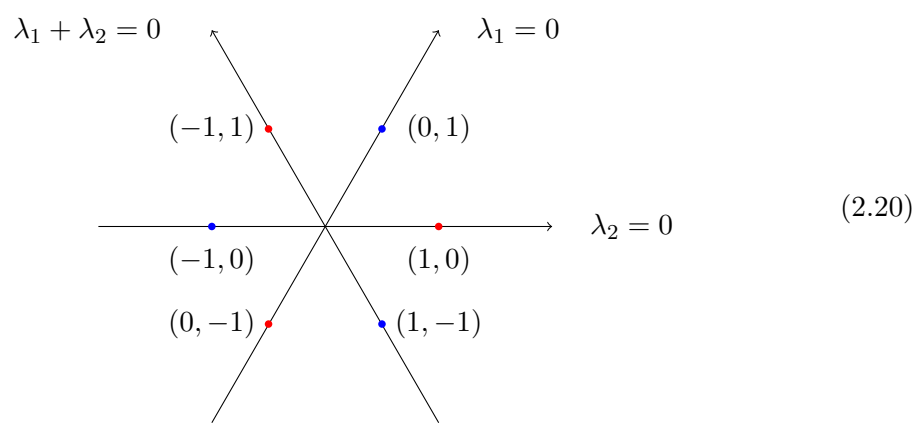
Geometrically, the only thing that really matters is the partition of  $N_f$  defined by the factorization on the right-hand side. This partition is unchanged under the action of the Weyl group on the weight space element  $\lambda = \lambda_1 \varpi_1 + \dots + \lambda_{N_f-1} \varpi_{N_f-1}$  of  $A_{N_f-1}$ . Focusing as previously on minimal deformations translates in this language into looking at Weyl orbits of fundamental weights. The space of FI parameters can be seen, in this example, as the space of  $A_{N_f-1}$  weights. It admits a natural stratification in terms of facets of the Weyl chambers. The dimension 1 walls, which are generated by fundamental weights, correspond to the minimal deformations. For the fundamental weight  $\varpi_i$ , the equation (2.18) becomes

$$XY = Z^i (Z - 1)^{N_f-i} . \tag{2.19}$$

Note that the weights  $\varpi_i$  and  $\varpi_{N_f-i}$  correspond to the same deformation.

**Example.** If we consider  $N_f = 3$ , the equation is  $XY = Z(Z - \lambda_1)(Z - \lambda_1 - \lambda_2)$ . We have a two-dimensional space spanned by  $(\lambda_1, \lambda_2)$ . There are singularities when the polynomial on the right-hand side has double roots, i.e. when either  $\lambda_1 = 0$  or  $\lambda_2 = 0$  or

$\lambda_1 + \lambda_2 = 0$ . Let's represent this graphically:

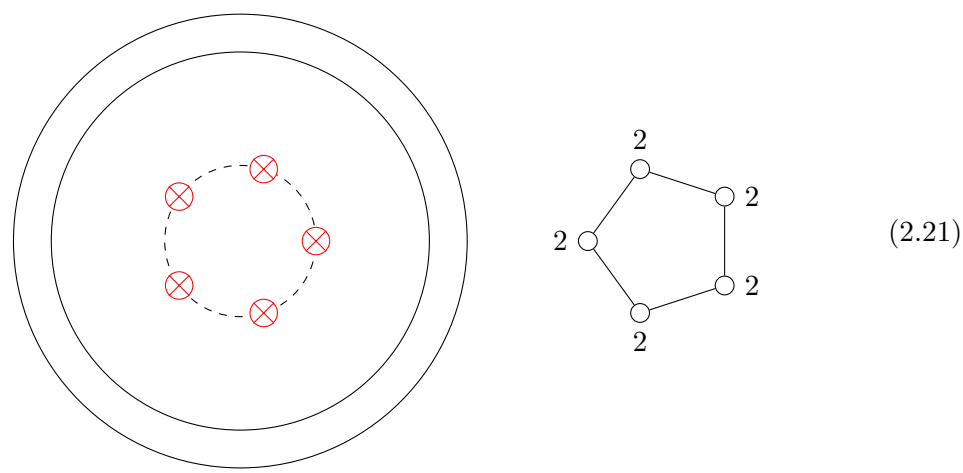


The dimension 1 facets of the Weyl chambers are the lines. On these lines the theory is mass deformed as (2.8) with  $N_f = 3$  and  $i = 1$ . This is a precise illustration of the cartoon shown in figure 1.

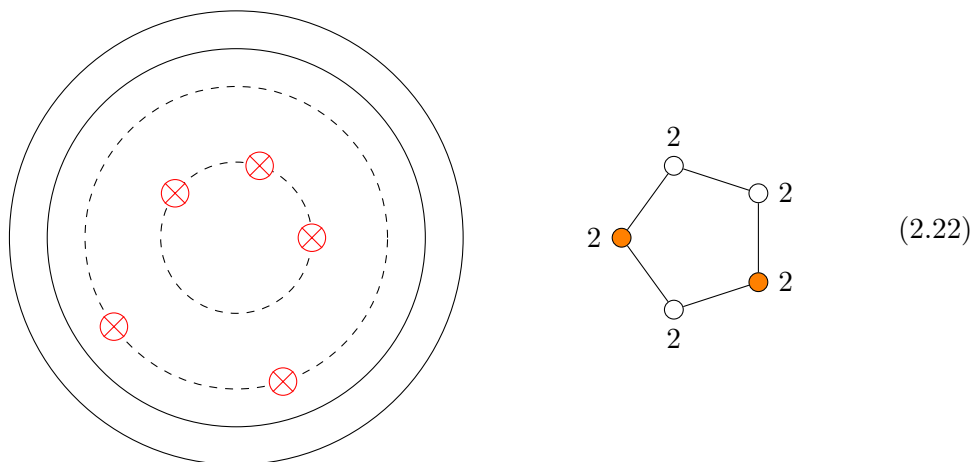
**Summary.** We have seen several aspects of the mass deformations in SQED. Minimal mass deformations (2.8) correspond to minimal FI deformations in the mirror, and the latter can be implemented algebraically at the level of the equations of motions (2.19), or equivalently using quiver subtraction.

**2.1.1 Affine A-Type Dynkin Quiver with higher rank nodes**

Let us consider the brane system (2.10) with two D3 branes instead of one



We can now turn on an FI term for the same nodes as in (2.11). We get



The Higgs branch of the quiver in (2.22)<sup>9</sup> has three most singular points:

1. Both D3 branes probe the ‘inner most’ NS5 branes. In this case we have the FI quiver subtraction

2. Both D3 branes probe the ‘outer most’ NS5 branes. In this case we have the FI quiver subtraction

3. There is another option, where one D3 brane probes the inner NS5 branes while the other D3 brane probes the outer NS5 branes. This corresponds to an FI quiver

<sup>9</sup>The Coulomb branch Hilbert series of the quiver in (2.21) cannot be computed through the monopole formula of [28] as it diverges, this doesn’t affect our discussion however.

subtraction of two quivers<sup>10</sup>

$$\begin{array}{c} \text{Quiver 1} \end{array} - \begin{array}{c} \text{Quiver 2} \end{array} - \begin{array}{c} \text{Quiver 3} \end{array} = \begin{array}{c} \text{Quiver 4} \end{array} \tag{2.25}$$

This last case deserves some further remarks. The result of the FI deformation is a disjoint union of two quivers, the moduli space of this theory is the product of the two individual moduli spaces of each quiver. In the limit of  $\lambda \rightarrow \infty$  the two sets of NS5 branes are infinitely far apart, yet there is a D3 brane probing each of them. The two D3 branes don't talk to each other since they are infinitely far apart, and hence their worldvolume theory is a disjoint union.

### 2.1.2 Affine A-Type Dynkin Quiver with higher rank nodes and one flavor

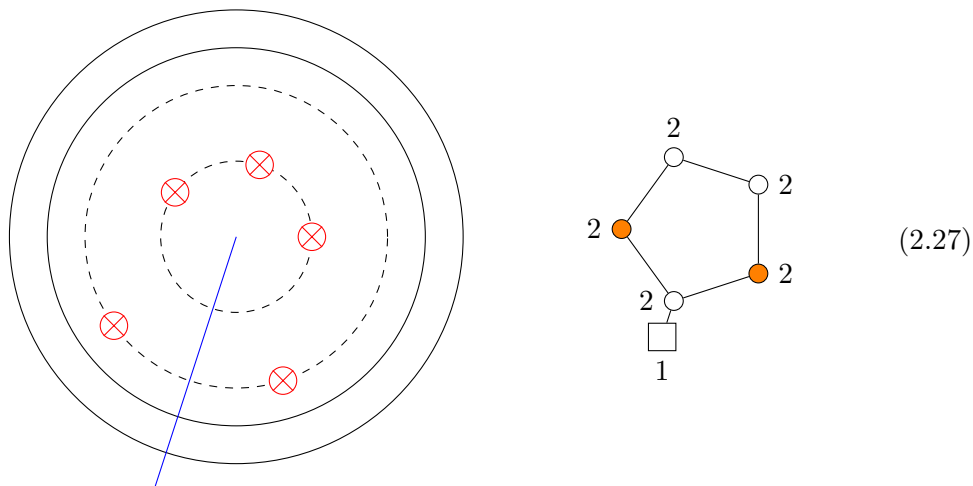
Let us now consider the brane system (2.21) with an added D5 brane providing a flavor to one of the nodes.<sup>11</sup>

$$\begin{array}{c} \text{Brane System} \end{array} \quad \begin{array}{c} \text{Quiver} \end{array} \tag{2.26}$$

<sup>10</sup>See e.g. [18, (2.8) and below] for a previous example of such a double FI quiver subtraction.

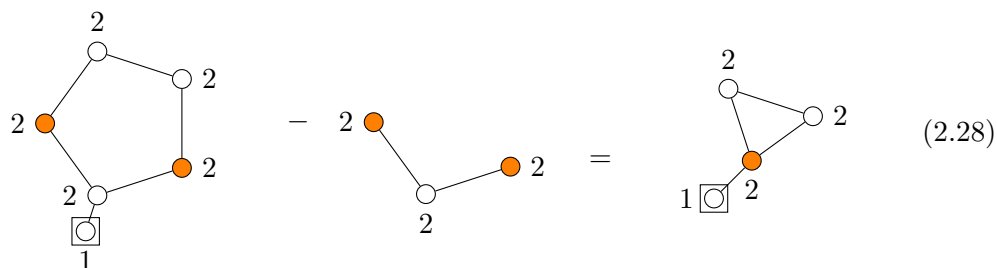
<sup>11</sup>The Coulomb branch of the resulting quiver is a moduli space of instantons and its Hilbert series can be computed straight forwardly using the monopole formula. Other FI deformations of this quiver are discussed in section 5.

Again we turn on FI terms on two nodes just as before

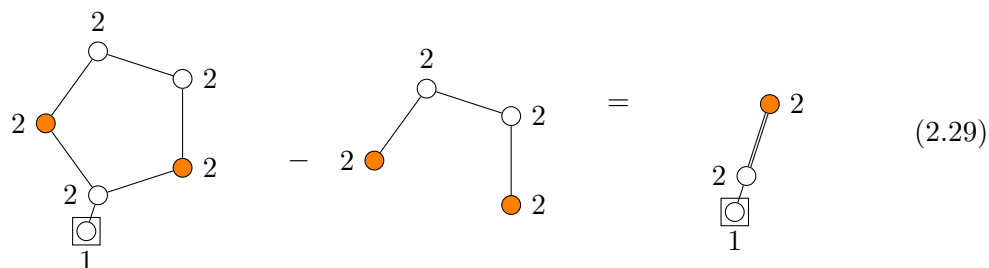


Again there are three most singular points in the resolved Higgs branch:

1. Both D3 branes probe the ‘inner most’ NS5 branes. In this case we have the FI quiver subtraction



2. Both D3 branes probe the ‘outer most’ NS5 branes. In this case we have the FI quiver subtraction



3. One D3 brane probes the inner NS5 branes while the other D3 brane probes the outer

NS5 branes

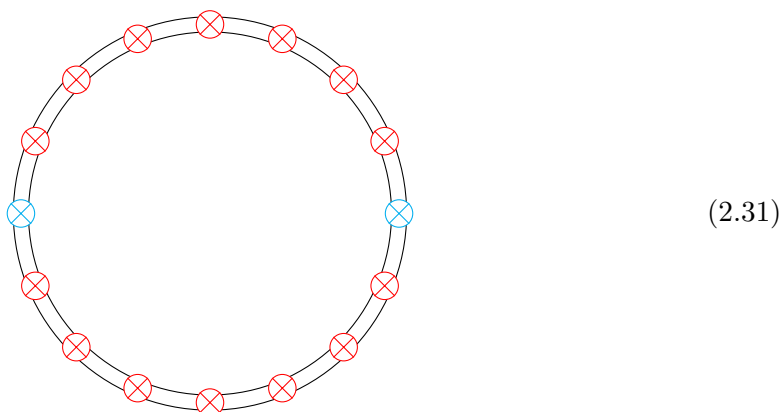
$$\begin{array}{c}
 \begin{array}{c}
 \circlearrowleft 2 \\
 \circlearrowleft 2 \\
 \circlearrowleft 2 \\
 \square 1 \\
 \circlearrowleft 2
 \end{array}
 \quad - \quad
 \begin{array}{c}
 \circlearrowleft 1 \\
 \circlearrowleft 1 \\
 \bullet 1
 \end{array}
 \quad - \quad
 \begin{array}{c}
 \bullet 1 \\
 \circlearrowleft 1 \\
 \bullet 1
 \end{array}
 \quad = \quad
 \begin{array}{c}
 \circlearrowleft 1 \\
 \circlearrowleft 1 \\
 \bullet 1 \\
 \square 1 \\
 \circlearrowleft 1
 \end{array}
 \end{array}
 \tag{2.30}$$

The resulting unframed quiver is connected, it can be disconnected however e.g. by framing the U(1) node which corresponds to the (flavour) D5 brane in the brane system.

### 2.2 Type D

We now turn to the SU(2) gauge theory with fundamental matter (2.2).

**Branes.** The right hand side of (2.2) is realized in a brane system on a circular dimension with two ON<sup>-</sup> planes as follows (drawn here for N<sub>f</sub> = 7) [11, 29, 30]:



The orientifold planes act as  $(x^6, x^7, x^8, x^9) \rightarrow (-x^6, -x^7, -x^8, -x^9)$ , which corresponds in this picture to a reflection through the horizontal line containing the two orientifolds and a reflection with respect to the circle they belong to.

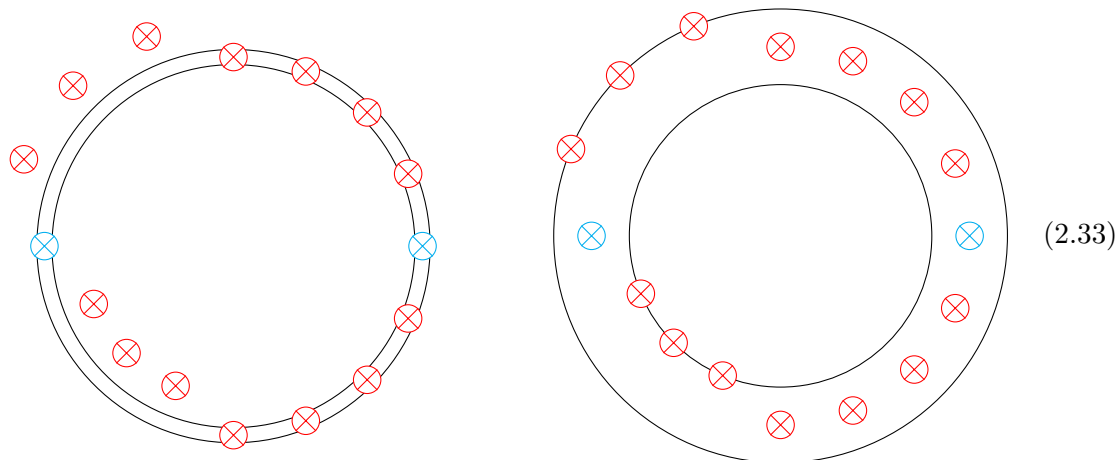
Consider for instance the FI deformations

$$\begin{array}{c}
 -2\lambda \\
 \bullet 1 \\
 \circlearrowleft 1 \\
 \circlearrowleft 2 \\
 \bullet 2 \\
 \circlearrowleft 2 \\
 \circlearrowleft 2 \\
 \circlearrowleft 1 \\
 \bullet 1
 \end{array}
 \tag{2.32}$$

The non abelian nodes in this quiver correspond to the four D3 brane intervals that stretch between the five central NS5 branes in (2.31), while the abelian nodes correspond to the two D3 brane intervals next to the orientifold planes. Therefore the FI deformation is accomplished in the brane system by lifting three NS5 branes adjacent to the orientifold

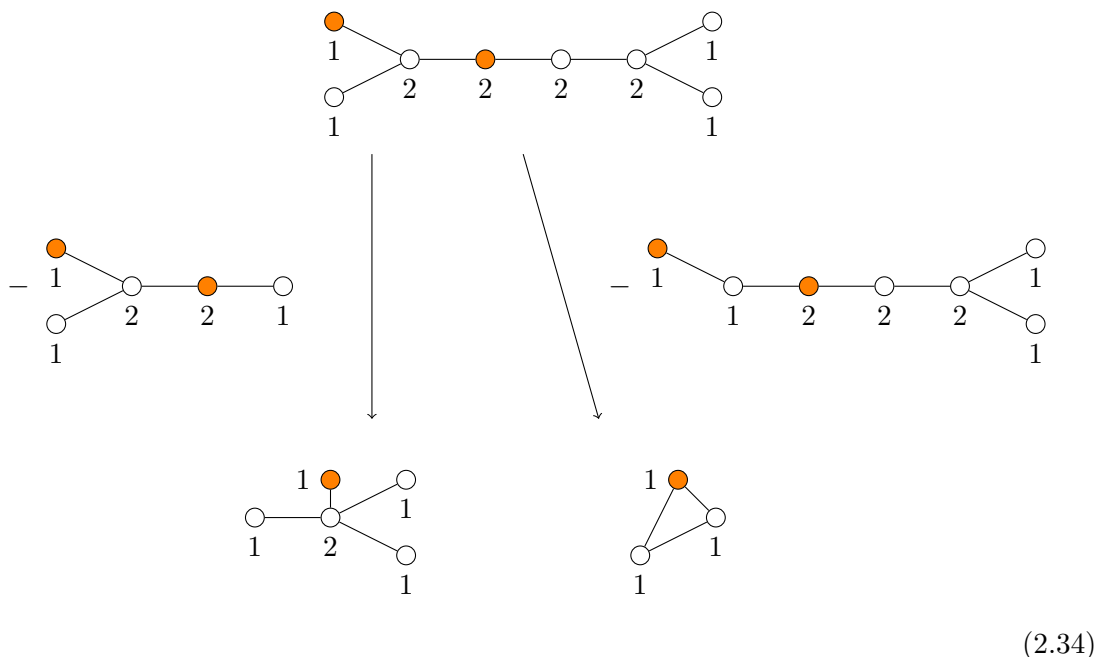


on the left. The D3 branes, whose motion is restricted by the orientifold action, give rise to two distinct phases:



In one phase (left), the world-volume of the D3 branes contains the same branes as in (2.31) but with  $N_f = 4$ . In the other phase (right), the D3 branes have left the orientifold fixed locus, and the local physics on their world-volumes is that of (2.10) with  $N_f = 3$ . This constitutes the brane proof that the singularity  $D_7$  splits under the FI deformation to two singularities  $D_4$  and  $A_2$ .

The previous result can be recovered directly via quiver subtraction as follows:



The quivers that need to be subtracted can be read directly from the brane systems (2.33). Note that on the left we subtract a *finite* Dynkin diagram of type  $D_5$ , while on the right we subtract another quiver that has the shape of the  $D_7$  Dynkin diagram but different ranks. Both quivers are *ugly*, in the terminology of [13], and their 3d  $\mathcal{N} = 4$  Coulomb branches are freely generated.

As is hopefully clear from these examples, the FI deformations can be implemented easily from a quiver subtraction algorithm, without referring to a brane system. However, the brane system was essential in identifying which quiver to subtract. In general situation, with an arbitrary quiver, brane systems are in general not available. Therefore, we need an *independent way of identifying which quivers to subtract*. Note in particular that we should be able to reproduce the subtraction of disconnected quivers as in (2.25). The whole problem of FI deformations reduces to this question, which we now address in full generality in the next section.

### 3 FI-flows via FI-subtractions

When the Higgs branch of a given theory can be described by a magnetic quiver, assumed to be unitary and simply laced, its mass deformations correspond to FI deformations for the magnetic quiver. It is therefore of interest to *identify and characterize the minimal FI deformations of a unitary quiver*.

In this section, we formalize this question and show that it is in general a difficult algebraic problem. We show that it can always be treated as a quiver subtraction procedure, generalizing what we saw in the previous section, but identifying which quivers to subtract is the central difficulty. In particular, it should be stressed that it is not enough to subtract finite Dynkin quivers or restrict to subtracting quivers with a freely generated Coulomb branch.

#### 3.1 Rephrasing into linear algebra

Consider a quiver with unitary gauge nodes and only bifundamental matter.<sup>12</sup> We assume that every gauge node  $U(k)$  has at least  $2k$  fundamentals. Formally, the quiver is defined by a set of vertices  $V$ , a list<sup>13</sup>  $E$  of edges  $e \in V^2$  and a list of ranks  $k_v \in \mathbb{Z}_{>0}$  for each  $v \in V$ . We turn on FI terms  $\zeta = (\zeta_v)_{v \in V} \in \mathbb{C}^V$  at the vertices, which have to satisfy

$$\sum_{v \in V} \zeta_v k_v = 0. \tag{3.1}$$

In terms of fields, we associate to each edge  $e = (e_1, e_2)$ , with  $e_1, e_2 \in V$ , two chiral multiplets  $Q_e$  and  $\tilde{Q}_e$  transforming respectively in the representations  $\mathbf{e}_1 \times \overline{\mathbf{e}_2}$  and  $\mathbf{e}_2 \times \overline{\mathbf{e}_1}$ . We see  $Q_e$  as a  $e_1 \times e_2$  matrix and  $\tilde{Q}_e$  as a  $e_2 \times e_1$  matrix. To each edge  $e = (e_1, e_2)$  one can associate two mesons:  $M_e = Q_e \tilde{Q}_e$ , transforming in the adjoint representation of  $U(k_{e_1})$ , and  $\tilde{M}_e = \tilde{Q}_e Q_e$  transforming in the adjoint representation of  $U(k_{e_2})$ . The F-term equations read

$$\sum_{e|e_1=v} M_e - \sum_{e|e_2=v} \tilde{M}_e = \zeta_v \mathbf{1}_{k_v}. \tag{3.2}$$

The Higgs branch of the magnetic quiver is parametrized by the gauge invariant combinations of the  $Q_e$  and  $\tilde{Q}_e$  subject to (3.2).

<sup>12</sup>Throughout this paper, we use quivers without framing, it being understood that a diagonal  $U(1)$  has to be ungauged. In some of the examples we used framed versions for convenience.

<sup>13</sup>The list can have repetitions. Note that the edges are oriented.

The problem can now be stated as follows. Given a quiver, and a list of FI parameters  $(\zeta_v)_{v \in V}$ , what is the set of mesons  $(M_e, \tilde{M}_e)$  satisfying (3.2), up to gauge transformations? There are two aspects to this question, which we attack in two steps. First, we need to characterize the possible pairs  $(M_e, \tilde{M}_e)$  of matrices associated to a given edge, and second, we need to find an arrangement of these matrices in such a way that the sum (3.2) at each vertex is satisfied. Both steps involve simple linear algebra, but in combination they yield a difficult problem. We look at these in turn.

- **Edges:** Let us look closer at the relation between  $M_e$  and  $\tilde{M}_e$  for a given edge  $e \in E$ . This boils down to the following linear algebra problem: what is the relation between two matrices of the form  $Q\tilde{Q}$  and  $\tilde{Q}Q$ ? The answer to this question is provided by the Theorem 1 stated and proved in appendix A. The bottom line is that the Jordan blocks of  $M_e$  and  $\tilde{M}_e$  with non zero eigenvalues are the same, while the Jordan blocks with 0 eigenvalue have sizes that can differ by at most one. Two matrices that satisfy this condition can always be written as  $Q\tilde{Q}$  and  $\tilde{Q}Q$  for some rectangular matrices  $Q$  and  $\tilde{Q}$  of appropriate shape.
- **Vertices:** The vertices  $v$  are distinguished by the number of edges reaching them, and the value of  $\zeta_v$ . If only two edges reach  $v$ , then (3.2) is straightforward to solve. Assume for simplicity that the orientations are such that the equation reads  $M_e - \tilde{M}_{e'} = \zeta_v \mathbf{1}_{k_v}$ . Then  $M_e = \tilde{M}_{e'} + \zeta_v \mathbf{1}_{k_v}$ , and this simply shifts the eigenvalue of all the Jordan blocks of  $\tilde{M}_{e'}$  by  $\zeta_v$ . At bifurcations however the problem is more intricate, even if  $\zeta_v = 0$ . Consider for instance the equation  $M_e = \tilde{M}_{e'} + \tilde{M}_{e''}$ . The constraints from the edges characterize the types of Jordan blocks for these three matrices, it is difficult to characterize the blocks of a sum from those of its summands.

Given a set of meson pairs  $(M_e, \tilde{M}_e)$  satisfying (3.2), one constructs a subquiver  $S$  of  $Q$  as follows. The sets of vertices and nodes are the same as those of  $Q$ , and the ranks are

$$k'_v = \max \left( \max_{e|v \in e} r_e, k_v(1 - \delta_{\zeta_v}) \right) \tag{3.3}$$

where  $\delta_{\zeta_v}$  is a delta function whose value is zero whenever the FI parameter at  $v$  vanishes and is one otherwise and

$$r_e = \max(\text{rank}(M_e), \text{rank}(\tilde{M}_e)). \tag{3.4}$$

The quivers  $S$  that can be obtained this way are called *solutions* of the FI-Meson problem.

The set  $\mathcal{S}$  of all solutions is partially ordered in the obvious way: for two solutions  $S^1$  and  $S^2$  (with nodes of ranks  $k_v^1$  and  $k_v^2$ ) we say that  $S^1 \preceq S^2$  if for all  $v \in V$ ,  $k_v^1 \leq k_v^2$ . With this partial order the solution set  $\mathcal{S}$ , which is finite, has a number of minimal elements that we call the *extremal solutions*:

$$\mathcal{S}^{\text{extr}} = \min \mathcal{S} = \{S_i | i = 1, \dots, n\}. \tag{3.5}$$

**Notations.** In the following, it is convenient to show solutions of (3.2) in a graphical way, without having to explicitly name the edges and vertices. We do this using the following notation. For each edge, we show the two matrices corresponding to  $M_e$  and  $\tilde{M}_e$  at the ends of the edge  $e$ , next to the vertex for which these matrices transform in the adjoint representation:

$$\begin{array}{ccc} \circ & \text{---} & \circ \\ k_1 & & k_2 \\ & M & \tilde{M} \end{array} \tag{3.6}$$

This notation means that  $M$  is an  $k_1 \times k_1$  matrix,  $\tilde{M}$  is an  $k_2 \times k_2$  matrix, and they are related as given by Theorem 1. For instance,

$$\begin{array}{ccc} \circ & \text{---} & \circ \\ 2 & & 3 \\ \begin{pmatrix} 1 & 0 \\ 0 & 1 \end{pmatrix} & & \begin{pmatrix} 2 & -1 & -1 \\ 1 & 0 & -1 \\ 1 & -1 & 0 \end{pmatrix} \end{array} \tag{3.7}$$

is admissible, as the Jordan block decomposition of the  $3 \times 3$  matrix is  $J_2(1) \oplus J_1(0)$ . Here we use the following standard notation for  $k \times k$  Jordan blocks:

$$J_k(\lambda) = \begin{pmatrix} \lambda & 1 & & & \\ & \lambda & 1 & & \\ & & \lambda & \ddots & \\ & & & \ddots & 1 \\ & & & & \lambda \end{pmatrix}. \tag{3.8}$$

Vertices  $v$  where  $\zeta_v = 0$  are painted in white, and the sum of adjacent matrices has to sum to 0 (with appropriate signs). Vertices  $v$  with  $\zeta_v \neq 0$  are painted in orange, the value of  $\zeta_v$  is indicated in orange next to the vertex, and the adjacent matrices have to sum to  $\zeta_v$  times the identity matrix (again with appropriate signs). When only two nodes are painted, there is no need to indicate the value of  $\zeta_v$  as it is fixed up to an overall constant. Thus, for a given quiver the solution in terms of mesons can be drawn by putting all the (non-zero) meson matrices as in (3.6). From there the solution quivers  $S$  can be read directly by looking at the ranks of the meson matrices on edges adjacent to each vertex. For instance, the D-type Klein singularities studied in section 2.2 are shown in figure 7. One can check that the solutions presented there are extremal.

**Subtraction algorithm.** Let us first assume that the solution is irreducible, i.e. there is no basis in which all the matrices  $M_e$  and  $\tilde{M}_e$  can be written into block diagonal form in a non trivial way, with each block being a solution of the equations. In this case, there is only a  $U(1)$  group, acting on the  $Q_e$  and  $\tilde{Q}_e$ , that leaves the set of all these matrices invariant. This  $U(1)$  is what replaces the group

$$\prod_{v \in V} U(k'_v). \tag{3.9}$$

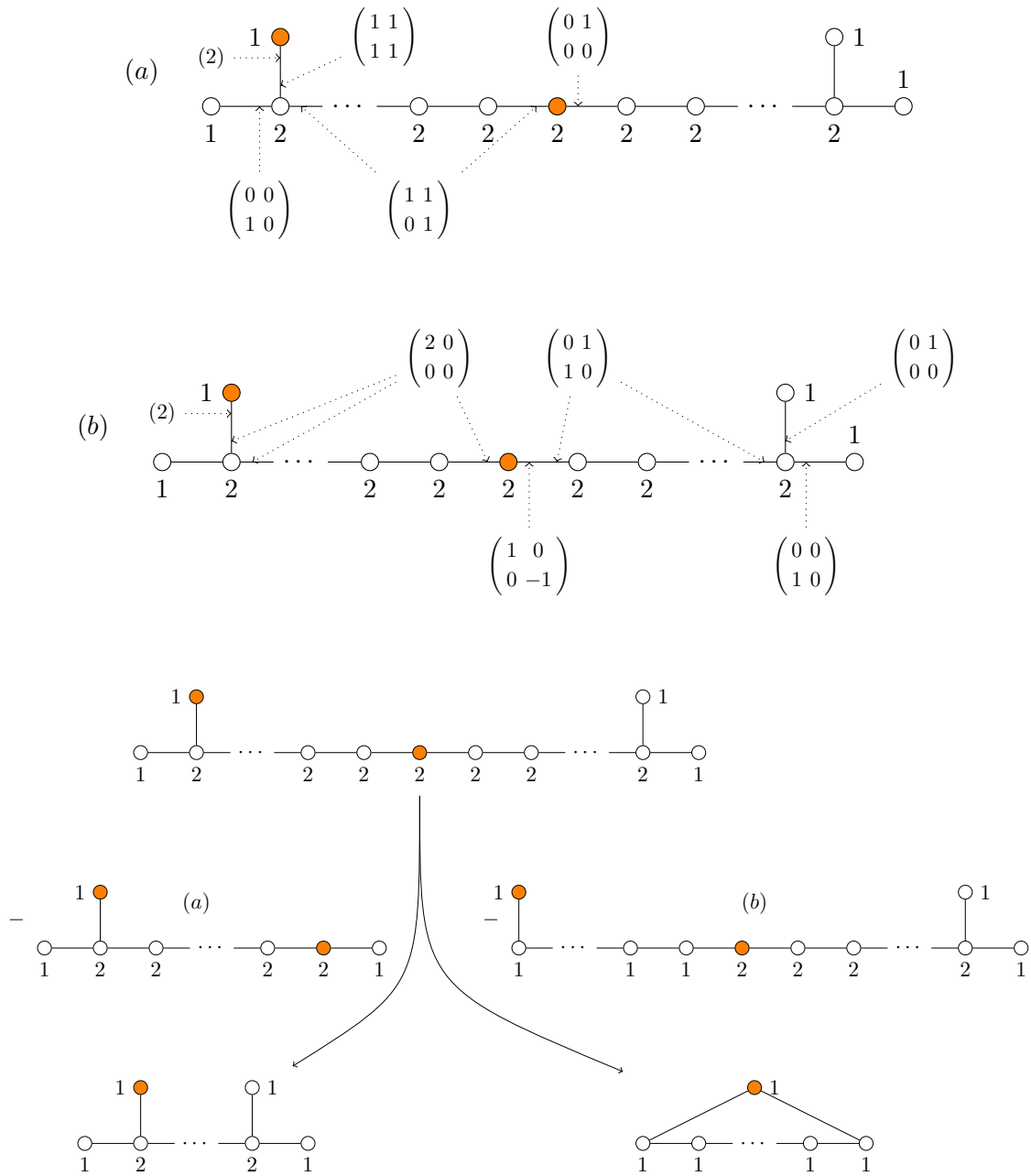


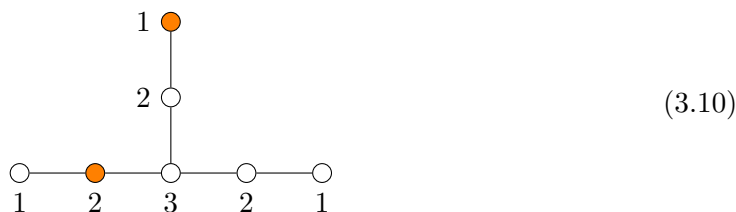
**Figure 7.** Two solutions for D type and corresponding subtractions. The subtractions realize the splitting  $D_n \rightarrow A_{k-1}D_{n-k}$ . The orange node in the middle is the  $k$ th starting from the left. This reproduces the subtraction (2.34) obtained from the brane system.

This is illustrated in figure 7. More generally, if the solution can be decomposed into the direct sum of  $K$  copies of a given solution, the group is broken to  $U(K)$ . A new quiver is obtained, with nodes  $U(k_v - k'_v)$  and an additional node  $U(K)$  and edges used to rebalance. If the solution can be decomposed into  $K_1$  times a solution, plus  $K_2$  times another one, etc, then one adds nodes  $U(K_1)$ ,  $U(K_2)$ , etc. This is what is at play in the “double subtraction” in (2.25). Several other examples of this are given in section 4.1.

### 3.2 Example solutions and complexity

In general, it is difficult to find explicit matrix solutions to (3.2). The reason is that while the Jordan structure of the matrices at each junction is known, the basis in which the canonical Jordan form is reached depends on each leg. To make the problem manifest, we look at two examples among the possible deformations of  $E$ -type Klein singularities. It should be noted that these are still very simple spaces, but the complexity of the linear algebra problem already requires computer assistance.

**Example 1.** For an illustration of the complexity of the problem, one can have a look at the quiver



We consider the affine  $E_6$  quiver, and turn on FI terms as indicated by the orange numbers. For simplicity, label the three legs by 1, 2, 3, oriented from the central node, leg 1 being the one where an FI term is turned on for a  $U(1)$  node, leg 2 having an FI term for a  $U(2)$ , and leg 3 having no FI term. In any given solution, leg  $i$  gives a  $3 \times 3$  matrix  $M_i$ , and these have to satisfy  $M_1 + M_2 + M_3 = 0$ . Let’s try to solve this equation. Consider first the Jordan types of the  $M_i$ , which are constrained by Theorem 1 in appendix A:

- We begin with  $M_1$ : since the Jordan type of the  $1 \times 1$  matrix at the end of the leg is  $J_1(2)$ , the type of  $M_1$  is either  $J_1(2) \oplus J_2(0)$  or  $J_1(2) \oplus J_1(0) \oplus J_1(0)$ .
- For  $M_2$ , the type of the  $2 \times 2$  matrix before the FI node is either  $J_2(0)$  or  $J_1(0) \oplus J_1(0)$ . Therefore the type of  $M_2$  is either  $J_2(1) \oplus J_1(0)$  or  $J_1(1) \oplus J_1(1) \oplus J_1(0)$ .
- Finally,  $M_3$  is nilpotent, its Jordan type is either  $J_3(0)$ ,  $J_2(0) \oplus J_1(0)$  or  $J_1(0) \oplus J_1(0) \oplus J_1(0)$ .

We now are left with solving the equation  $M_1 + M_2 + M_3 = 0$  with these Jordan form constraints. Using brute force computation, we find exactly two extremal solutions up to conjugation. This is summarized in table 1. Once these solutions are known, it is easy to complete all the meson matrices, as depicted in figure 8. This means that two quiver subtractions are possible: they are shown in figure 8. Geometrically, this means that the  $E_6$  singularity is deformed to a space with two singularities, of types  $A_1$  and  $A_4$ .

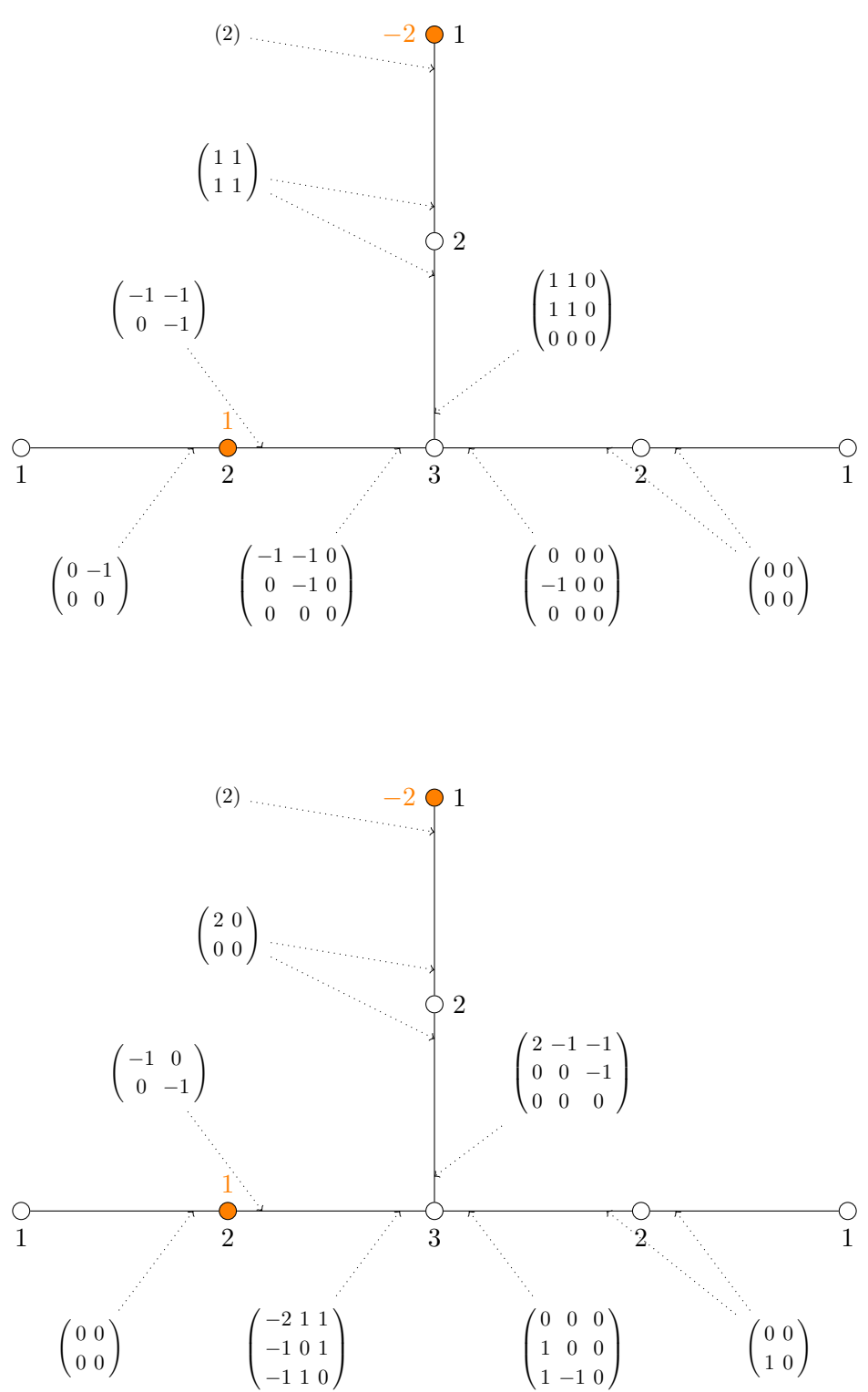
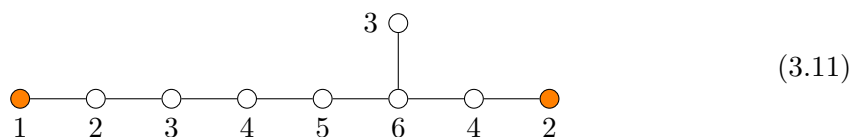


**Figure 8.** The two minimal deformations corresponding to the given FI in orange. The top quiver displays Solution 1 in table 1, and the bottom quiver displays Solution 2.

Matrices	$M_1$	$M_2$	$M_3$
Possibilities	$J_1(2) \oplus J_2(0)$ $J_1(2) \oplus J_1(0) \oplus J_1(0)$	$J_2(-1) \oplus J_1(0)$ $J_1(-1) \oplus J_1(-1) \oplus J_1(0)$	$J_3(0)$ $J_2(0) \oplus J_1(0)$ $J_1(0) \oplus J_1(0) \oplus J_1(0)$
Solution 1	$J_1(2) \oplus J_1(0) \oplus J_1(0)$ $\begin{pmatrix} 1 & 1 & 0 \\ 1 & 1 & 0 \\ 0 & 0 & 0 \end{pmatrix}$	$J_2(-1) \oplus J_1(0)$ $\begin{pmatrix} -1 & -1 & 0 \\ 0 & -1 & 0 \\ 0 & 0 & 0 \end{pmatrix}$	$J_2(0) \oplus J_1(0)$ $\begin{pmatrix} 0 & 0 & 0 \\ -1 & 0 & 0 \\ 0 & 0 & 0 \end{pmatrix}$
Solution 2	$J_1(2) \oplus J_2(0)$ $\begin{pmatrix} 2 & -1 & -1 \\ 0 & 0 & -1 \\ 0 & 0 & 0 \end{pmatrix}$	$J_1(-1) \oplus J_1(-1) \oplus J_1(0)$ $\begin{pmatrix} -2 & 1 & 1 \\ -1 & 0 & 1 \\ -1 & 1 & 0 \end{pmatrix}$	$J_3(0)$ $\begin{pmatrix} 0 & 0 & 0 \\ 1 & 0 & 0 \\ 1 & -1 & 0 \end{pmatrix}$

**Table 1.** Solutions for the FI deformations (3.10). The columns are labelled by the  $3 \times 3$  meson matrices, one for each leg in the quiver. The possibilities are the possible Jordan types compatible with the FI constraints. Then we show the two extremal solutions in terms of Jordan forms, and with a choice of representative.

**Example 2.** We now turn to the quiver



One can perform exactly the same analysis as for the previous example. Given the lengths of the legs and using the theorem, the possibilities are given respectively by the 7 partitions of 5, the 3 partitions of 4 with no entry  $> 2$ , and the 4 partitions of 6 with no entry  $> 2$ . This is summarized in table 2. We find a unique extremal solution up to conjugation, and it leads to the subtraction shown in the appendix, see (D.22).

### 3.3 How to find extremal solutions?

The previous subsection shows that finding extremal solutions for a given quiver  $Q$  and FI parameters  $\zeta$  can be difficult in general. Here we list a few methods that have helped us identifying extremal solutions for specific examples.

- The first method is brute force computation, exploring all possible cases. We first use Theorem 1 in appendix A to restrict the possible Jordan forms of various meson matrices, and solve the graph constraints using generic basis transformations on the intersecting nodes. This boils down to studying an algebraic variety embedded in affine space of dimension  $\sim \sum_v k_v^2$ . This quickly becomes intractable as the ranks increase.
- A handy set of extremal solutions is provided by the Klein singularities  $\mathbb{C}^2/\Gamma_{ADE}$ . Indeed, there is a well known resolution of the singularities involving a set of  $r$



Matrices	$M_1$	$M_2$	$M_3$
Possibilities	$J_1(2) \oplus 5J_1(0)$		
	$J_1(2) \oplus J_2(0) \oplus 3J_1(0)$		$6J_1(0)$
	$J_1(2) \oplus 2J_2(0) \oplus J_1(0)$	$J_1(-1) \oplus J_1(-1) \oplus 4J_1(0)$	$J_2(0) \oplus 4J_1(0)$
	$J_1(2) \oplus J_3(0) \oplus 2J_1(0)$	$J_1(-1) \oplus J_1(-1) \oplus J_2(0) \oplus 2J_1(0)$	$2J_2(0) \oplus 2J_1(0)$
	$J_1(2) \oplus J_3(0) \oplus J_2(0)$	$J_1(-1) \oplus J_1(-1) \oplus 2J_2(0)$	$3J_2(0)$
	$J_1(2) \oplus J_4(0) \oplus J_1(0)$		
	$J_1(2) \oplus J_5(0)$		
Solution	$J_1(2) \oplus J_3(0) \oplus 2J_1(0)$	$J_1(-1) \oplus J_1(-1) \oplus J_2(0) \oplus 2J_1(0)$	$2J_2(0) \oplus 2J_1(0)$
	$\begin{pmatrix} 1 & -1 & 0 & -1 \\ -1 & 3 & 1 & 1 \\ 1 & -3 & -1 & -1 \\ 1 & -2 & -1 & -1 \end{pmatrix}$	$\begin{pmatrix} -1 & 0 & 0 & 0 \\ 0 & -1 & 0 & 0 \\ 0 & 0 & 0 & -1 \\ 0 & 0 & 0 & 0 \end{pmatrix}$	$\begin{pmatrix} 0 & 1 & 0 & 1 \\ 1 & -2 & -1 & -1 \\ -1 & 3 & 1 & 2 \\ -1 & 2 & 1 & 1 \end{pmatrix}$

**Table 2.** Solutions for the FI deformations (3.11). Note that a trivial block  $2J_1(0)$  appears in the solution everywhere, and we show only the non trivial  $4 \times 4$  block in the explicit solution.

compact  $\mathbb{P}^1$  divisors intersecting transversely [31], where  $r$  is the rank of the ADE algebra. A minimal FI deformation corresponds to a partial resolution where one of these compact divisors is blown up, while the  $r - 1$  other compact divisors can be kept at zero size. This guarantees that there is exactly one minimal FI deformation for each simple root  $\alpha_i$  of the algebra, i.e. each node in the finite ADE Dynkin diagram. In our language, an FI term is turned on at that node, and at the affine node, in order to guarantee the vanishing (3.1). Then we have exactly one extremal solution to the FI-Meson problem for each connected component of the finite Dynkin diagram with node  $\alpha_i$  removed. It turns out they correspond to *free quivers*. All these cases are shown explicitly in appendix D.

- Building up on the previous point, we have observed that given a quiver  $Q$  with prescribed FI deformation  $\zeta$ , one can usually easily find solutions  $S_i^{\text{free}}$  which are *free quivers* (meaning that their 3d Coulomb branch is spanned by free hypermultiplets). In the case of the Klein singularities, these are extremal. *This is not the case in general*, as many examples in sections 4 and 5 demonstrate. However, it appears heuristically useful to use the free solutions  $S_i^{\text{free}}$  as starting points in the poset of solutions  $\mathcal{S}(\zeta)$ , and to find extremal solutions  $S_i^{\text{extremal}} \preceq S_i^{\text{free}}$ , see figure 9.
- Given an extremal solution  $S$  for a quiver  $Q$ , if we replace in  $Q$  a node  $U(k)$  by a chain of nodes  $U(k)$ , thus forming a new quiver  $\tilde{Q}$ , then an extremal solution  $\tilde{S}$  is obtained by performing a similar replacement of a node by a chain in  $S$ .

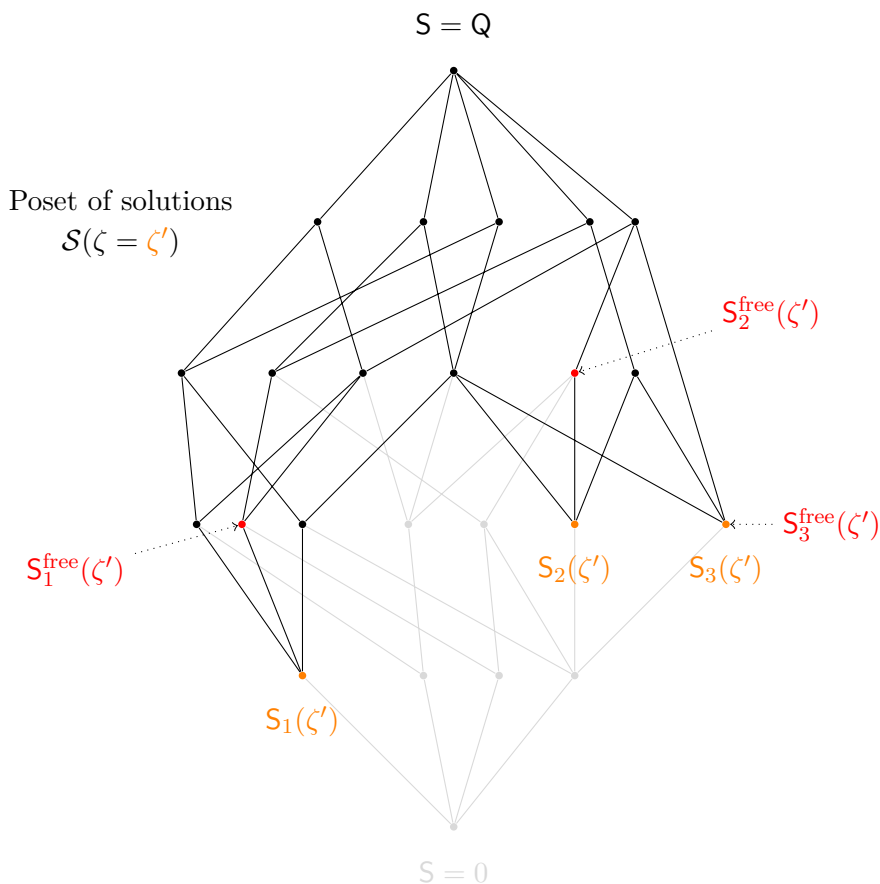


**Figure 9.** Given an FI deformation  $\zeta'$  one can look for free quiver solutions, shown here in red. They can happen to be extremal (as is the case here for  $S_3^{\text{free}}(\zeta') = S_3(\zeta')$ ). If they are not, they can be used as seeds to restrict the space of potential extremal solutions to explore to the solutions that lie below the free solutions.

### 4 SQCD

In this section, we consider  $U(k)$  and  $SU(k)$  SQCD with  $N_f \geq 4$  flavors. The relevant mirror pairs are well-known [13, 26]:

$$\begin{array}{c} N_f \\ \square \\ | \\ \bigcirc \\ U(k) \end{array} \leftrightarrow \begin{array}{c} 1 \\ \bigcirc \\ / \quad \backslash \\ \bigcirc \quad \bigcirc \\ | \quad | \\ \dots \quad \dots \\ \bigcirc \quad \bigcirc \quad \bigcirc \quad \bigcirc \quad \bigcirc \quad \bigcirc \\ | \quad | \quad | \quad | \quad | \quad | \\ 1 \quad \dots \quad k \quad k \quad \dots \quad k \quad k \quad \dots \quad 1 \\ \underbrace{\hspace{10em}}_{N_f - 1} \end{array} \tag{4.1}$$

Equation (4.2) shows a duality between two quiver diagrams. On the left, a square node labeled  $N_f$  is connected to a circle node labeled  $SU(k)$ . An arrow points to the right, where a chain of nodes is shown. The chain starts with a circle node labeled 1, followed by an ellipsis, then a circle node labeled  $k$  with a circle node labeled 1 above it. This is followed by another circle node labeled  $k$ , an ellipsis, another circle node labeled  $k$  with a circle node labeled 1 above it, and finally a circle node labeled 1. A bracket underneath the chain of nodes from the first  $k$  to the last  $k$  is labeled  $N_f - 1$ .

This is a good testing ground for our methods as the mass deformations of the SQCD theories are easily understood, and we furthermore have a straightforward brane system to engineer the theories. On the other side, the FI-flows on the magnetic quivers shown above display a vast array of phenomena. Rather than attempting a cumbersome fully general discussion in terms of  $N_f$  and  $k$ , we focus on specific examples and put emphasis on interesting phenomena: subtraction of bad and ugly quivers, rebalancing with multiple nodes, and Weyl group symmetry.

### 4.1 Unitary gauge group

Let us focus on  $U(2)$  SQCD with  $N_f = 10$  flavors and study its mass deformations. The brane system describing the magnetic theory is

Equation (4.3) shows a brane system represented by a series of vertical red lines. There are 10 vertical lines in total. Two diagonal blue lines are drawn between the first and second lines, and between the sixth and seventh lines. A horizontal black line runs across the bottom of the vertical lines.

Now we turn on a mass deformation in the electric theory, which in the brane system is implemented by moving a subset of NS5 branes. Let us consider for example moving the first, 5th, 6th and 10th branes in the above figure. Clearly this requires rearranging the D3 branes in order to preserve supersymmetry. We have three possibilities and for each one of them we provide the corresponding brane system in figure 10.

The mass deformation is equivalent to the following FI deformation in the magnetic quiver  $Q$ :

Equation (4.4) shows a quiver diagram. At the top is a white circle node labeled 1. Below it is a horizontal chain of nodes. From left to right: a red circle node labeled  $\lambda$  with 1 below it; a white circle node labeled 2 with 2 below it; a white circle node labeled 2 with 2 below it; a red circle node labeled  $-\lambda$  with 2 below it; a white circle node labeled 2 with 2 below it; a red circle node labeled  $\lambda$  with 2 below it; a white circle node labeled 2 with 2 below it; a white circle node labeled 2 with 2 below it; and a red circle node labeled  $-\lambda$  with 1 below it.

In this context the three frames arise because there are three extremal solutions to the FI-Meson problem. The first frame is realized by propagating the vev from the leftmost node in (4.4) to the rightmost going through the abelian node on top. The second frame is obtained by propagating the vev along the  $A_9$  quiver, without involving the abelian node on top. The third frame instead arises by leaving the central  $U(2)$  node unbroken. These extremal solutions  $S_F$ , for each frame  $F = I, II, III$ , are drawn in figure 10, along with the resulting quivers  $Q_F = Q - S_F$ .

Interestingly, it can be checked that the same results can be obtained by simplifying the FI deformation taking into account the action of the Weyl group of the global symmetry, as explained in appendix B. Here the global symmetry is  $A_{N_f-1} = A_9$ , which is

generated in the magnetic quiver by the 9 balanced nodes in the chain. The FI deformation is labeled by a weight of  $A_9$ , that we write in the basis of fundamental weights  $\varpi = [1, 0, 0, -1, 0, 0, 1, 0, 0, -1]$ . We observe that  $\varpi$  is in the Weyl orbit of the fundamental weight  $\varpi_4 := [0, 0, 0, 1, 0, 0, 0, 0, 0, 0]$ , and therefore we can equivalently consider the deformation

(4.5)

The quivers that need to be subtracted are depicted in the rightmost column of figure 11. For Frames I and III, the solutions to the F-term equations are clear (they are similar to those shown in figure 7 for the D-type singularities). Frame II is more interesting, and an extremal solution to the FI-Meson problem is easily worked out to be

(4.6)

This solution instructs us to subtract a “bad” quiver:

(4.7)

Note however that the matrices in (4.6) provide a rationale why this is, and show that an alternative interpretation is as shown in figure 11 (Frame II, weight  $[0, 0, 0, 1, 0, 0, 0, 0, 0, 0]$ ).

In the more general case of  $U(N_c)$  SQCD we find for every minimal FI deformation  $N_c + 1$  frames, depending on how we distribute the  $D3$  branes between the two stacks of five branes. Let us illustrate this at the level of the brane system for  $U(3)$  SQCD, where we take the number of flavors to be 12 for definiteness. The relevant brane diagram in Type IIB is

(4.8)

If we now displace the  $D5$  branes 1, 2, 6, 7, 11, 12 along the direction wrapped by the  $NS5$  branes we find the following four frames:

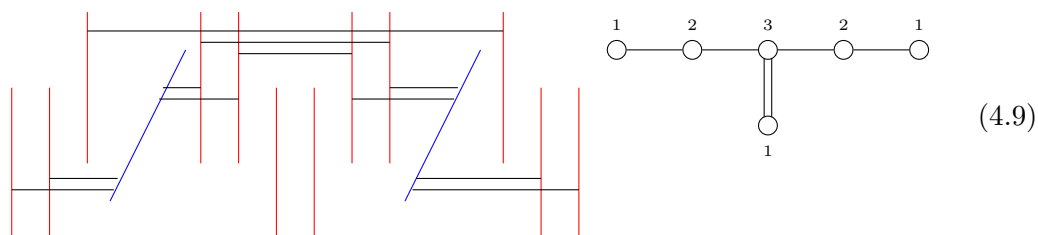
Frame $F$	Brane system	Solution $S_F$	Quiver $Q_F = Q - S_F$
I			
II			
III			

**Figure 10.** This table summarizes the FI flows for the deformation (4.4). First we use brane systems and identify three phases, that we call frames  $F \in \{I, II, III\}$ . Correspondingly, there are three extremal solutions  $S_F$ , and three resulting quivers  $Q_F$ .

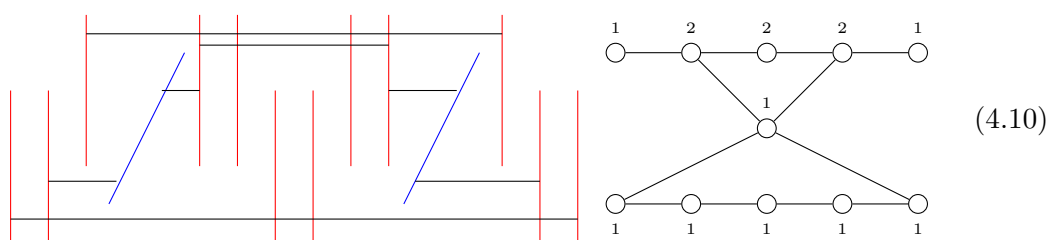
Frame	Weight $[1, 0, 0, -1, 0, 1, 0, 0, -1]$	Weight $[0, 0, 0, 1, 0, 0, 0, 0, 0]$
I		
II		
III		

**Figure 11.** Quivers to be subtracted in each frame, for two different weights in the same Weyl orbit. For the weight  $[1, 0, 0, -1, 0, 1, 0, 0, -1]$ , there are three quivers to subtract (counting multiplicities), so the rebalancing nodes form a rank 3 group, while for the other weight, it forms a rank 1 group. Therefore the sum of ranks of quivers in the  $[1, 0, 0, -1, 0, 1, 0, 0, -1]$  column is two more than the corresponding quiver in the  $[0, 0, 0, 1, 0, 0, 0, 0, 0]$  column.

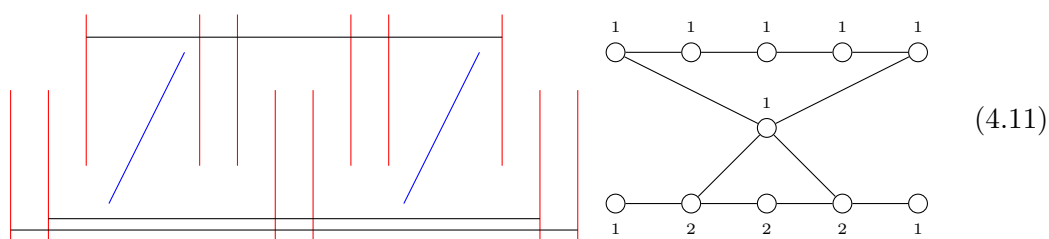
• **Frame I**



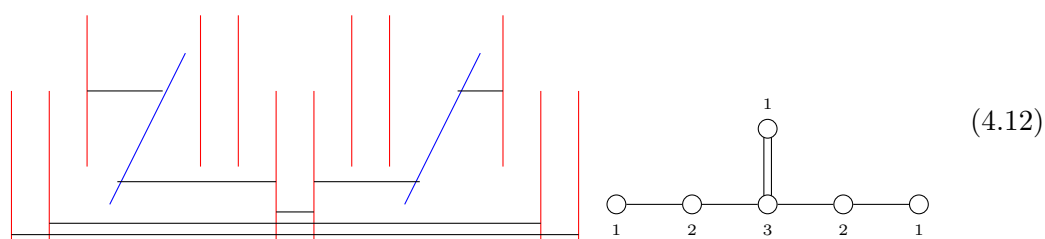
• **Frame II**



• **Frame III**



• **Frame IV**



One easily checks that these results can be recovered via quiver subtraction, as we have done for U(2) SQCD in table 11.

### 4.2 Special unitary gauge group

**A new mirror pair.** Let us now discuss the special unitary case (4.2). One particularly interesting subset of mass deformations is described by the following FI deformation of the

mirror dual:

$$(4.13)$$

In this case, the FI-Meson problem is trivial, the unique extremal solution  $\mathbf{S}$  is the direct sum of  $k$  quivers  $A_{N_f-2k}$ . The subtraction algorithm instructs us to subtract these quivers (or equivalently subtract a linear quiver of length  $N_f + 1 - 2k$  with  $U(k)$  nodes) and rebalance with a  $U(k)$  node. The result is the quiver on the right, which is just a special case of (1.5a) with  $B = 2M = 2k$  and can be interpreted as the mirror dual of the following theory (see (1.5b)):

$$(4.14)$$

with gauge group  $SU(N) \times U(1) \times SU(k)$ ,  $N_f - 2k$  hypermultiplets in the fundamental representation of  $SU(N)$  of charge  $k$  under  $U(1)$  and  $2k$  hypermultiplets in the antifundamental representation of  $SU(k)$  of charge  $N$  under  $U(1)$ , and gauged 1-form  $\mathbb{Z}_{kN}$  symmetry indicated by the quotient. Graphically, the number of hypermultiplets is indicated above the double lines, while the  $U(1)$  charges are inserted within the line. As supporting evidence for our claim, we observe that the moduli space dimensions and Hilbert series of the candidate dual theories match. We actually find that the matching of Hilbert series extends to the more general family (1.5a) and (1.5b). We defer a detailed discussion of the Hilbert series to appendix C.

In the special case  $k = 1$  the theory (4.14) is equivalent to a  $U(N)$  gauge theory with  $N_f - 2$  fundamentals and two hypermultiplets in the determinant representation. If we instead set  $N = 1$  (4.14) reduces to a  $U(k)$  gauge theory with  $2k$  fundamentals and  $N_f - 2k$  hypermultiplets in the determinant representation, whose mirror dual according to (4.13) is

$$(4.15)$$

Based on the above results, it is natural to propose that the mirror dual of  $U(N)$  SQCD with  $N_f \geq 2N$  flavors and  $n$  hypermultiplets in the determinant representation is given by



the quiver

This reproduces the result found in [23] (and of course the case  $N_f = 2N + 1, n = 1$  discussed in [18, 25]) and is clearly consistent with the special cases we have considered above.

**An exhaustive case study.** In this subsection we carry out the exhaustive study of deformations for the case (4.2) with  $k = 3$  and  $N_f = 7$ . More precisely, we consider all the FI-deformations which involve exactly two nodes in the magnetic quiver.<sup>14</sup> In general, for the SQCD theory  $SU(k)$  with an odd number  $N_f > 2k$  of flavors, and using charge conjugation symmetries to eliminate redundant cases, there are precisely  $(\frac{N_f+1}{2})^2$  cases to consider. Here, with  $N_f = 7$  this gives 16 deformations; in each case the number of extremal solutions appears to be between one and three. The results are gathered in tables 3, 4, and 5, where we have picked a numbering of the 16 minimal deformations, from #1 to #16.

Many extremal solutions correspond to cases that have already appeared in earlier examples: those involving two nodes of the same rank were discussed in section 4.2, and those involving a  $U(1)$  node and a  $U(2)$  node were given in figure 7. We are left with deformations involving one  $U(3)$  node and either a  $U(1)$  or a  $U(2)$  node, which are more interesting and which we discuss now in detail. For case #3, there are three solutions, but two of them are related by a graph isomorphism, so it is enough to give the two non-isomorphic solutions, which are given explicitly as follows:

<sup>14</sup>For these deformations we don't write explicitly the value of the FI terms on the quivers, as it is fixed uniquely up to an irrelevant overall magnitude by the ratio of the ranks of the two gauge nodes. It is enough to paint two nodes in orange to fully specify the FI deformation.

and

$$\begin{array}{cccc}
 & & \begin{matrix} \textcircled{1} \\ \downarrow \\ (3) \end{matrix} & & \begin{matrix} \textcircled{1} \\ \downarrow \\ \begin{pmatrix} 1 & 1 & 1 \\ 1 & 1 & 1 \\ 1 & 1 & 1 \end{pmatrix} \end{matrix} & & \begin{matrix} \begin{pmatrix} 0 & 0 & 0 \\ 0 & 0 & 0 \\ 0 & 1 & 0 \end{pmatrix} \\ \downarrow \\ \textcircled{1} \end{matrix} \\
 & & & & & & \\
 \begin{matrix} \textcircled{1} \\ \downarrow \\ \begin{pmatrix} 0 & 0 & 0 \\ 1 & 0 & 0 \\ 1 & 0 & 0 \end{pmatrix} \end{matrix} & & \begin{matrix} \textcircled{3} \\ \downarrow \\ \begin{pmatrix} 0 & 1 & 1 \\ 0 & 0 & 1 \\ 0 & 1 & 0 \end{pmatrix} \end{matrix} & & \begin{matrix} \textcircled{3} \\ \downarrow \\ \begin{pmatrix} 0 & 0 & 0 \\ 0 & 0 & 1 \\ 0 & 1 & 0 \end{pmatrix} \end{matrix} & & \begin{matrix} \textcircled{1} \\ \downarrow \\ \begin{pmatrix} 0 & 0 & 0 \\ 0 & 0 & 1 \\ 0 & 0 & 0 \end{pmatrix} \end{matrix} \\
 \textcircled{1} & & \textcircled{3} & & \textcircled{3} & & \textcircled{1}
 \end{array} \tag{4.18}$$

For case #4, the first two solutions are deduced straightforwardly from (4.17) and (4.18). The third solution appears in the deformations of the Klein  $E_6$  surface, and for this reason is given in figure 8 in appendix D. Next, we move on to case #9, where the  $E_6$  solution is used again (with a trivial extension in the third solution). The same applies to the first solution in case #10. For the second solution, one can use a slight modification of (4.18). The most difficult case is #13, where both nodes with FI terms are non-abelian. The first extremal solution is given explicitly as follows:

$$\begin{array}{cccc}
 & & \begin{matrix} \textcircled{1} \\ \downarrow \\ \begin{pmatrix} 3 & 0 \\ 0 & 3 \end{pmatrix} \end{matrix} & & \begin{matrix} \begin{pmatrix} 2/3 & 0 & -1 \\ 0 & 0 & 0 \\ 4/9 & 0 & -2/3 \end{pmatrix} \\ \downarrow \\ \textcircled{3} \end{matrix} & & \begin{matrix} \begin{pmatrix} 0 & 0 \\ 1 & 0 \end{pmatrix} \\ \downarrow \\ \textcircled{1} \end{matrix} \\
 & & & & & & \\
 \begin{matrix} \begin{pmatrix} 0 & 0 & 0 \\ 0 & 3 & 0 \\ 0 & 0 & 3 \end{pmatrix} \\ \downarrow \\ \textcircled{2} \end{matrix} & & \begin{matrix} \begin{pmatrix} -4/3 & 0 & -1 \\ 0 & 1 & 0 \\ 4/9 & 0 & 1/3 \end{pmatrix} \\ \downarrow \\ \textcircled{3} \end{matrix} & & \begin{matrix} \begin{pmatrix} 0 & 1 \\ 1 & 0 \end{pmatrix} \\ \downarrow \\ \textcircled{2} \end{matrix} & & \begin{matrix} \begin{pmatrix} 0 & 1 \\ 0 & 0 \end{pmatrix} \\ \downarrow \\ \textcircled{1} \end{matrix} \\
 \textcircled{2} & & \textcircled{3} & & \textcircled{2} & & \textcircled{1}
 \end{array} \tag{4.19}$$

The other solutions are obtained by making use of the pair of matrices (D.6). Case number #14 is similar, with the only exception being the last entry in case #14, for which we find

the following solution

$$\begin{array}{ccccccc}
 & & & \circ 1 & & \circ 1 & \\
 & & & | & & | & \\
 & & & \begin{pmatrix} 0 & 0 & 0 \\ 1 & 0 & 0 \\ 0 & 0 & 0 \end{pmatrix} & & \begin{pmatrix} \frac{1}{2} & \frac{1}{2} & -1 \\ \frac{1}{2} & \frac{1}{2} & -1 \\ \frac{1}{2} & \frac{1}{2} & -1 \end{pmatrix} & \\
 & & & \vdots & & \vdots & \\
 \circ 1 & \text{---} & \circ 2 & \text{---} & \circ 3 & \text{---} & \circ 3 & \text{---} & \circ 1 \\
 & & \begin{pmatrix} 0 & 1 \\ 0 & 0 \end{pmatrix} & & \begin{pmatrix} 3 & 1 & 0 \\ 0 & 3 & 0 \\ 0 & 0 & 0 \end{pmatrix} & & \begin{pmatrix} 3 & 1 & 0 \\ 1 & 3 & 0 \\ 0 & 0 & 0 \end{pmatrix} & & \begin{pmatrix} \frac{1}{2} & \frac{1}{2} & 1 \\ \frac{1}{2} & \frac{1}{2} & 1 \\ -\frac{1}{2} & -\frac{1}{2} & -1 \end{pmatrix}
 \end{array} \tag{4.20}$$

We note that we can only conjecture these solutions are extremal, and we acknowledge it would be helpful to have a systematic way to check extremality.

### 5 SCFTs and non-Lagrangian theories

In this section we will explore FI deformations of magnetic quivers for higher dimensional theories. In particular we will discuss mass deformations for rank two  $\mathcal{N} = 2$  SCFTs in four dimensions, which are quite well-understood, and then show how FI deformations relate multi instanton moduli spaces to non-minimal nilpotent orbits for the same group  $G$ .

#### 5.1 4d SCFTs

Four dimensional SCFTs form a set of theories of prime importance, and display a large varieties of behaviors: the theories can be Lagrangian or not, they can have Coulomb branch operators of fractional scaling dimension (Argyres-Douglas theories [32]), some possess a conformal manifold while others are isolated, etc. The low rank theories have been studied in [8, 33–35]. Their Higgs branches can be studied using magnetic quivers [11, 17, 34, 36–60]. For theories of ranks 1 and 2, a systematic exploration of the magnetic quivers was given in [43, 61]. This shows that a full description of 4d SCFTs requires at least non simply laced quivers, with orthogonal and symplectic gauge groups in addition to unitary ones. Here, in line with the rest of this paper, we will focus for simplicity on 4d theories with a simply-laced unitary magnetic quiver. For concreteness, we concentrate on rank 2 theories, where the mass deformations have been analyzed in detail in [62], and is reproduced with magnetic quivers in [61, figure 3]. In this section, we show how these results are confirmed by our FI-flows.

The top of the mass deformation tree is given by two models: the rank two E-string theory and the  $\mathfrak{so}(20)$  model. The corresponding magnetic quivers are drawn on top of figure 12. We will now identify the FI deformations which implement the RG flows to their descendant theories.

#	Deformation	Extremal Solutions	Subtractions	Interpretation
1				
2				
3				
4				
5				
6				
7				

**Table 3.** Analysis for SU(3) with 7 flavors (1/3).

#	Deformation	Extremal Solutions	Subtractions	Interpretation
8				
9				
10				
11				
12				

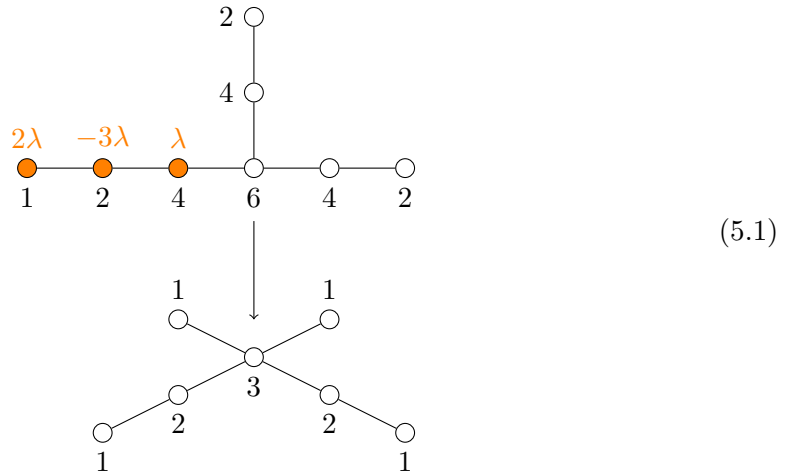
Table 4. Analysis for SU(3) with 7 flavors (2/3).

#	Deformation	Extremal Solutions	Subtractions	Interpretation
13		   	   	   
14		  	  	  
15				
16				

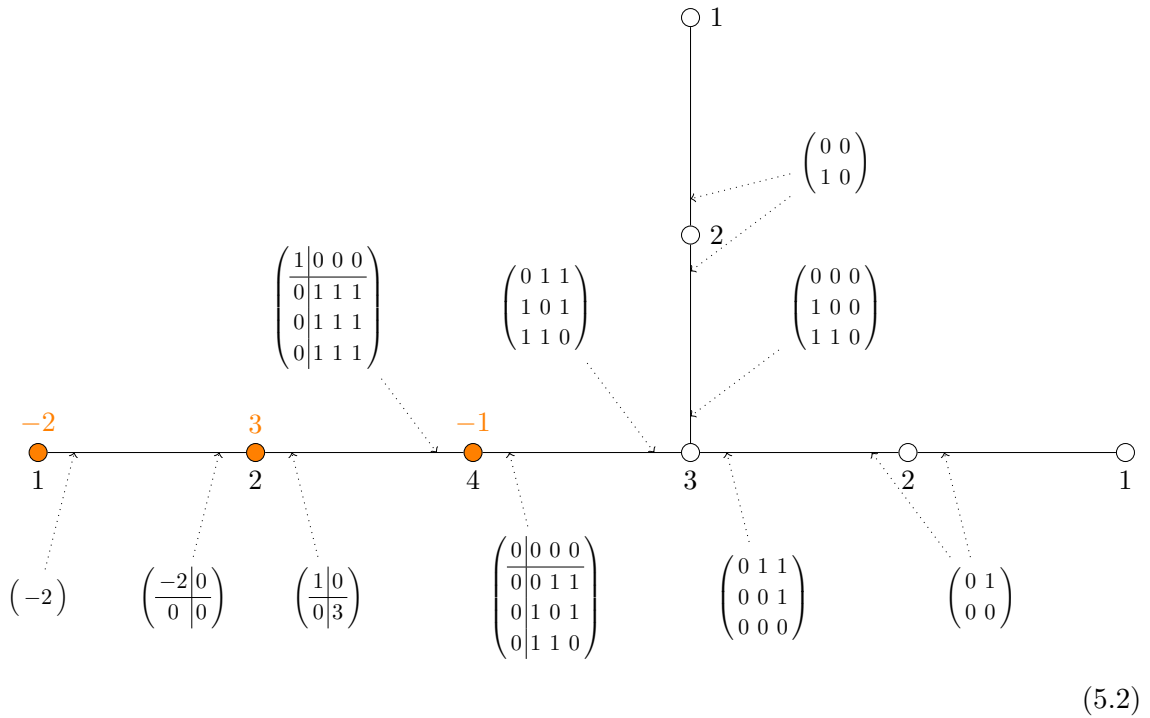
**Table 5.** Analysis for  $SU(3)$  with 7 flavors (3/3). The first column specifies the FI deformation, the second column shows the extremal solutions and the third column gives the result of the subtraction. The last column gives a 3d mirror.

Let us start from the rank two E-string theory. It was already shown in [18] that we can flow to the rank two  $\epsilon_7$  theory and then from there to the  $\epsilon_6$  theory reproducing the known pattern for rank one models. A novelty with respect to the rank one case is the

existence of the flow from the rank two  $\mathfrak{e}_6$  theory to  $\mathfrak{su}(3)$  SQCD with six flavors



An explicit solution for this case is



The solution is not irreducible, as indicated by the separation in the matrices. This means the subtraction involves two quivers, or equivalently, the rebalancing is done with two  $U(1)$  nodes. These are the two abelian nodes on top of the resulting quiver in (5.1).

Apart from these flows, we also have the mass deformation to the  $\mathfrak{e}_8$  model discussed in [34, 63]:

(5.3)

Finally, we can also reproduce the flow to the  $\mathfrak{so}(14) \times \mathfrak{u}(1)$  SCFT:

(5.4)

Notice that also in this case the deformation is implemented by subtracting two quivers:

(5.5)

and the rebalancing is done with a  $U(1)$  node and also a  $U(5)$  which ends up being the central node of the magnetic quiver for the  $\mathfrak{so}(14) \times \mathfrak{u}(1)$  SCFT.



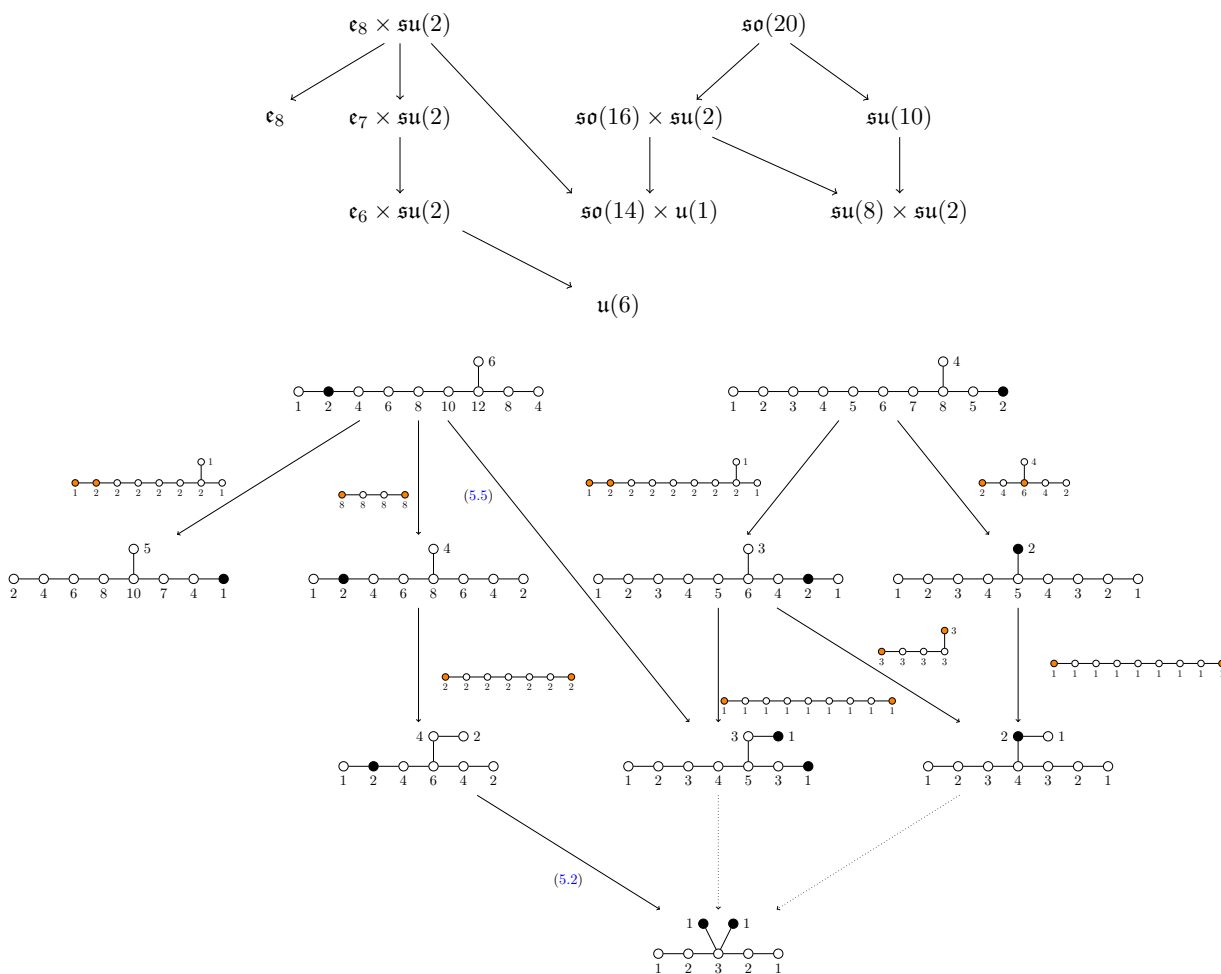


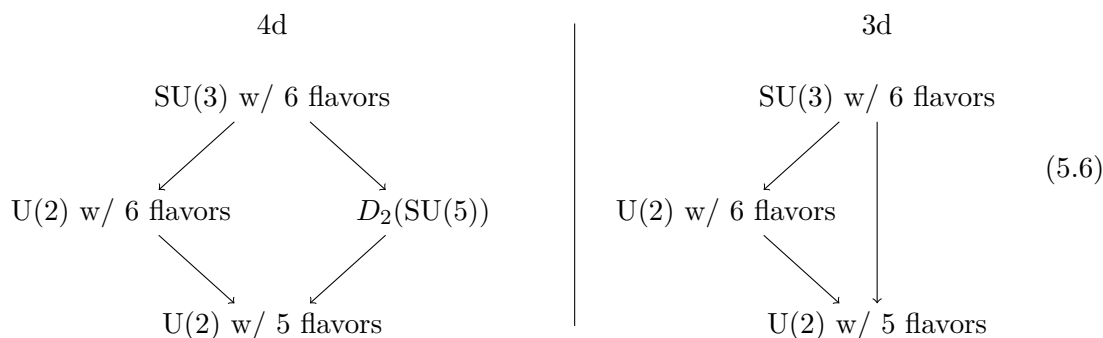
**Figure 12.** Top: part of the graph of mass deformation for 4d  $\mathcal{N} = 2$  SCFTs of rank 2. We stop at the point where the theories become Lagrangian (here the SU(3) SQCD theory). Bottom: corresponding graph of magnetic quivers, along with the solutions to be subtracted to implement the mass deformations. Most subtractions are straightforward. The non-trivial ones are discussed in the text.

Let us now consider the mass deformations of the  $\mathfrak{so}(20)$  model. These involve only subtractions of finite quivers of types A and D. Overall, we recover the known tree of mass deformations of 4d  $\mathcal{N} = 2$  rank two SCFTs which admit a simply-laced magnetic quiver [62],<sup>15</sup> shown in figure 12.

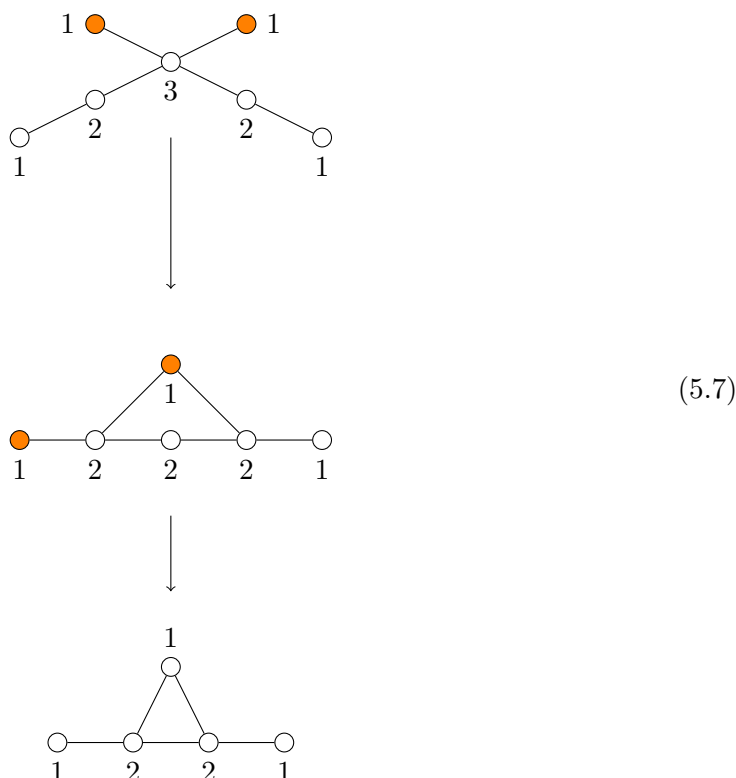
As a final remark, we notice that studying mass deformations of 4d  $\mathcal{N} = 2$  Lagrangian SCFTs via their magnetic quivers is subtle, since minimal mass deformations can look non-minimal at the level of FI deformations of the corresponding magnetic quivers and for this reason we refrain from discussing them in detail. In order to illustrate this point, let us focus on the SU(3) theory with six flavors we have mentioned before. It is known that

<sup>15</sup>Here we have omitted the RG flows involving two or more mass parameters, focusing on the minimal FI deformations.

this model can be mass deformed both to the  $D_2(\text{SU}(5))$  SCFT (see [62, 64]) and to  $\text{U}(2)$  SQCD with six flavors.<sup>16</sup> Moreover, both models can be mass deformed to  $\text{U}(2)$  SQCD with five flavors. The main point now is that upon dimensional reduction to 3d the  $D_2(\text{SU}(5))$  theory becomes equivalent to  $\text{U}(2)$  with five flavors [50, 65] and therefore the flow from  $\text{SU}(3)$  SQCD with six flavors to  $D_2(\text{SU}(5))$ , which is a minimal mass deformation in 4d, in 3d is equivalent to a sequence of two deformations: to  $\text{U}(2)$  SQCD with six flavors first and then to the  $\text{U}(2)$  theory with five flavors and this is precisely what we see at the level of FI deformations of the magnetic quiver. The above discussion can be summarized as follows:



The corresponding FI deformations leading from  $\text{SU}(3)$  SQCD to the  $\text{U}(2)$  theory with five flavors are



<sup>16</sup>More precisely, the flow to  $\text{U}(2)$  SQCD with six flavors involves both giving a common mass to all the flavors and also moving on the Coulomb branch of the theory.

The phenomenon we have just described is rather common and arises also for rank one SCFTs: the  $SU(2)$  theory with four flavors can be mass deformed either to  $D_2(SU(3))$  or to SQED with four flavors (see e.g. [9]) and these two theories can both flow to SQED with three flavors. Upon compactification to 3d, it is known that the  $D_2(SU(3))$  SCFT reduces to SQED with three flavors [66, 67].

## 5.2 Instanton moduli spaces

In this section we will see that via FI deformations the magnetic quivers describing  $G$  instanton moduli spaces reduce to those describing nilpotent orbits of  $G$ . This statement can be understood by considering the cases  $G = A, D$ : the moduli space of  $k$  instantons of  $SU(N)$  is known to coincide with the Higgs branch of  $U(k)$  SQCD with  $N$  flavors and one adjoint hypermultiplet. This theory has  $SU(2) \times SU(N)$  symmetry and the  $SU(2)$  clearly acts on the adjoint field only. By turning on a mass term for  $SU(2)$  we make the adjoint massive and the theory reduces to  $U(k)$  SQCD with  $N$  flavors, whose Higgs branch describes the nilpotent orbit of  $SU(N)$  labeled by the partition  $[N - k, k]$ .

At the level of magnetic quivers this is implemented as follows: as is well known, the mirror dual of the adjoint SQCD theory is given by the quiver [2]

$$(5.8)$$

where we have colored in orange the nodes at which we turn on the FI deformation describing the  $SU(2)$  mass term. The equations of motion can be solved by setting the vev of the  $U(1) \times U(k)$  bifundamentals  $Q$  and  $\tilde{Q}$  to

$$\tilde{Q}^T = Q = \sqrt{\lambda}(1, 1, \dots, 1). \tag{5.9}$$

As a result, the vev of the meson in the  $U(k)$  adjoint becomes a  $k \times k$  matrix whose entries are all equal to  $\lambda$ . It is then consistent to assign nilpotent vev to the adjoint mesons built out of  $U(k) \times U(k)$  bifundamentals on the left and on the right of the top  $U(k)$  gauge node in (5.8): one meson will have all entries above the main diagonal equal to  $\lambda$  whereas the other will have non-vanishing entries below the main diagonal only. These vevs will propagate along the quiver, partially higgsing the various  $U(k)$  groups. This results in the

following RG flow

$$(5.10)$$

where on the right of (5.10) we recognize the magnetic quiver of  $U(k)$  SQCD with  $N$  flavors and no adjoints, as expected.

We can similarly analyze the  $k$ -instanton moduli space of  $SO(2N)$ , which coincides with the Higgs branch of  $USp(2k)$  SQCD with  $N$  hypermultiplets in the fundamental representation and one in the rank-2 antisymmetric. As in the previous case, the global symmetry of the theory is  $SO(2N) \times SU(2)$  where the  $SU(2)$  acts on the antisymmetric only. If we turn on a mass term for the  $SU(2)$  we therefore remove the hyper in the antisymmetric from the infrared spectrum and the theory reduces to the  $USp(2k)$  theory with  $N$  fundamentals.

Let us reproduce this result from the mirror dual side using FI deformations. We focus for simplicity on the case  $k = 2$ . The mirror dual of  $USp(4)$  SQCD with  $N > 3$  flavors and an antisymmetric hypermultiplet is given by the quiver (see [2] and also [68, 69] for the corresponding brane construction)

$$(5.11)$$

and, as in the previous case, turning on a  $SU(2)$  mass term is equivalent to activating a FI deformation at the abelian node and at the  $U(2)$  next to it. As we have seen, this RG flow is described by a D-type quiver subtraction:

$$(5.12)$$

where the bottom quiver in (5.12) is the mirror dual of  $USp(4)$  SQCD with  $N$  fundamentals as expected (see [29]).

In the exceptional case we have to rely on the magnetic quiver analysis only, since we do not have a Lagrangian description of the theory whose Higgs branch is the instanton moduli space of  $E_{6,7,8}$ . We consider again the two instanton case and turn on FI deformations which correspond to a mass term for the  $SU(2)$  global symmetry. Also in this case the deformation is implemented via quiver subtraction and we end up with the magnetic quivers associated with the next-to-minimal nilpotent orbits of  $E_{6,7,8}$  [70].

(5.13)

## 6 Outlook

In this paper we have seen that we can efficiently study mass deformations of field theories with eight supercharges by considering FI deformations of their magnetic quivers. Remarkably this holds true even when the theory is strongly coupled, providing us with an efficient tool to study RG flows which would be otherwise intractable. As the many examples we have discussed in the paper clearly show, the method is very general and allows us to understand deformations for a wide variety of moduli spaces.

Although we have not found an algorithmic method to solve the algebraic problem in general, the reformulation in terms of quiver subtractions allows us to greatly simplify the analysis and in several cases identify the answer rather easily. Moreover, for a large class of quivers the problem can be addressed by exploiting brane technology, making it much simpler to identify the infrared quiver.

Apart from finding a systematic way of solving the FI-meson problem, there are several interesting directions for future investigations. One is the study of FI deformations for non

simply-laced quivers, which have no known Lagrangian description. Sometimes these can be understood by first unfolding the quiver, deforming it and then refolding, although this method is not applicable in general. Studying this problem in detail would definitely shed light on the physics of non simply-laced quivers. Another point we did not address in this paper is the role of adjoint matter (or even more general representations) in the quiver when considering FI deformations. This is known to arise e.g. in magnetic quivers for SCFTs in dimensions 4-6. A more challenging problem is to generalize the technique to orthosymplectic quivers, where the FI deformation involves monopole operators and therefore does not have a simple Lagrangian description. We hope to come back to some of these problems in the future.

Finally, we would like to remark that in this work we have primarily focused on understanding the RG flow triggered by a given FI deformation. This however is one side of the problem: in order to study systematically RG flows for SCFTs with eight supercharges with this method, one also needs to understand the correspondence between relevant deformations of the SCFT and FI deformations of the corresponding magnetic quiver. More precisely, it would be important to identify the map between the generalized Coulomb branch (which includes the space parameterized by mass parameters) of the SCFT and the space of FI deformations. In this work we have exploited as a guiding principle to identify the relevant FI deformation the global symmetry preserved along the RG flow. This significantly constrains the set of candidate FI deformations and in many cases allows us to identify it unambiguously, up to the action of the Weyl group of the Coulomb branch global symmetry of the quiver. In general however, this is not enough to fully specify the map we are after. In [18] a partial answer was provided in the context of relevant deformations of 5d SCFTs, by noticing that the generalized toric polygon describing the 5d theory provides constraints on the choice of FI deformation. It would be important to fill in this gap and provide a general rule to identify the FI deformation describing the RG flow of interest.

## Acknowledgments

We thank Andrew Dancer, Amihay Hanany and Dan Waldram for discussions. AB is supported by the ERC Consolidator Grant 772408-Stringlandscape, and by the LabEx ENS-ICFP: ANR-10-LABX-0010/ANR-10-IDEX-0001-02 PSL\*. The work of SG is supported by the INFN grant “Per attività di formazione per sostenere progetti di ricerca” (GRANT 73/STRONGQFT). JFG is supported by STFC grant ST/T000791/1.

## A The meson propagation theorem

In this appendix, we prove the central theorem which underlies the FI-Meson problem. It gives a necessary and sufficient condition for two matrices to be expressible as  $AB$  and  $BA$  respectively. This plays a central role in section 3.

Let  $M$  and  $\tilde{M}$  be two square matrices with complex coefficients, of respective sizes  $m$  and  $n$ . We write

$$M \rightsquigarrow \tilde{M} \tag{A.1}$$

if there exists two matrices  $A$  and  $B$ , of sizes respectively  $m \times n$  and  $n \times m$ , such that  $M = AB$  and  $\tilde{M} = BA$ . In the notation of (3.6), this is the necessary and sufficient condition to be able to write

$$\begin{array}{ccc}
 \circ & \text{---} & \circ \\
 n & & m \\
 & \swarrow \quad \searrow & \\
 & M \quad \tilde{M} &
 \end{array}
 \tag{A.2}$$

Note that although the relation  $\leftrightarrow$  is reflexive and symmetric, it is not transitive, and therefore it does not define an equivalence relation. We begin with three elementary properties. The first one ensures that one can safely reduce  $M$  and  $\tilde{M}$  to their Jordan normal form, and the second and third one relates the characteristic polynomials and ranks of  $M$  and  $\tilde{M}$ .

**Lemma 1.** *Let  $M \in \mathbb{C}^{m \times m}$ ,  $\tilde{M} \in \mathbb{C}^{n \times n}$ ,  $P \in \text{GL}(m, \mathbb{C})$  and  $Q \in \text{GL}(n, \mathbb{C})$ . We have*

$$M \leftrightarrow \tilde{M} \iff P^{-1}MP \leftrightarrow Q^{-1}\tilde{M}Q.
 \tag{A.3}$$

*Proof:* This follows from the fact that if  $M = AB$  and  $\tilde{M} = BA$ , then  $P^{-1}MP = (P^{-1}AQ)(Q^{-1}BP)$  and  $Q^{-1}\tilde{M}Q = (Q^{-1}BP)(P^{-1}AQ)$ .

**Lemma 2.** *Let  $M \in \mathbb{C}^{m \times m}$ ,  $\tilde{M} \in \mathbb{C}^{n \times n}$ . If  $M \leftrightarrow \tilde{M}$  then  $x^n \chi_M(x) = x^m \chi_{\tilde{M}}(x)$ .*

*Proof:* This is a consequence of  $\det(AB) = \det(BA)$ .

**Lemma 3.** *Let  $A \in \mathbb{C}^{m \times n}$ ,  $B \in \mathbb{C}^{n \times m}$ . Then*

$$2r(BA) - n \leq r(AB).
 \tag{A.4}$$

*Proof:* This follows from Sylvester's rank inequality, which states that  $r(A) + r(B) - n \leq r(AB)$ . Since we also know that  $r(BA) \leq r(A)$  and  $r(BA) \leq r(B)$ , the lemma follows.

We now turn to the central point of the argument. The previous lemmas show how certain conjugacy invariant quantities (eigenvalues, rank) behave with respect to the relation (A.1). It turns out one can entirely characterize this relation by inspecting the Jordan decompositions.

**Lemma 4.** *Let  $M \in \mathbb{C}^{m \times m}$ ,  $\tilde{M} \in \mathbb{C}^{n \times n}$  with  $m \leq n$ . Assume that  $M$  has Jordan decomposition  $J_m(\lambda)$ .*

- *If  $\lambda \neq 0$  then:  $M \leftrightarrow \tilde{M}$  if and only if  $\tilde{M}$  has Jordan decomposition  $J_m(\lambda) \oplus (J_1(0))^{\oplus n-m}$*
- *If  $\lambda = 0$  then:  $M \leftrightarrow \tilde{M}$  if and only if  $\tilde{M}$  has Jordan decomposition  $J_m(0) \oplus (J_1(0))^{\oplus n-m}$  or  $J_{m\pm 1}(0) \oplus (J_1(0))^{\oplus n-m\mp 1}$ .*

*Proof:* Using Lemma 1, we can assume the matrices  $\tilde{M}$  and  $M$  are in the form of Jordan blocks. Let  $A \in \mathbb{C}^{m \times n}$ ,  $B \in \mathbb{C}^{n \times m}$  such that  $M = AB$  and  $\tilde{M} = BA$ . We introduce the decomposition

$$A = (A_1, A_2), \quad B = \begin{pmatrix} B_1 \\ B_2 \end{pmatrix} \tag{A.5}$$

with  $A_1, B_1 \in \mathbb{C}^{m \times m}$ . Then

$$M = AB = (A_1 B_1 + A_2 B_2), \quad N = BA = \begin{pmatrix} B_1 A_1 & B_1 A_2 \\ B_2 A_1 & B_2 A_2 \end{pmatrix}. \tag{A.6}$$

- We start with the case  $\lambda \neq 0$ . Using Lemma 2, we know that the eigenvalues of  $\tilde{M}$  are  $\lambda$  with multiplicity  $m$  and 0 with multiplicity  $n - m$ . Therefore we know that  $\tilde{M}$ , which is in Jordan form, is block diagonal with blocks of sizes  $m$  and  $n - m$ . We get that  $B_1 A_1 = J_m(\lambda)$  is a non-singular matrix since  $\lambda \neq 0$ , therefore  $A_1$  is non-singular. Since  $B_2 A_1 = 0$  because of the block diagonal form of  $N$ , this implies  $B_2 = 0$ , and therefore  $B_2 A_2 = 0$ . We conclude  $\tilde{M} = J_m(\lambda) \oplus (J_1(0))^{\oplus n-m}$ . The converse is deduced from an elementary computation.
- Let us now move on to  $\lambda = 0$ . Now both  $\tilde{M}$  and  $M$  are nilpotent. Using Lemma 3, we have

$$m - 2 = 2r(AB) - m \leq r(BA) \leq m, \tag{A.7}$$

so<sup>17</sup>

$$|r(M) - r(\tilde{M})| \leq 1. \tag{A.8}$$

Let's now have a closer look at the maps involved:

$$\begin{array}{ccccc}
 & & \mathbb{C}^m & \xrightarrow{M} & \mathbb{C}^m & & \\
 & \nearrow A & & & & \searrow B & \\
 \mathbb{C}^n & \xrightarrow{\tilde{M}} & \mathbb{C}^n & \xrightarrow{\tilde{M}} & \mathbb{C}^n & & \\
 & \searrow B & & & & \nearrow A & \\
 & & \mathbb{C}^m & \xrightarrow{M} & \mathbb{C}^m & & 
 \end{array} \tag{A.9}$$

Since the rank of  $M$  is  $m - 1$ ,  $r(ABA) \geq r(A) - 1$ . On the other hand  $r(ABA) < r(A)$  (otherwise  $BA = \tilde{M}$  would be invertible). Therefore  $r(ABA) = r(A) - 1$ , so  $\text{Im}(ABA)$  is a vector subspace of  $\text{Im}(A)$  with codimension 1. Therefore  $r(BA) - r(BABA)$  is either 0 or 1. It can't be 0 as  $\tilde{M} = BA$  is nilpotent, so it is 1. This means that  $r(\tilde{M}^2) = r(\tilde{M}) - 1$ , so there is at most one Jordan block in  $\tilde{M}$  with size  $> 1$ . From the inequality (A.8), this block has size  $m - 1$ ,  $m$  or  $m + 1$ , which proves the lemma (again, the converse is deduced from an elementary computation).

From this, one obtains a complete characterization of the relation (A.1) as follows.

---

<sup>17</sup>One can also argue with the nilpotency index: if  $k_M$  is the nilpotency index of  $M$  and  $k_{\tilde{M}}$  the nilpotency index of  $\tilde{M}$ , we have  $\tilde{M}^{k_M+1} = BM^{k_M}A = 0$  so  $k_{\tilde{M}} \leq k_M + 1$ . Conversely,  $k_M \leq k_{\tilde{M}} + 1$ , so  $|k_M - k_{\tilde{M}}| \leq 1$ .



**Theorem 1.** Let  $M \in \mathbb{C}^{m \times m}$ ,  $\tilde{M} \in \mathbb{C}^{n \times n}$  with  $m \leq n$ . Assume that  $M$  has a block decomposition  $M_{\mathbf{p}} \oplus \bigoplus J_{m_i}(\lambda_i)$ , with  $M_{\mathbf{p}}$  nilpotent in the orbit  $\mathcal{O}_{\mathbf{p}}$  and  $\lambda_i \neq 0$  and  $\tilde{M}$  has a block decomposition  $\tilde{M}_{\mathbf{q}} \oplus \bigoplus J_{n_j}(\mu_j)$ , with  $\tilde{M}_{\mathbf{q}}$  nilpotent in the orbit  $\mathcal{O}_{\mathbf{q}}$  and  $\mu_j \neq 0$ . Then  $M \leftrightarrow \tilde{M}$  if and only if up to reordering  $m_i = n_j$  and  $\lambda_i = \mu_j$  and the partitions  $\mathbf{p}$  and  $\mathbf{q}$  are related by

$$|\mathbf{p}_k - \mathbf{q}_k| \leq 1 \tag{A.10}$$

for a certain ordering of the entries, and including zeros.

In other words, the invertible Jordan blocks stay the same, and the nilpotent Jordan block can see their sizes change by at most one unit.

**Examples.** To illustrate let us give a few examples. The following transition is allowed:

$$\begin{array}{ccc}
 \circ & \text{---} & \circ \\
 3 & & 2 \\
 \vdots & & \vdots \\
 \begin{pmatrix} -4/3 & 0 & -1 \\ 0 & 1 & 0 \\ 4/9 & 0 & 1/3 \end{pmatrix} & & \begin{pmatrix} 0 & 1 \\ 1 & 0 \end{pmatrix}
 \end{array} \tag{A.11}$$

as the Jordan decompositions are respectively  $J_1(1) \oplus J_1(-1) \oplus J_1(0)$  and  $J_1(1) \oplus J_1(-1)$ . This particular example appears in equation (4.19).

## B Weyl orbits

In this section we consider framed quivers with a set of balanced gauge nodes. For framed quivers there is no condition (2.9) on the FI parameters. If the quiver is viewed in its unframed version, then the additional  $U(1)$  gauge node will carry an FI parameter specified by solving (2.9), which could either be zero or non-zero.

For a balanced subset of nodes in the shape of the Dynkin diagram of an algebra  $g$  we find, that several choices of FI parameters lead to the same deformation of the Higgs branch. The equivalent choices are related by an action of the Weyl group of  $g$ . This is visible particularly well from the linking number of NS5 branes in a Hanany-Witten system.

**Example 1.** Let us consider a specific example, the quiver:



The balanced nodes form an  $A_3$  Dynkin diagram, circled in blue.

We can now turn on an FI term  $\lambda$  on the  $U(1)$  gauge node, which corresponds to the weight  $[1, 0, 0]$  of the  $A_3$  algebra.

$$\begin{array}{c} \lambda \\ \bullet \\ 1 \end{array} \text{---} \begin{array}{c} \circ \\ 2 \end{array} \text{---} \begin{array}{c} \circ \\ 3 \end{array} \begin{array}{c} \square \\ 4 \\ | \\ \circ \\ 3 \end{array} \longleftrightarrow [1, 0, 0] \tag{B.2}$$

The Weyl group orbit of this weight is

$$\{ [1, 0, 0], [-1, 1, 0], [0, -1, 1], [0, 0, -1] \}. \tag{B.3}$$

This implies that the following FI deformations are equivalent:

$$\begin{array}{c} \lambda \\ \bullet \\ 1 \end{array} \text{---} \begin{array}{c} \circ \\ 2 \end{array} \text{---} \begin{array}{c} \circ \\ 3 \end{array} \begin{array}{c} \square \\ 4 \\ | \\ \circ \\ 3 \end{array}, \quad \begin{array}{c} -\lambda \\ \bullet \\ 1 \end{array} \text{---} \begin{array}{c} \lambda \\ \bullet \\ 2 \end{array} \text{---} \begin{array}{c} \circ \\ 3 \end{array} \begin{array}{c} \square \\ 4 \\ | \\ \circ \\ 3 \end{array}, \quad \begin{array}{c} \circ \\ 1 \end{array} \text{---} \begin{array}{c} -\lambda \\ \bullet \\ 2 \end{array} \text{---} \begin{array}{c} \lambda \\ \bullet \\ 3 \end{array} \begin{array}{c} \square \\ 4 \\ | \\ \circ \\ 3 \end{array}, \quad \begin{array}{c} \circ \\ 1 \end{array} \text{---} \begin{array}{c} \circ \\ 2 \end{array} \text{---} \begin{array}{c} \bullet \\ 3 \end{array} \begin{array}{c} \square \\ 4 \\ | \\ \circ \\ 3 \end{array} \text{---} -\lambda \tag{B.4}$$

We can use the brane system to check that all choices of FI parameters indeed lead to the same answer. The brane system with FI parameters turned off, in the Coulomb phase, is

$$\tag{B.5}$$

In order to do the FI deformation, we move to the Higgs phase

$$\tag{B.6}$$

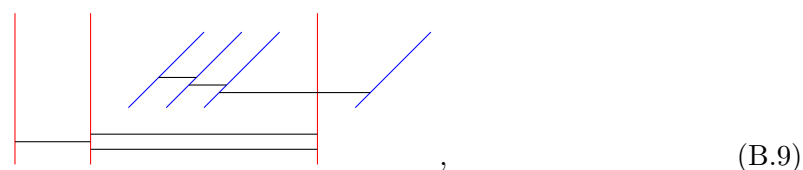
For a more symmetric picture we perform a Hanany-Witten transition.

$$\tag{B.7}$$

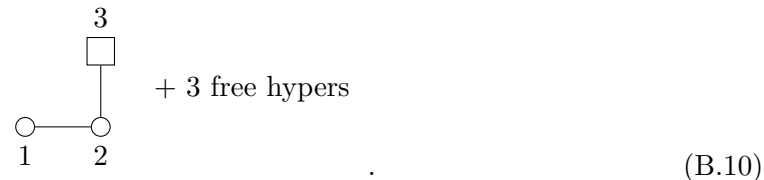
An FI deformation corresponds to moving an NS5 brane. The four choices in (B.3) correspond to moving one of the four NS5 branes (and the frozen D3 brane connected to it). No matter which NS5 brane is sent away to infinity, one obtains the same brane system:

$$\tag{B.8}$$

Moving to the (partial) Coulomb phase, after performing some Hanany-Witten transitions



we can read off the resulting theory



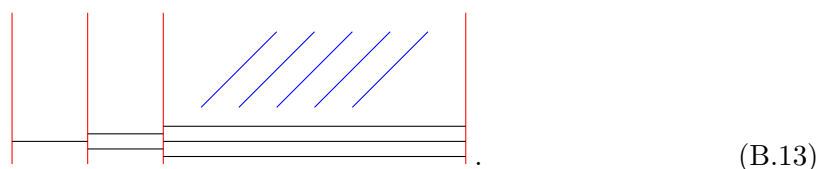
**Example 2.** Based on the last example one could ask, whether it never matters which NS5 brane one moves in a brane system. This is obviously not the case, as we demonstrate with another simple example. Consider the theory



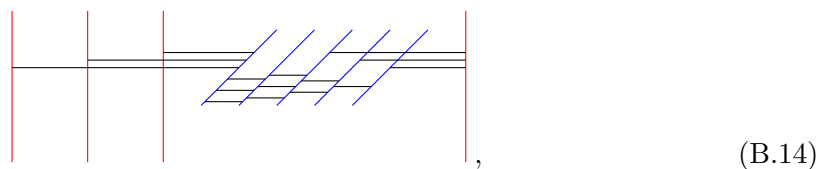
The set of balanced nodes, circled in blue, make up an  $A_2$  Dynkin diagram. Let us again turn on an FI term on the first node, corresponding to the weight  $[1, 0]$  of  $A_2$ . The Weyl group orbit of this weight is

$$\{ [1, 0], [-1, 1], [0, -1] \} . \tag{B.12}$$

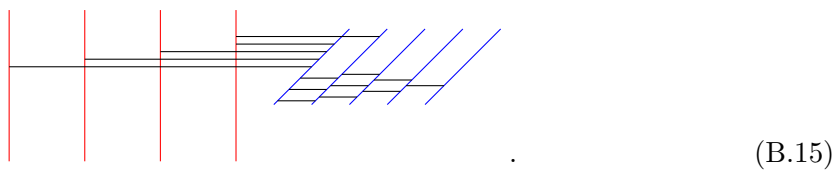
The brane system with FI parameters turned off, in the Coulomb phase, is



We can again move to the Higgs phase



and perform a Hanany-Witten transition, bringing all NS5 branes to the left



Here we see that moving the first three NS5 branes away leads to the same brane system. However, moving the last NS5 brane leads to a different brane system.

**Applications:** the Weyl orbit can be used to simplify an FI deformation. Take for example the quiver and FI deformation

$\lambda$   
 $1$  ●  
 ●  $\lambda$  ●  $-\lambda$  ○  
 ○  $2$  ○  $3$  ○  $4$   
 ○ ○  
 ○ ○

(B.16)

We can frame the quiver in the following way

$1$  □  
 ○  $\lambda$  ●  $-\lambda$  ○  
 ○  $2$  ○  $3$  ○  $4$   
 ○ ○  
 ○ ○

(B.17)

leaving intact the subset of balanced gauge nodes which make up a  $D_6$  Dynkin diagram. The FI deformation corresponds to the weight  $[0, 1, -1, 0, 0, 0]$ . In the same Weyl orbit we have the weight  $[1, 0, 0, 0, 0, 0]$ . Therefore we have an equivalent FI deformation

$1$  □  
 ●  $\lambda$  ○ ○ ○  
 ○  $1$  ○  $2$  ○  $3$  ○  $4$   
 ○ ○  
 ○ ○

(B.18)

Which in its unframed form is

$-\lambda$   
 $1$  ●  
 ●  $\lambda$  ○ ○ ○  
 ○  $1$  ○  $2$  ○  $3$  ○  $4$   
 ○ ○  
 ○ ○

(B.19)

Indeed one can check that both FI deformations (B.16) and (B.19) are equivalent. Hence the action of the Weyl group can turn seemingly more complicated FI deformations into simpler ones, involving less nodes.

**Linear Quivers.** We can do the general case of linear framed quivers. Let  $n$  be a positive integer, we consider a linear framed quiver with gauge nodes  $U(k_i)$  and flavors  $N_i$  for  $i = 1, \dots, n$ . This defines two partitions as follows:

$$\lambda_i = k_{i+1} - k_i + \sum_{j=1}^i N_j \tag{B.20}$$

$$\mu_i^T = \sum_{j=1}^{n+1-i} N_j. \tag{B.21}$$

These correspond to linking numbers of branes: the  $\lambda_i$  ( $i = 1, \dots, n$ ) are the linking numbers of the NS5 and the  $\mu_j$  ( $j = 1, \dots, n^T$ ). Turning on FI corresponds to picking one NS5 and moving it out of the local brane system. Moving two branes with the same linking number gives equivalent FI deformations. In terms of partitions, we choose an integer  $\ell$  in the partition  $\lambda$ . The resulting theory is defined by  $\lambda'$ ,  $\mu'$  where  $\lambda'$  is obtained from  $\lambda$  by removing one occurrence of  $\ell$  and  $\mu' = \mu - [1^\ell, 0, \dots]$ .

### C Hilbert series check of the mirror pair

In this appendix we provide a computational check of the mirror pair (1.5a)–(1.5b) by checking the equality of the Hilbert series for the Higgs and Coulomb branches of both quivers. The first equality is

$$\text{HS}(\mathcal{C}[1.5a]; t) = \text{HS}(\mathcal{H}[1.5b]; t), \tag{C.1}$$

and it is straightforward to check, as the 1-form symmetry gauging in (1.5b) does not affect this Hilbert series, and one can use the standard hyper-Kähler quotient. We focus instead here on the other check, involving the Coulomb branch Hilbert series of (1.5b), which is sensitive to the quotient. The computation of  $\text{HS}(\mathcal{C}[1.5b]; t)$  uses the monopole formula. We spell out the details, as there are subtleties due to the SU gauge groups and the gauging of 1-form symmetry.

**Hilbert series before gauging the 1-form symmetry.** Consider first the  $\mathfrak{su}(N)$  algebra, with fundamental weights  $(\varpi_1, \dots, \varpi_{N-1})$ . We parametrize its coweights, which are identified to the weights as the algebra is simply laced, by  $\varpi = a_1\varpi_1 + \dots + a_{N-1}\varpi_{N-1}$  with  $a_i \in \mathbb{Z}$ . The fundamental Weyl chamber is given by  $a_i \in \mathbb{N}$ . We parametrize coweights of the  $\mathfrak{u}(1)$  algebra by  $b \in \mathbb{Z}$ , and the coweights of  $\mathfrak{su}(N)$  by  $c_i \in \mathbb{Z}$ . The Hilbert series for the quiver before gauging the 1-form symmetry is

$$\sum_{a_1, \dots, a_{N-1} \in \mathbb{N}} \sum_{b \in \mathbb{Z}} \sum_{c_1, \dots, c_{M-1} \in \mathbb{N}} t^{\Delta(a,b,c)} \frac{P^{\text{SU}}(a; t) P^{\text{SU}}(c; t)}{1 - t^2} \times \delta \left( N \mid \sum_{i=1}^{N-1} i a_i \right) \delta \left( M \mid \sum_{i=1}^{M-1} i c_i \right), \tag{C.2}$$

where  $\Delta(a, b, c)$  is the monopole operator conformal dimension [28],  $P^{\text{SU}}(a; t)$  is a dressing factor defined below, and  $\delta_{N \mid \sum i a_i} \delta_{M \mid \sum i c_i}$  imposes that the sum is restricted to the weights of the Langlands dual groups  $\text{PSU}(N)$  and  $\text{PSU}(M)$ , i.e. the root lattice. The dressing factor  $P^{\text{SU}}(a; t)$  depends only on which of the  $a_i$  are vanishing, encoding which facet of the Weyl chamber the weight belongs to. If there are  $r$  strings of zeros of lengths  $l_1, \dots, l_r$  in the string  $a_1, \dots, a_{N-1}$  then

$$P^{\text{SU}}(a; t) = \text{PE} \left[ \left( N - 1 - \sum_{i=1}^r l_i \right) t^2 + \sum_{i=1}^r \sum_{j=1}^{l_i} t^{2+2j} \right]. \tag{C.3}$$

**Gauging the 1-form symmetry.** In order to implement gauging the 1-form symmetry, we use the embedding:

$$\begin{aligned} \mathbb{Z} &\rightarrow Z(\mathrm{SU}(N) \times \mathrm{U}(1) \times \mathrm{SU}(M)) \\ I &\mapsto (e^{-2\pi i \frac{I}{N}} \mathbf{1}_N, e^{2\pi i \frac{I}{NM}}, e^{-2\pi i \frac{I}{M}} \mathbf{1}_M) \end{aligned} \tag{C.4}$$

specified by the charge of the hypers in (1.5b). The kernel of this morphism is  $NM\mathbb{Z}$  so the image is isomorphic to  $\mathbb{Z}_{NM}$ . We shift the magnetic lattices accordingly [71], which leads us to introduce the sums

$$\begin{aligned} H[I] &= \sum_{a_1, \dots, a_{N-1} \in \mathbb{N}} \sum_{b \in \mathbb{Z} + \frac{I}{MN}} \sum_{c_1, \dots, c_{M-1} \in \mathbb{N}} \frac{t^{\Delta(a,b,c)} P^{\mathrm{SU}}(a; t) P^{\mathrm{SU}}(c; t)}{1 - t^2} \\ &\times \delta \left( N \left| -I + \sum_{i=1}^{N-1} ia_i \right. \right) \delta \left( M \left| -I + \sum_{i=1}^{M-1} ic_i \right. \right), \end{aligned} \tag{C.5}$$

for any integer  $I \in \mathbb{Z}$ . The final result is then given by

$$\mathrm{HS}(\mathcal{C}[1.5b]; t) = \sum_{I \in \mathbb{Z}_{NM}} H[I]. \tag{C.6}$$

One finds that this agrees with the Higgs branch Hilbert series for the mirror, thus providing a strong argument for the validity of the mirror pair.

## D Minimal deformations of ADE singularities

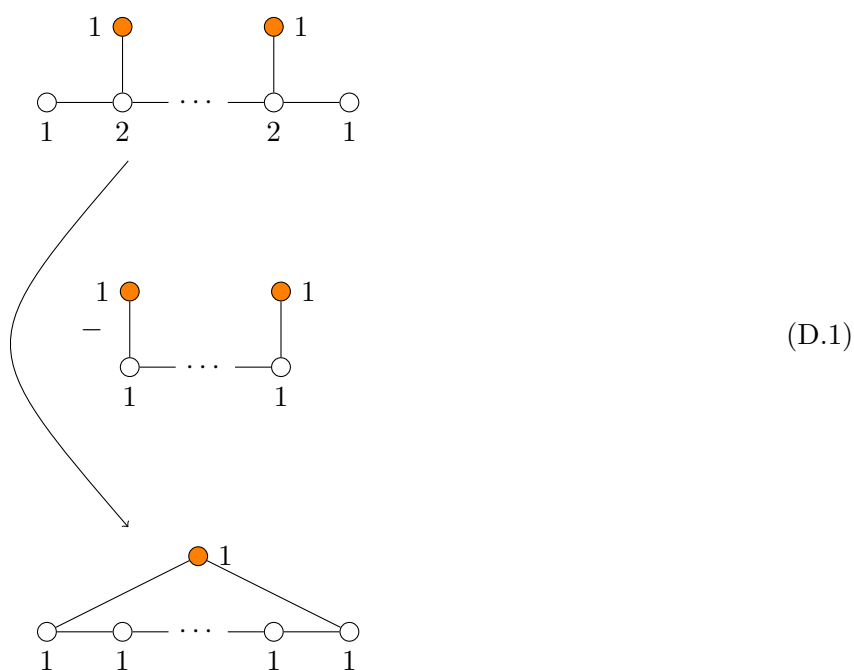
We perform the minimal deformations of ADE-type singularities using finite quiver subtraction. It is known that the minimal deformations of Kleinian singularities are in bijection with the fundamental weights of the associated algebra. Therefore we turn on FI parameters for the affine node as well as one of the other nodes for each such minimal deformation. The quivers to subtract are obtained by finding all minimal free sub-quivers which contain both nodes with non-zero FI.

**D.1 Type  $A_n$**

For type  $A$ , the only breaking pattern is  $A_n \rightarrow A_k A_{n-k-1}$ . The subtractions are shown in section 2.

**D.2 Type  $D_n$**

**D.2.1  $D_n \rightarrow A_{n-1}$**

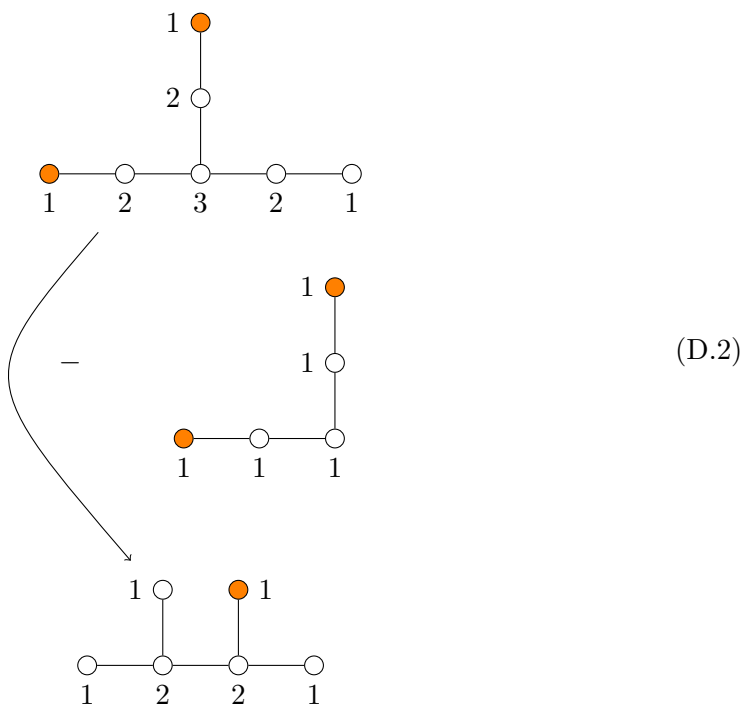


**D.2.2  $D_n \rightarrow A_{k-1} D_{n-k}$**

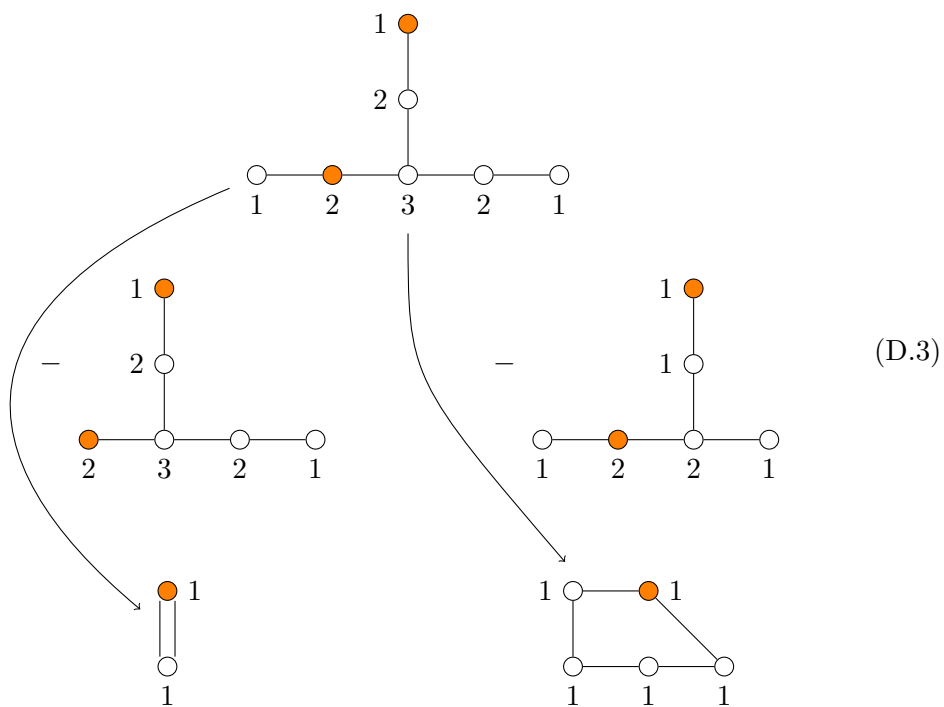
See figure 7.

**D.3 Type  $E_6$**

**D.3.1  $E_6 \rightarrow D_5$**

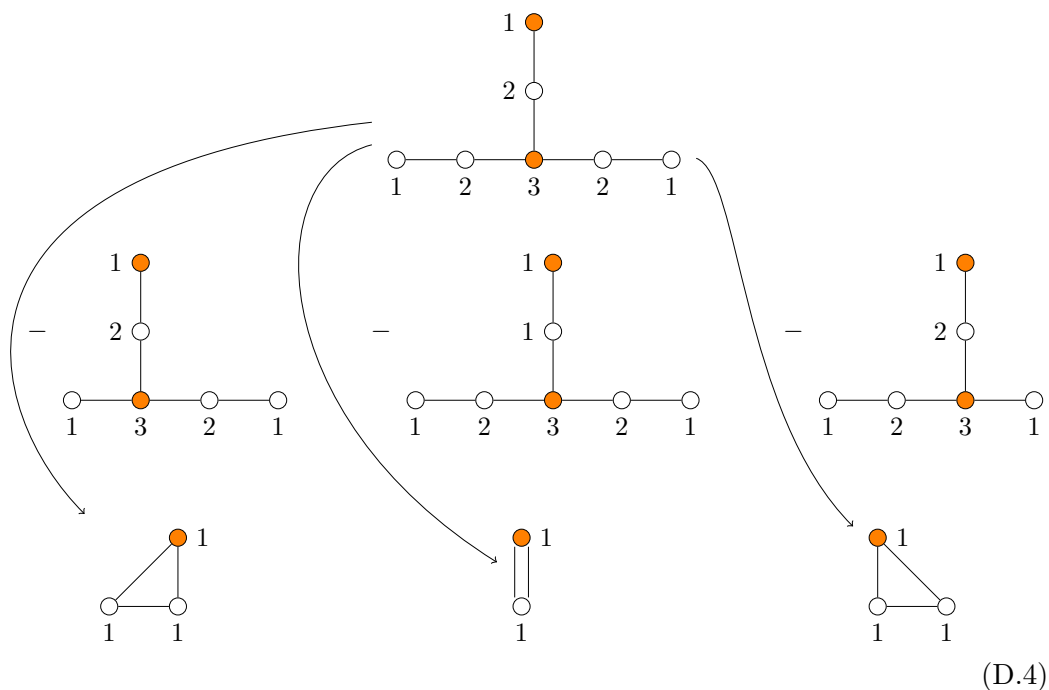


**D.3.2  $E_6 \rightarrow A_1A_4$**

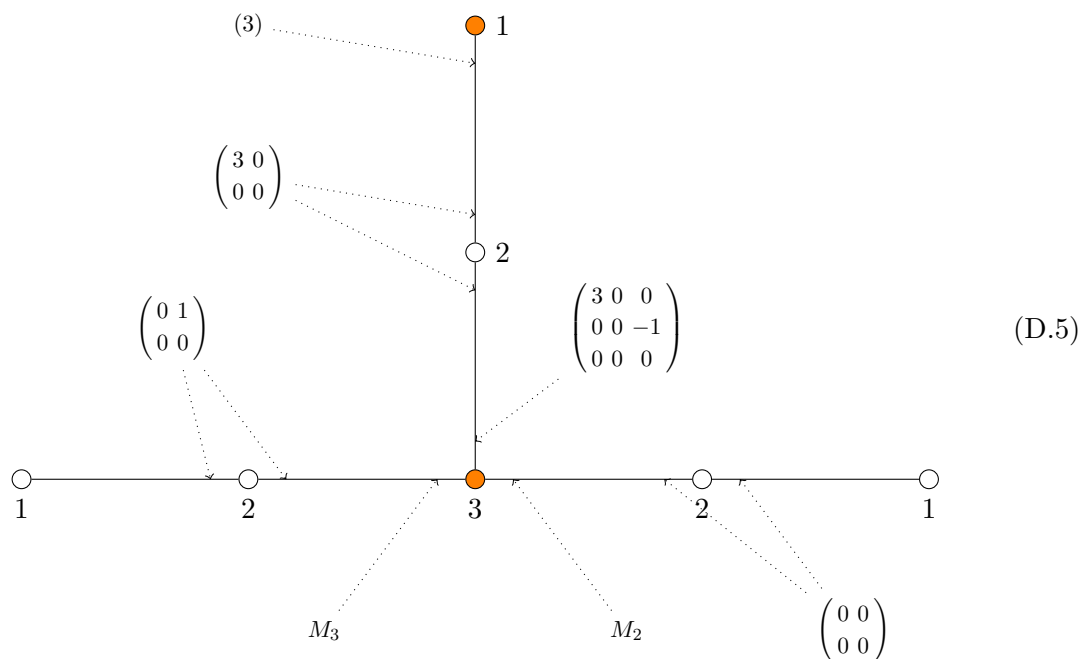




**D.3.3**  $E_6 \rightarrow A_2 A_1 A_2$



An explicit solution for the first and third subtractions here is given as follows:



We note that the solution requires to find three matrices, say  $M_1$ ,  $M_2$  and  $M_3$  such that  $M_1$  has Jordan form  $J_1(3) \oplus J_2(0)$ ,  $M_2$  is nilpotent of order 2 and  $M_3$  is nilpotent of order 3, and  $M_1 + M_2 + M_3 = \mathbf{1}_3$ . Abstractly, we are looking for three endomorphisms of a 3-dimensional vector space satisfying with prescribed Jordan forms and constrained by an overall linear relation. Without loss of generality we can put one of the endomorphisms in

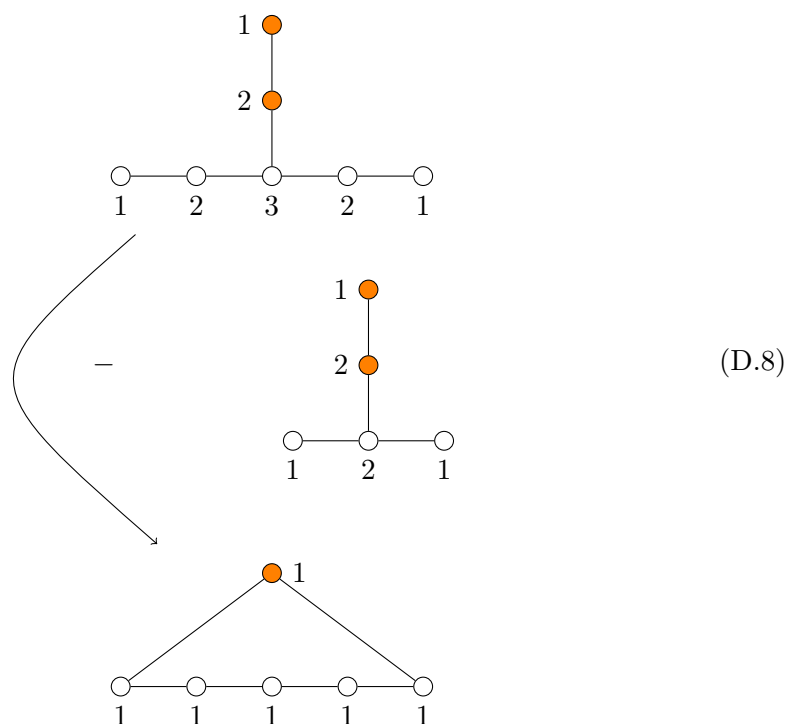
Jordan form by picking an appropriate basis. The question becomes: write the following matrix as the sum of two nilpotent matrices  $M_2$  and  $M_3$  with nilpotency degrees 2 and 3:

$$\begin{pmatrix} -2 & 0 & 0 \\ 0 & 1 & 1 \\ 0 & 0 & 1 \end{pmatrix} = M_2 + M_3, \quad M_2^2 = M_3^3 = 0. \tag{D.6}$$

One way to address this question is to write the most general nilpotent matrix (the orbit of  $J_3(0)$ ) and impose that the difference with (D.6) squares to 0. This provides many solutions, none of which appear to be particularly simple. We pick one solution

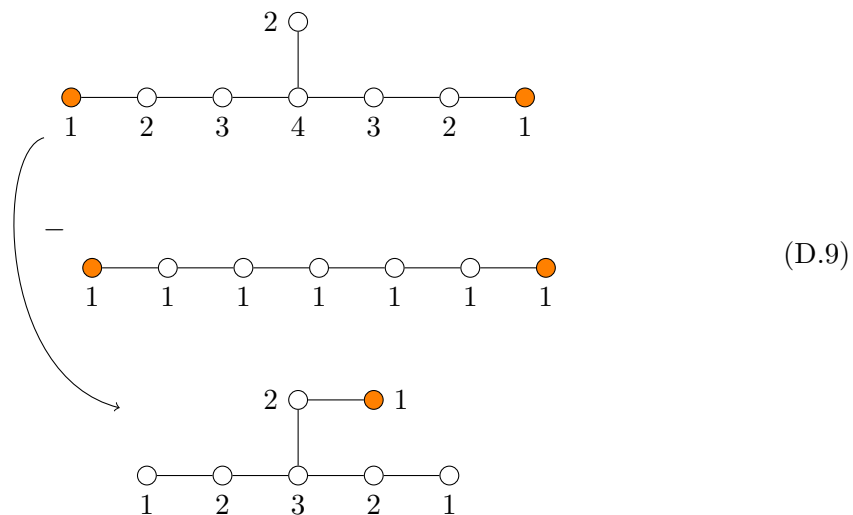
$$M_2 = \begin{pmatrix} \frac{8}{9} & -\frac{2}{3} & \frac{10}{9} \\ \frac{4}{9} & -\frac{1}{3} & \frac{5}{9} \\ -\frac{4}{9} & \frac{1}{3} & -\frac{5}{9} \end{pmatrix} \quad M_3 = \begin{pmatrix} \frac{10}{9} & \frac{2}{3} & -\frac{10}{9} \\ -\frac{4}{9} & -\frac{2}{3} & \frac{4}{9} \\ \frac{4}{9} & -\frac{1}{3} & -\frac{4}{9} \end{pmatrix}. \tag{D.7}$$

**D.3.4**  $E_6 \rightarrow A_5$

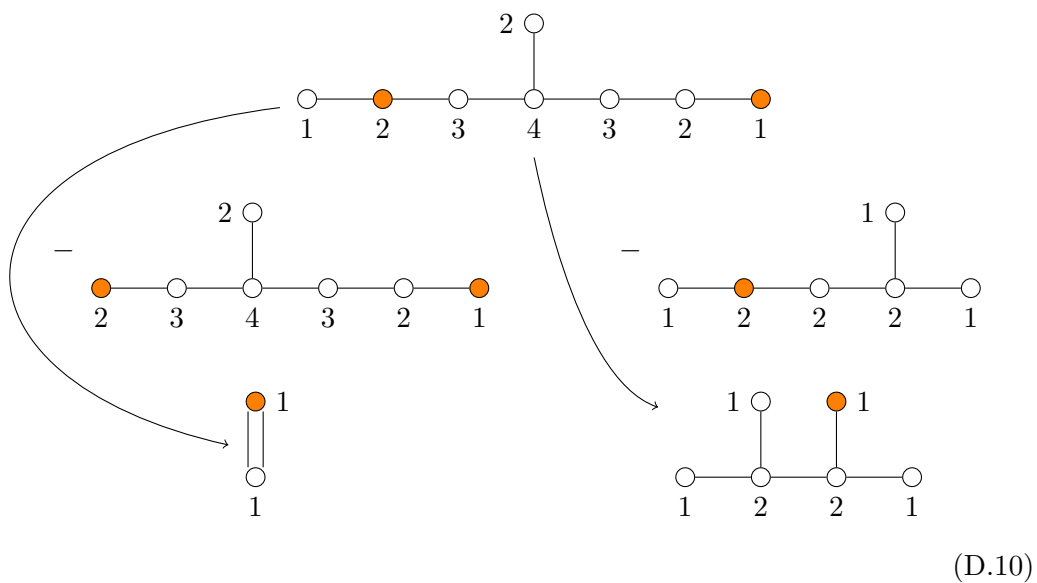


**D.4 Type  $E_7$**

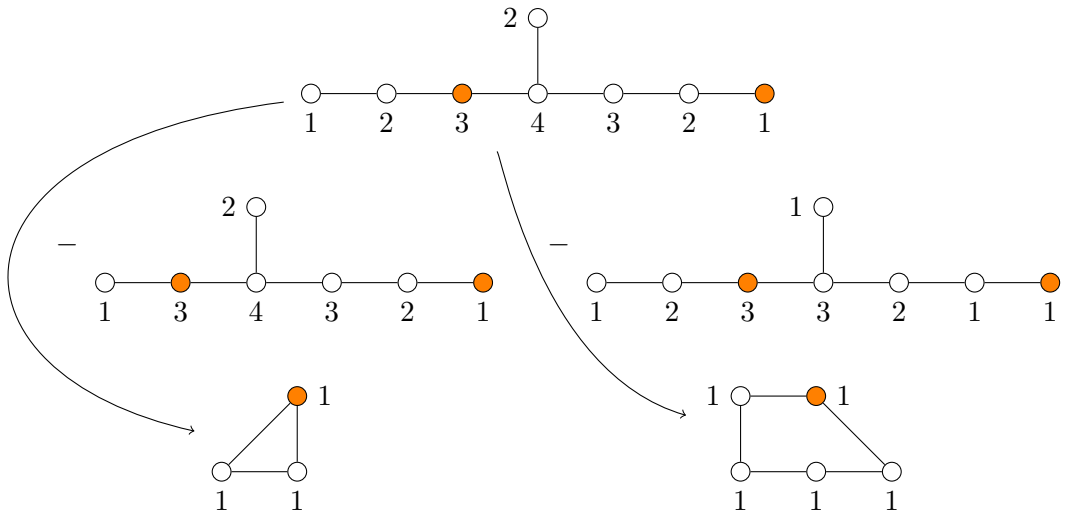
**D.4.1  $E_7 \rightarrow E_6$**



**D.4.2  $E_7 \rightarrow A_1 D_5$**

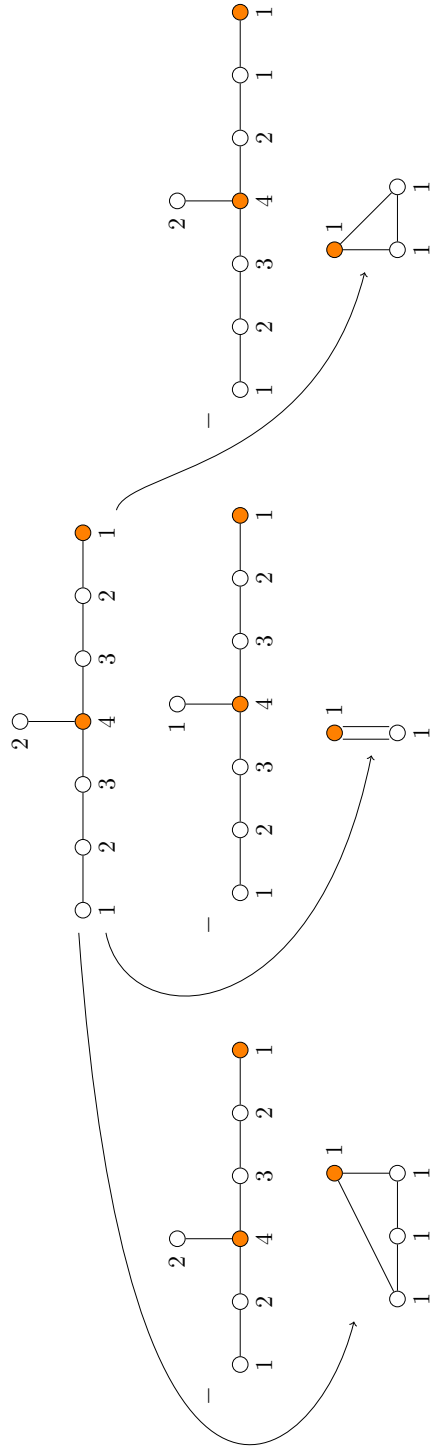


D.4.3  $E_7 \rightarrow A_2A_4$



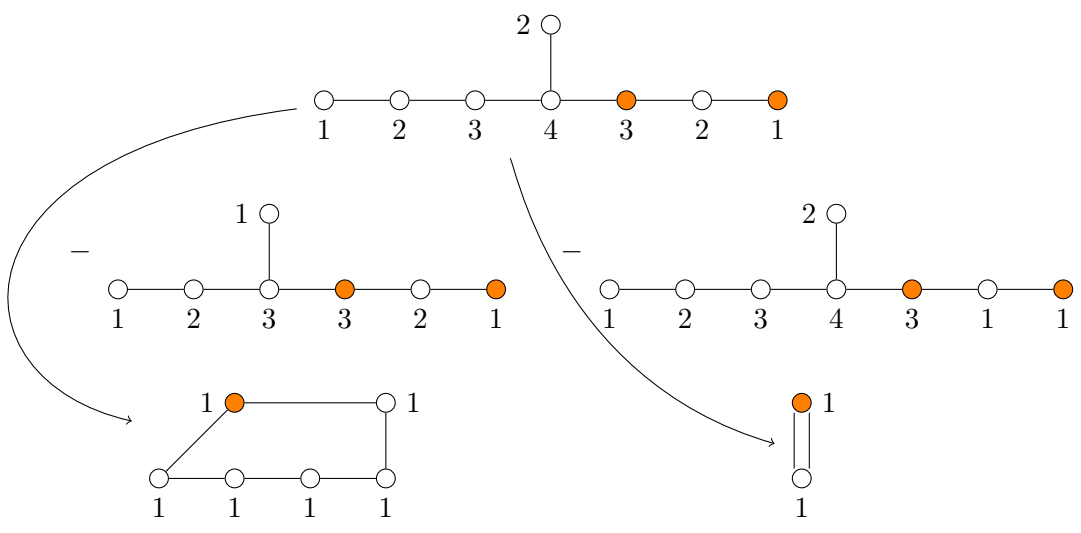
(D.11)

D.4.4  $E_7 \rightarrow A_3 A_1 A_2$



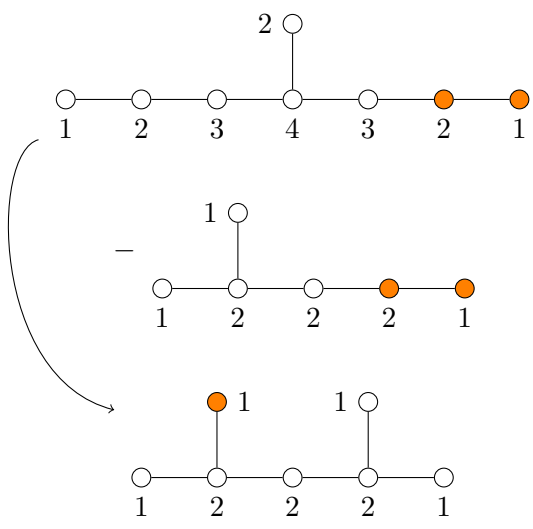
(D.12)

**D.4.5**  $E_7 \rightarrow A_5A_1$



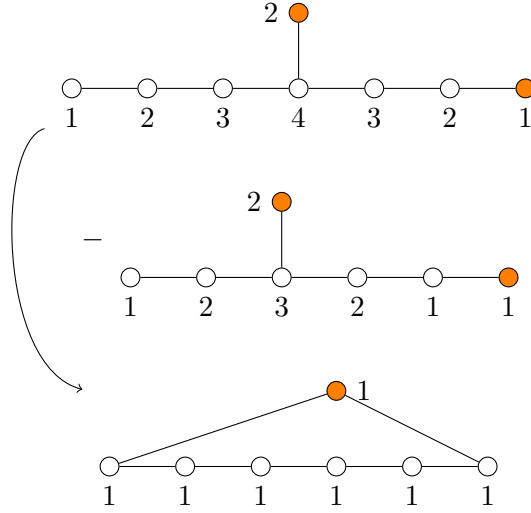
(D.13)

**D.4.6**  $E_7 \rightarrow D_6$



(D.14)

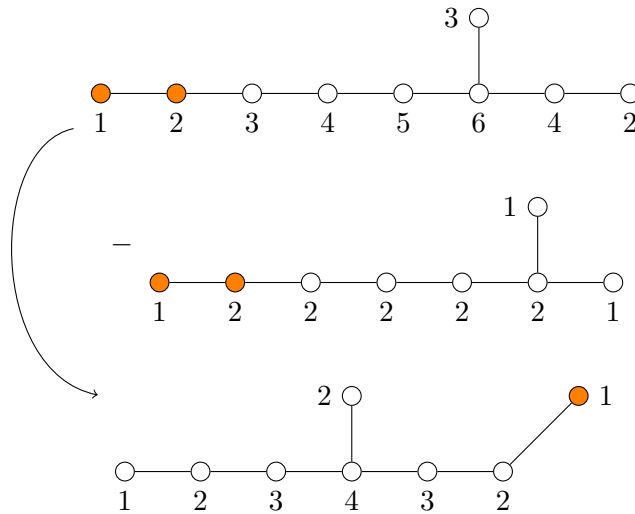
D.4.7  $E_7 \rightarrow A_6$



(D.15)

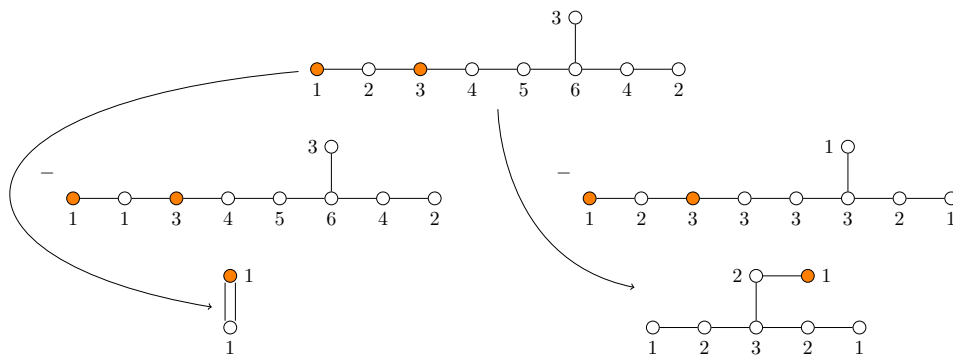
D.5 Type  $E_8$

D.5.1  $E_8 \rightarrow E_7$



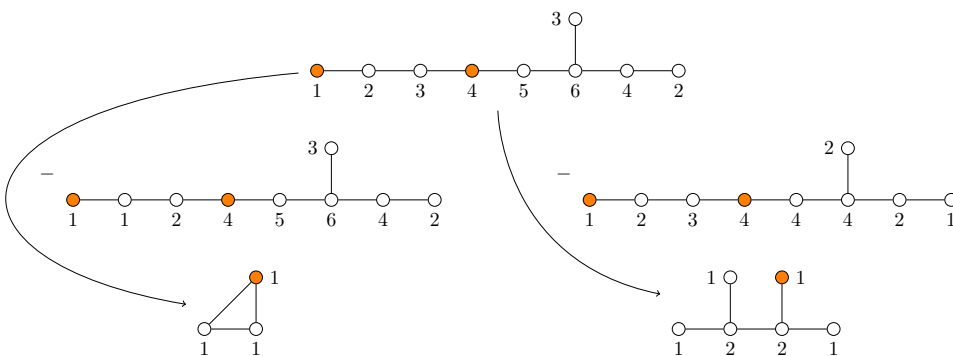
(D.16)

**D.5.2**  $E_8 \rightarrow A_1 E_6$



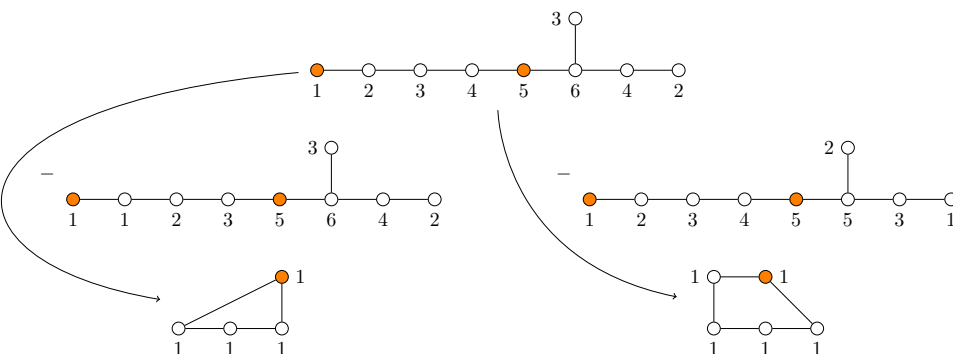
(D.17)

**D.5.3**  $E_8 \rightarrow A_2 D_5$



(D.18)

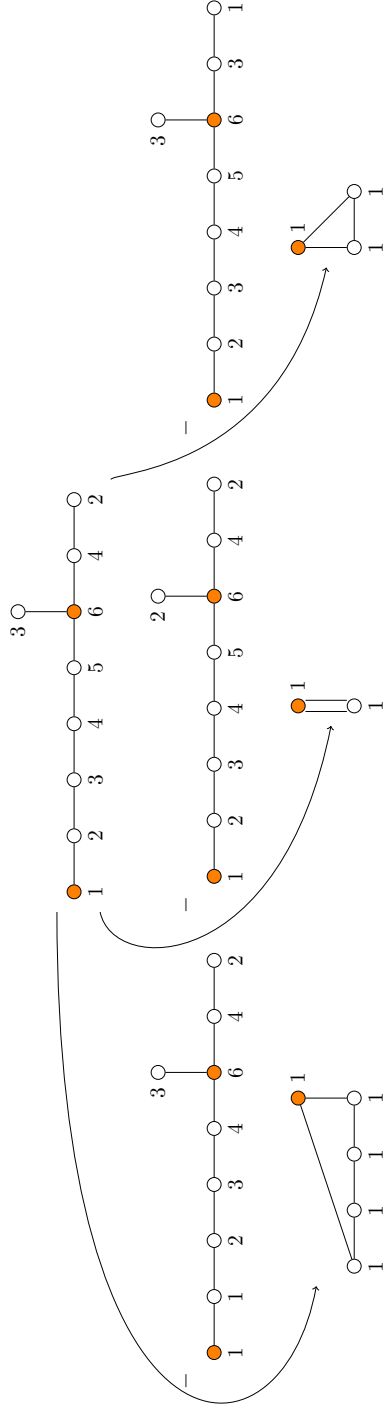
**D.5.4**  $E_8 \rightarrow A_3 A_4$



(D.19)

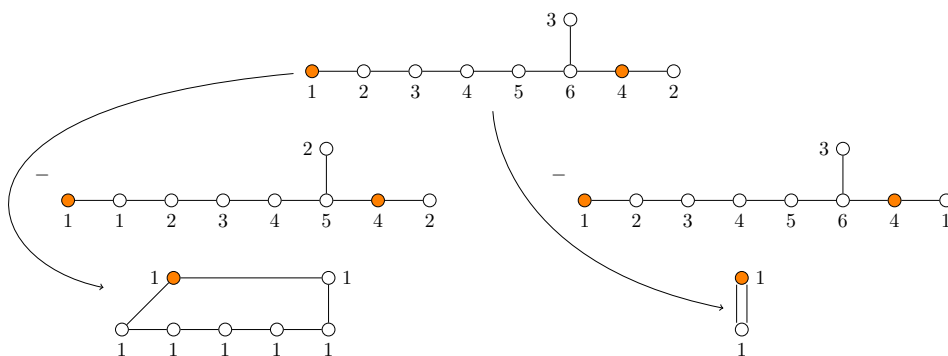


D.5.5  $E_8 \rightarrow A_4 A_1 A_2$



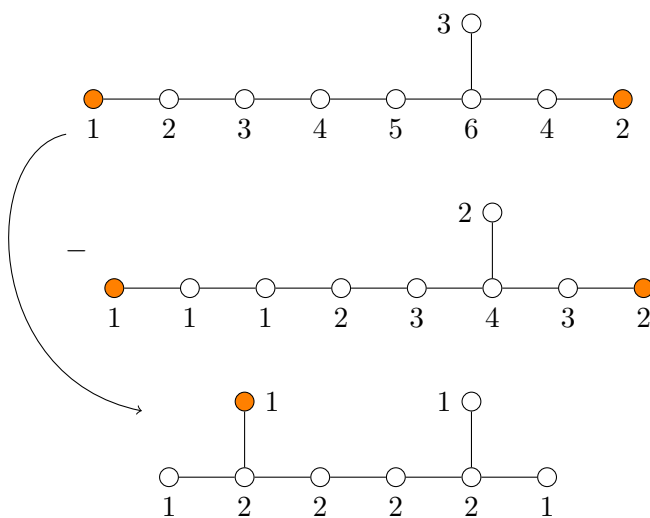
(D.20)

**D.5.6**  $E_8 \rightarrow A_6A_1$



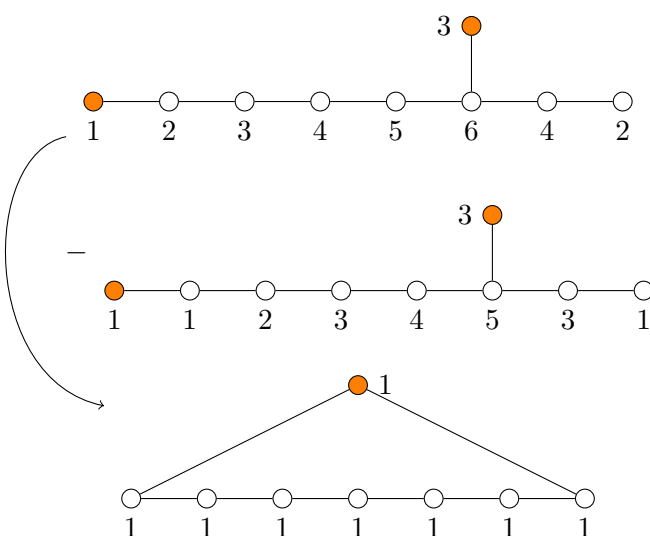
(D.21)

**D.5.7**  $E_8 \rightarrow D_7$



(D.22)

**D.5.8**  $E_8 \rightarrow A_7$



(D.23)

**Open Access.** This article is distributed under the terms of the Creative Commons Attribution License ([CC-BY 4.0](https://creativecommons.org/licenses/by/4.0/)), which permits any use, distribution and reproduction in any medium, provided the original author(s) and source are credited. SCOAP<sup>3</sup> supports the goals of the International Year of Basic Sciences for Sustainable Development.

## References

- [1] P. Fayet and J. Iliopoulos, *Spontaneously Broken Supergauge Symmetries and Goldstone Spinors*, *Phys. Lett. B* **51** (1974) 461 [[INSPIRE](#)].
- [2] K.A. Intriligator and N. Seiberg, *Mirror symmetry in three-dimensional gauge theories*, *Phys. Lett. B* **387** (1996) 513 [[hep-th/9607207](#)] [[INSPIRE](#)].
- [3] V. Ginzburg, *Lectures on Nakajima’s Quiver Varieties*, [arXiv:0905.0686](#).
- [4] N.J. Hitchin, A. Karlhede, U. Lindstrom and M. Rocek, *Hyperkahler Metrics and Supersymmetry*, *Commun. Math. Phys.* **108** (1987) 535 [[INSPIRE](#)].
- [5] U. Lindstrom, M. Rocek and R. von Unge, *HyperKahler quotients and algebraic curves*, *JHEP* **01** (2000) 022 [[hep-th/9908082](#)] [[INSPIRE](#)].
- [6] E. Witten, *Toroidal compactification without vector structure*, *JHEP* **02** (1998) 006 [[hep-th/9712028](#)] [[INSPIRE](#)].
- [7] Y. Tachikawa, *Frozen singularities in M and F theory*, *JHEP* **06** (2016) 128 [[arXiv:1508.06679](#)] [[INSPIRE](#)].
- [8] P. Argyres, M. Lotito, Y. Lü and M. Martone, *Geometric constraints on the space of  $\mathcal{N} = 2$  SCFTs. Part I: physical constraints on relevant deformations*, *JHEP* **02** (2018) 001 [[arXiv:1505.04814](#)] [[INSPIRE](#)].
- [9] P.C. Argyres, M. Lotito, Y. Lü and M. Martone, *Geometric constraints on the space of  $\mathcal{N} = 2$  SCFTs. Part II: construction of special Kähler geometries and RG flows*, *JHEP* **02** (2018) 002 [[arXiv:1601.00011](#)] [[INSPIRE](#)].
- [10] P. Argyres, M. Lotito, Y. Lü and M. Martone, *Geometric constraints on the space of  $\mathcal{N} = 2$  SCFTs. Part III: enhanced Coulomb branches and central charges*, *JHEP* **02** (2018) 003 [[arXiv:1609.04404](#)] [[INSPIRE](#)].
- [11] S. Cremonesi, G. Ferlito, A. Hanany and N. Mekareeya, *Coulomb Branch and The Moduli Space of Instantons*, *JHEP* **12** (2014) 103 [[arXiv:1408.6835](#)] [[INSPIRE](#)].
- [12] K. Gledhill and A. Hanany, *Coulomb branch global symmetry and quiver addition*, *JHEP* **12** (2021) 127 [[arXiv:2109.07237](#)] [[INSPIRE](#)].
- [13] D. Gaiotto and E. Witten, *S-Duality of Boundary Conditions In  $N=4$  Super Yang-Mills Theory*, *Adv. Theor. Math. Phys.* **13** (2009) 721 [[arXiv:0807.3720](#)] [[INSPIRE](#)].
- [14] I. Yaakov, *Redeeming Bad Theories*, *JHEP* **11** (2013) 189 [[arXiv:1303.2769](#)] [[INSPIRE](#)].
- [15] B. Assel and S. Cremonesi, *The Infrared Physics of Bad Theories*, *SciPost Phys.* **3** (2017) 024 [[arXiv:1707.03403](#)] [[INSPIRE](#)].
- [16] A. Bourget et al., *Higgs branches of U/SU quivers via brane locking*, *JHEP* **08** (2022) 061 [[arXiv:2111.04745](#)] [[INSPIRE](#)].
- [17] A. Bourget et al., *S-fold magnetic quivers*, *JHEP* **02** (2021) 054 [[arXiv:2010.05889](#)] [[INSPIRE](#)].

- [18] M. van Beest and S. Giacomelli, *Connecting 5d Higgs branches via Fayet-Iliopoulos deformations*, *JHEP* **12** (2021) 202 [[arXiv:2110.02872](#)] [[INSPIRE](#)].
- [19] S. Giacomelli, M. Moleti and R. Savelli, *Probing 7-branes on orbifolds*, *JHEP* **08** (2022) 163 [[arXiv:2205.08578](#)] [[INSPIRE](#)].
- [20] S. Cabrera and A. Hanany, *Quiver Subtractions*, *JHEP* **09** (2018) 008 [[arXiv:1803.11205](#)] [[INSPIRE](#)].
- [21] A. Bourget et al., *The Higgs mechanism — Hasse diagrams for symplectic singularities*, *JHEP* **01** (2020) 157 [[arXiv:1908.04245](#)] [[INSPIRE](#)].
- [22] A. Bourget et al., *Branes, Quivers, and the Affine Grassmannian*, [arXiv:2102.06190](#) [[INSPIRE](#)].
- [23] A. Dey, *Exploring Seiberg-like Dualities with Eight Supercharges*, [arXiv:2210.04921](#) [[INSPIRE](#)].
- [24] A. Dey, *Exploring Seiberg-like N-ality with Eight Supercharges*, [arXiv:2210.09319](#) [[INSPIRE](#)].
- [25] A. Dey, *Higgs branches of Argyres-Douglas theories as quiver varieties*, *JHEP* **03** (2023) 059 [[arXiv:2109.07493](#)] [[INSPIRE](#)].
- [26] A. Hanany and E. Witten, *Type IIB superstrings, BPS monopoles, and three-dimensional gauge dynamics*, *Nucl. Phys. B* **492** (1997) 152 [[hep-th/9611230](#)] [[INSPIRE](#)].
- [27] J.F. Grimminger and A. Hanany, *Hasse diagrams for 3d  $\mathcal{N} = 4$  quiver gauge theories — Inversion and the full moduli space*, *JHEP* **09** (2020) 159 [[arXiv:2004.01675](#)] [[INSPIRE](#)].
- [28] S. Cremonesi, A. Hanany and A. Zaffaroni, *Monopole operators and Hilbert series of Coulomb branches of 3d  $\mathcal{N} = 4$  gauge theories*, *JHEP* **01** (2014) 005 [[arXiv:1309.2657](#)] [[INSPIRE](#)].
- [29] A. Hanany and A. Zaffaroni, *Issues on orientifolds: On the brane construction of gauge theories with  $SO(2n)$  global symmetry*, *JHEP* **07** (1999) 009 [[hep-th/9903242](#)] [[INSPIRE](#)].
- [30] A. Hanany and J. Troost, *Orientifold planes, affine algebras and magnetic monopoles*, *JHEP* **08** (2001) 021 [[hep-th/0107153](#)] [[INSPIRE](#)].
- [31] P. Slodowy, *Four lectures on simple groups and singularities*, Rijksuniversiteit, Mathematical Institute (1980).
- [32] P.C. Argyres and M.R. Douglas, *New phenomena in  $SU(3)$  supersymmetric gauge theory*, *Nucl. Phys. B* **448** (1995) 93 [[hep-th/9505062](#)] [[INSPIRE](#)].
- [33] P.C. Argyres, M. Lotito, Y. Lü and M. Martone, *Expanding the landscape of  $\mathcal{N} = 2$  rank 1 SCFTs*, *JHEP* **05** (2016) 088 [[arXiv:1602.02764](#)] [[INSPIRE](#)].
- [34] M. Martone, *Testing our understanding of SCFTs: a catalogue of rank-2  $\mathcal{N} = 2$  theories in four dimensions*, *JHEP* **07** (2022) 123 [[arXiv:2102.02443](#)] [[INSPIRE](#)].
- [35] P.C. Argyres and M. Martone, *The rank 2 classification problem I: scale invariant geometries*, [arXiv:2209.09248](#) [[INSPIRE](#)].
- [36] F. Benini, Y. Tachikawa and D. Xie, *Mirrors of 3d Sicilian theories*, *JHEP* **09** (2010) 063 [[arXiv:1007.0992](#)] [[INSPIRE](#)].
- [37] D. Xie, *General Argyres-Douglas Theory*, *JHEP* **01** (2013) 100 [[arXiv:1204.2270](#)] [[INSPIRE](#)].
- [38] M. Del Zotto and A. Hanany, *Complete Graphs, Hilbert Series, and the Higgs branch of the 4d  $\mathcal{N} = 2$  ( $A_n, A_m$ ) SCFTs*, *Nucl. Phys. B* **894** (2015) 439 [[arXiv:1403.6523](#)] [[INSPIRE](#)].

- [39] S. Cabrera, A. Hanany and F. Yagi, *Tropical Geometry and Five Dimensional Higgs Branches at Infinite Coupling*, *JHEP* **01** (2019) 068 [[arXiv:1810.01379](#)] [[INSPIRE](#)].
- [40] S. Cabrera, A. Hanany and M. Sperling, *Magnetic quivers, Higgs branches, and 6d  $N=(1,0)$  theories*, *JHEP* **06** (2019) 071 [*Erratum ibid.* **07** (2019) 137] [[arXiv:1904.12293](#)] [[INSPIRE](#)].
- [41] S. Cabrera, A. Hanany and M. Sperling, *Magnetic quivers, Higgs branches, and 6d  $\mathcal{N} = (1, 0)$  theories — orthogonal and symplectic gauge groups*, *JHEP* **02** (2020) 184 [[arXiv:1912.02773](#)] [[INSPIRE](#)].
- [42] A. Bourget et al., *Brane Webs and Magnetic Quivers for SQCD*, *JHEP* **03** (2020) 176 [[arXiv:1909.00667](#)] [[INSPIRE](#)].
- [43] A. Bourget et al., *Magnetic quivers for rank 1 theories*, *JHEP* **09** (2020) 189 [[arXiv:2006.16994](#)] [[INSPIRE](#)].
- [44] A. Bourget et al., *Magnetic Quivers from Brane Webs with  $O5$  Planes*, *JHEP* **07** (2020) 204 [[arXiv:2004.04082](#)] [[INSPIRE](#)].
- [45] E. Beratto, S. Giacomelli, N. Mekareeya and M. Sacchi, *3d mirrors of the circle reduction of twisted  $A_{2N}$  theories of class S*, *JHEP* **09** (2020) 161 [[arXiv:2007.05019](#)] [[INSPIRE](#)].
- [46] C. Closset, S. Schafer-Nameki and Y.-N. Wang, *Coulomb and Higgs Branches from Canonical Singularities: Part 0*, *JHEP* **02** (2021) 003 [[arXiv:2007.15600](#)] [[INSPIRE](#)].
- [47] M. van Beest, A. Bourget, J. Eckhard and S. Schafer-Nameki, *(Symplectic) Leaves and (5d Higgs) Branches in the Poly(go)nesian Tropical Rain Forest*, *JHEP* **11** (2020) 124 [[arXiv:2008.05577](#)] [[INSPIRE](#)].
- [48] S. Giacomelli, M. Martone, Y. Tachikawa and G. Zafrir, *More on  $\mathcal{N} = 2$  S-folds*, *JHEP* **01** (2021) 054 [[arXiv:2010.03943](#)] [[INSPIRE](#)].
- [49] M. Van Beest, A. Bourget, J. Eckhard and S. Schäfer-Nameki, *(5d RG-flow) Trees in the Tropical Rain Forest*, *JHEP* **03** (2021) 241 [[arXiv:2011.07033](#)] [[INSPIRE](#)].
- [50] C. Closset, S. Giacomelli, S. Schafer-Nameki and Y.-N. Wang, *5d and 4d SCFTs: Canonical Singularities, Trinions and S-Dualities*, *JHEP* **05** (2021) 274 [[arXiv:2012.12827](#)] [[INSPIRE](#)].
- [51] M. Akhond et al., *Factorised 3d  $\mathcal{N} = 4$  orthosymplectic quivers*, *JHEP* **05** (2021) 269 [[arXiv:2101.12235](#)] [[INSPIRE](#)].
- [52] G. Arias-Tamargo, A. Bourget and A. Pini, *Discrete gauging and Hasse diagrams*, *SciPost Phys.* **11** (2021) 026 [[arXiv:2105.08755](#)] [[INSPIRE](#)].
- [53] A. Bourget et al., *Folding orthosymplectic quivers*, *JHEP* **12** (2021) 070 [[arXiv:2107.00754](#)] [[INSPIRE](#)].
- [54] F. Carta, S. Giacomelli, N. Mekareeya and A. Mininno, *Conformal manifolds and 3d mirrors of  $(D_n, D_m)$  theories*, *JHEP* **02** (2022) 014 [[arXiv:2110.06940](#)] [[INSPIRE](#)].
- [55] D. Xie, *3d mirror for Argyres-Douglas theories*, [arXiv:2107.05258](#) [[INSPIRE](#)].
- [56] S. Nawata, M. Sperling, H.E. Wang and Z. Zhong, *Magnetic quivers and line defects — On a duality between 3d  $\mathcal{N} = 4$  unitary and orthosymplectic quivers*, *JHEP* **02** (2022) 174 [[arXiv:2111.02831](#)] [[INSPIRE](#)].
- [57] C. Closset, S. Schäfer-Nameki and Y.-N. Wang, *Coulomb and Higgs branches from canonical singularities. Part I. Hypersurfaces with smooth Calabi-Yau resolutions*, *JHEP* **04** (2022) 061 [[arXiv:2111.13564](#)] [[INSPIRE](#)].

- [58] L. Bhardwaj, S. Giacomelli, M. Hübner and S. Schäfer-Nameki, *Relative defects in relative theories: Trapped higher-form symmetries and irregular punctures in class S*, *SciPost Phys.* **13** (2022) 101 [[arXiv:2201.00018](#)] [[INSPIRE](#)].
- [59] M.J. Kang et al., *Higgs branch, Coulomb branch, and Hall-Littlewood index*, *Phys. Rev. D* **106** (2022) 106021 [[arXiv:2207.05764](#)] [[INSPIRE](#)].
- [60] S. Nawata, M. Sperling, H.E. Wang and Z. Zhong, *3d  $\mathcal{N} = 4$  mirror symmetry with 1-form symmetry*, [arXiv:2301.02409](#) [[INSPIRE](#)].
- [61] A. Bourget, J.F. Grimminger, M. Martone and G. Zafrir, *Magnetic quivers for rank 2 theories*, *JHEP* **03** (2022) 208 [[arXiv:2110.11365](#)] [[INSPIRE](#)].
- [62] M. Martone and G. Zafrir, *On the compactification of 5d theories to 4d*, *JHEP* **08** (2021) 017 [[arXiv:2106.00686](#)] [[INSPIRE](#)].
- [63] S. Giacomelli, *RG flows with supersymmetry enhancement and geometric engineering*, *JHEP* **06** (2018) 156 [[arXiv:1710.06469](#)] [[INSPIRE](#)].
- [64] S. Cecotti, M. Del Zotto and S. Giacomelli, *More on the  $N=2$  superconformal systems of type  $D_p(G)$* , *JHEP* **04** (2013) 153 [[arXiv:1303.3149](#)] [[INSPIRE](#)].
- [65] S. Giacomelli, N. Mekareeya and M. Sacchi, *New aspects of Argyres–Douglas theories and their dimensional reduction*, *JHEP* **03** (2021) 242 [[arXiv:2012.12852](#)] [[INSPIRE](#)].
- [66] S. Benvenuti and S. Giacomelli, *Abelianization and sequential confinement in  $2 + 1$  dimensions*, *JHEP* **10** (2017) 173 [[arXiv:1706.04949](#)] [[INSPIRE](#)].
- [67] S. Benvenuti and S. Giacomelli, *Lagrangians for generalized Argyres–Douglas theories*, *JHEP* **10** (2017) 106 [[arXiv:1707.05113](#)] [[INSPIRE](#)].
- [68] J. de Boer, K. Hori, H. Ooguri and Y. Oz, *Mirror symmetry in three-dimensional gauge theories, quivers and D-branes*, *Nucl. Phys. B* **493** (1997) 101 [[hep-th/9611063](#)] [[INSPIRE](#)].
- [69] A. Kapustin,  *$D(n)$  quivers from branes*, *JHEP* **12** (1998) 015 [[hep-th/9806238](#)] [[INSPIRE](#)].
- [70] A. Hanany and R. Kalveks, *Quiver Theories and Formulae for Nilpotent Orbits of Exceptional Algebras*, *JHEP* **11** (2017) 126 [[arXiv:1709.05818](#)] [[INSPIRE](#)].
- [71] A. Bourget et al., *Magnetic Lattices for Orthosymplectic Quivers*, *JHEP* **12** (2020) 092 [[arXiv:2007.04667](#)] [[INSPIRE](#)].